HORIZONTAL AND VERTICAL DISPLACEMENT MONITORING ABOVE THE PCS SALT AND POTASH MINE NEAR SUSSEX, NEW BRUNSWICK.

by

Brian David Singleton

B.Sc., University of Natal, 1986.

A Report Submitted in Partial Fulfilment of
the Requirements for the Degree of

Master of Engineering

in the Graduate Academic Unit of
The Department of Geodesy and Geomatics Engineering.

Supervisor:	**Adam Chrzanowski**, PhD, *Dept. of Geodesy and Geomatics Engineering.*
Examining Board:	**Frank Rack**, PhD, Chair, *Dept. of Geodesy and Geomatics Engineering.*
	Wolfgang Faig, PhD, Dean of Engineering, *Dept. of Geodesy and Geomatics Engineering.*
	James Secord, PhD, *Dept. of Geodesy and Geomatics Engineering.*

THE UNIVERSITY OF NEW BRUNSWICK

September, 1997.

Abstract

Since 1989, the Engineering and Mining Surveys Research Group of the University of New Brunswick, under contract to the Potash Corporation of Saskatchewan-New Brunswick Division, has collected data for the purpose of monitoring ground displacements above the mine workings in Penobsquis, near Sussex, New Brunswick. Some of the latest surveying equipment was used to collect the horizontal and vertical data, namely: Leica's digital level, NA3000; and precision total station, TC2002; as well as Ashtech's Global Positioning System (GPS) receivers.

This report focuses on the horizontal integration of the conventional traverse and GPS data via a three-dimensional height-controlled least squares adjustment, using the commercial software package GeoLab™. An independent check on the WGS84 position of the projects' "fixed" station, via the International GPS Service for Geodynamics' Active Control System, was also performed. The assessment of relative accuracies for the observations used a limited version of the Iterated Minimum Norm Quadratic Estimation algorithm and various empirical observation accuracy models.

A horizontal trend analysis, via the Iterated Weighted Similarity Transformation algorithm, identified a maximum horizontal displacement rate of 23 mm/year. Vertical analysis, via profile graphs, revealed a maximum displacement rate of -24 mm/year, with a maximum accumulated subsidence, between 1989 and 1996, of -116mm.

Acknowledgements

As with most undertakings, this project could not have been completed without the assistance of a number of people, to whom I am indebted.

Firstly, I would like to thank my supervisor Dr. Adam Chrzanowski for his perseverance and financial support throughout the project and the writing of this report. Secondly, Brian Roulston and Greg Northrup of Potash Corporation of Saskatchewan - New Brunswick Division are thanked for their input.

The data collection for this project has been very extensive and so I would like to thank James Lutes, Geoffrey Bastin, Dany Gauthier, Kevin MacLeod, Justin Walford and John Ogundare of the Engineering and Mining Surveys Research Group for their much appreciated assistance and enthusiasm. As well, Jacek Grodecki, Mark Caissy, James Lutes and Justin Walford were responsible for writing much of the group's internal software and their efforts were greatly appreciated.

Noreen Bonnell, Theresa Pearce and Linda O'Brien of the Department of Geodesy and Geomatics Engineering are also thanked for their assistance with the various administrative tasks associated with this project.

Finally, I would like to thank my fellow graduate students for all those times when I was not working on this report, particularly Marta Wojnarowska for all the canoeing, cycling, skiing and hiking trips she made possible.

Table of Contents

List of Figures

List of Tables

Chapter 1

Introduction

In 1989, the Potash Company of America (now the Potash Corporation of Saskatchewan - New Brunswick Division) engaged the Engineering and Mining Surveys Research Group at the University of New Brunswick to monitor ground displacements above their salt and potash mine at Penobsquis, near Sussex, New Brunswick. Starting from a network of approximately 70 monuments and vertical displacements only, monitoring has expanded to over 100 monuments and both horizontal and vertical displacements using the latest measuring methods and instruments.

In 1983, Dr Chen completed his PhD Thesis in which he introduced a (UNB) generalised method for the analysis of deformation surveys [Chen, 1983]. Two of the techniques forming part of this UNB generalised method included the Iterative Minimum Norm Quadratic Estimation (IMINQE), for the assessment of observation accuracies, and the Iterative Weighted Similarity Transformation (IWST), for displacement trend analysis.

By 1994, software incorporating these two techniques had been written by members of the Engineering and Mining Surveys Research Group and were available for this project.

By 1993, the integration of Global Positioning System (GPS) and terrestrial data for monitoring horizontal displacements above the Potash Corporation of Saskatchewan-New Brunswick Division (PCS) mine had still not been resolved. Also, the three-dimensional adjustment package GeoLab™ had been acquired by the Engineering and Mining Surveys Research Group, which used a "height-controlled three-dimensional" system [Vincenty, 1980] in which to perform the least squares adjustment.

Given the above events, the objective, then, was: to combine GPS and terrestrial data in a three-dimensional height-controlled adjustment, together with techniques from the UNB generalised method of deformation analysis, for horizontal and vertical displacement monitoring above the PCS salt and potash mine near Sussex, New Brunswick. Implementation of the above objective was performed via a series of sub-objectives, namely:

1. to select a suitable datum for the combined adjustment of the GPS and terrestrial data and to establish the absolute position of a fixed point within this datum (Chapter 3);
2. to reconcile the different GPS (ellipsoidal) and levelling (nearly-orthometric) height systems through the modelling of local geoidal corrections (Chapter 3);
3. to assess the accuracies of the various observations in preparation for a combined, single epoch, least squares adjustment (Chapter 4);
4. to perform a combined least squares adjustment of the GPS and terrestrial data using the three-dimensional height-controlled system implemented by GeoLab™ (Chapter 5);

5. to identify horizontal and vertical displacement trends, suitable for the formulation of a strategy upon which to begin modelling the displacements (Chapter 6); and
6. to geometrically model the observed horizontal and vertical displacements.

Not all of these objectives were achieved, while others were achieved via means not originally intended. Most notably, it was discovered that an erroneous ellipsoidal height was being used to process the GPS baselines, hence the reconciliation of the GPS and levelled height systems was not theoretically correct. Secondly, the IMINQE algorithm failed to converge while assessing the traverse data, hence it could not be used to combine all observations together in an optimum estimation of their relative accuracies. Chapter 4, therefore, deals with the alternative procedures used to obtain, and consequently scale, the *a priori* variances for the combined adjustment. Finally, the geometrical modelling was not performed due to the time taken to resolve problems encountered in the previous objectives and also due to the complexity of the displacement sources.

Before discussing any of the objectives, however, it seemed appropriate to describe the data collection procedures and the instrumentation used on this project. Additionally, the three-dimensional height-controlled system required different, and considerably less, data reductions than the traditional two-dimensional horizontal adjustment techniques. These topics are thus covered in Chapter 2.

Chapter 2

Data Collection and Pre-processing

The monitoring network over the mine workings was initially intended for vertical displacement monitoring only. An extension to horizontal displacement monitoring effectively started in 1991. Consequently, between 1991 and 1996, three distinct survey methods were employed, namely: levelling; traversing; and static differential GPS positioning. The first two of these methods were the traditional "terrestrial" methods of vertical and horizontal data collection, respectively. The third method was the most recent, and had the distinct advantage of collecting information about all three dimensions simultaneously.

In this chapter, the equipment; observation techniques; and data preparation for each of the three aforementioned modes is presented separately. Here, "data preparation" was taken to represent those actions performed on the observation data in order to "prepare" it for the final, combined (GPS and terrestrial), three-dimensional, least squares

adjustment. It does not, however, include the process of assigning *a priori* weights for the final adjustment, as this is covered in Chapter 4.

2.1 Levelling

The levelling campaigns have been conducted in the summer of each year, generally in the months of June and July, between 1989 and 1996. The monitoring area is characterised by a number of levelling lines running perpendicular to the mine workings (cross-sections), which are connected via two major lines running parallel to the mine workings (profiles). The layout of monitoring stations with respect to the underground workings and surface topography is presented in Figure 2.1. Typically, two different types of ground conditions were encountered: either; firm, dry ground adjacent to paved roads; or soft, wet ground along the edges of cultivated fields. Ground conditions dictated the type of turning point used, so as to reduce the propagation of rod settlement errors.

2.1.1 Levelling Equipment

Over the series of levelling campaigns conducted near Sussex, only two types of levels have been used. In 1989, through to 1991, the Kern GK2-A automatic optical level was used in conjunction with two Wild double-scaled, invar levelling rods. The Kern GK2-A

Figure 2.1 Cross-sections, Profiles and Monument Layout

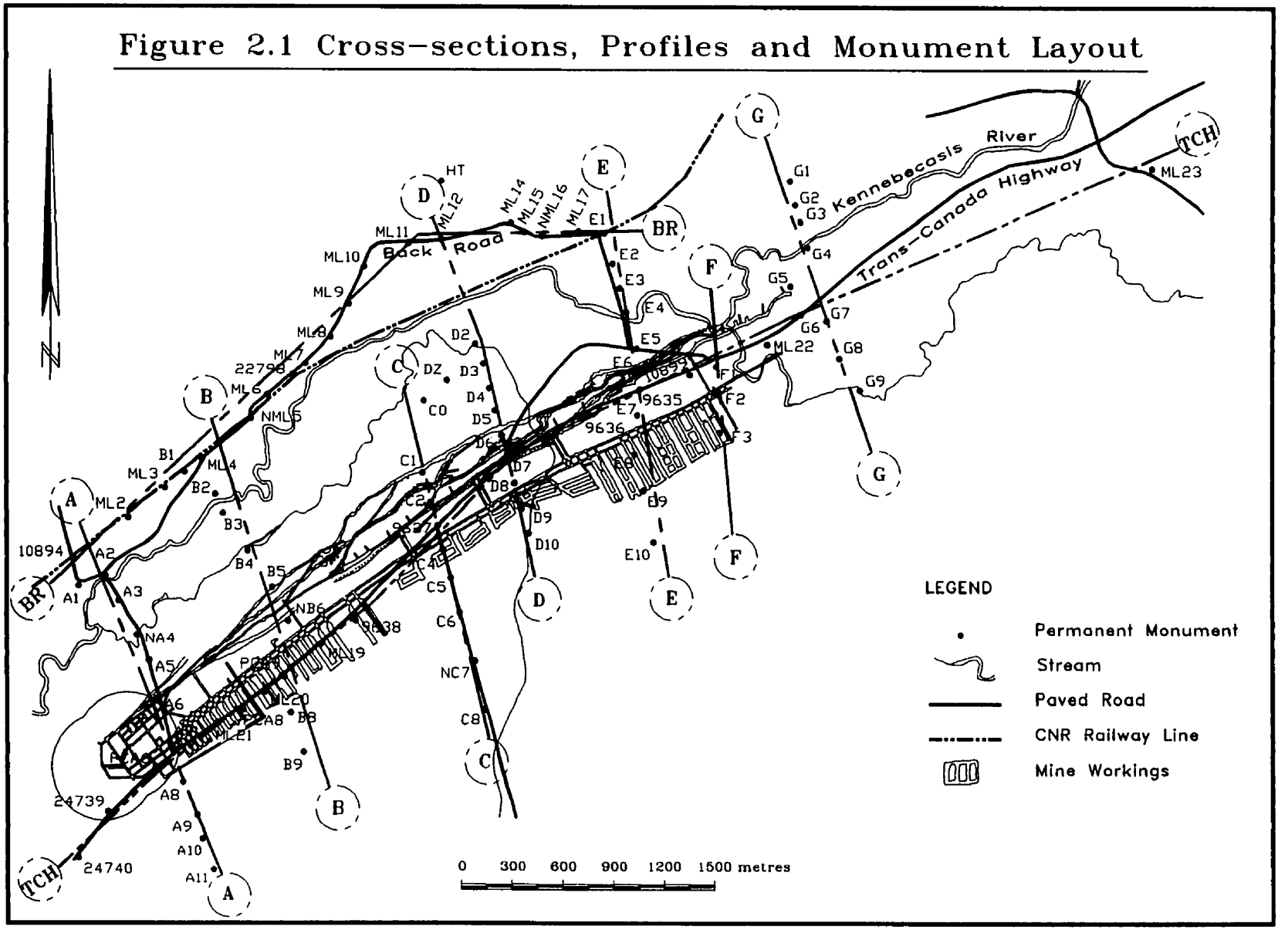

had an attachable parallel plate micrometer reading system, with a manufacture's claimed precision of ± 0.3 mm/km when used with invar levelling rods [Kern, 1987]. Additionally, it contained a pendulum compensator for the "automatic" levelling of the line of sight to within ± 0.3 ". The Wild levelling rods comprised a single section of 3 m length, with two separate scales graduated in centimetres on an invar band and marked from 0.00 m - 2.98 m (low scale) and 3.02 m - 5.99 m (high scale). A circular bubble was permanently attached to each rod.

In 1992, the Leica NA3000 precision digital automatic level (approved for first-order levelling by the Federal Geodetic Control Society (FGCS) in 1992 [Leica, 1993a]) was first used in conjunction with two 3 m long, Leica GPCL3 bar coded invar levelling rods. It has been used exclusively in the 1992 to 1994 campaigns, but jointly with the GK2-A in 1995 and 1996.

Prior to 1992, observations were recorded manually in field books, in traditional formats. In 1992, the Corvallis Microtechnology Inc. (CMT) MC-V hand computer was used for data collection and verification. Software programs were written in BASIC for manual data entry via the Kern GK2-A, and direct two-way communication with the NA3000.

2.1.2 Observation Methodology

The primary objectives of the data collection methods were: i) reduction of known systematic errors; ii) early detection of observation blunders; and iii) preparation of the

data for the next stage of processing.

The major systematic errors of concern were those of refraction, collimation, earth curvature, and rod and instrument settlement. Observation procedures for the minimisation of these errors can be found in the levelling specifications of national mapping organisations (see, for example, Specification Series, [1978] and Bossler, [1984]). While not a specification of the monitoring contract, the EMR (Energy, Mines and Resources) Canada recommendations for first order levelling [Specification Series, 1978] were generally followed in this project, subject to practical limitations. The following is a list of the observation procedures used between 1993 and 1996, for which a separate levelling rod was required on each of the forward and backward turning points:

i) rod readings were taken in a BS-FS-FS-BS sequence (alternating with a FS-BS-BS-FS sequence since 1994);

ii) sight distances were restricted to a maximum of 50 m;

iii) the imbalance between foresight and backsight distances was restricted to a maximum of 5 m, with the exception of river and Trans-Canada Highway (TCH) crossings;

iv) rod readings were restricted to a minimum height of 0.5 m;

v) heavy duty "turtles" were used as turning points for roadside sections, while nominal 355 mm long "pins" were used for all other sections;

vi) cross-sections were levelled forward and backward; and

vii) profiles (along TCH, railway and Back Road) were levelled in one direction only, prior to 1994, but in both directions since 1994.

Sections (taken here to be neighbouring monuments) levelled in both directions were considered acceptable if their misclosures were less than $\pm 4\ \text{mm}\sqrt{L}$, where L was the section length in kilometres. At the completion of each setup, but prior to the relocation of the level, a check for reading consistency to $\pm$ 0.5 mm was made. These checks were generally made in the field, and their execution was greatly facilitated with the advent of the data logger.

The hand computer, used as a data logger, enabled preparation of the data for later processing. In this manner the section height difference (one-way); the number of setups (and total levelled distance in the case of the NA3000); and monument labels were placed into a daily summary file. The raw observations were still recorded as a backup in a separate daily file. All file names included an instrument identification letter, the date and an identifying extension (e.g., N950701.PRT was a summary file of the NA3000 observations collected on the 1st of July, 1995).

2.1.3 Data Preparation

As the misclosures obtained in the field often included several neighbouring sections, all individual runs were subsequently collected together and sorted into forward and backward run pairs. Misclosures for each section were then computed. This was generally done each evening after the data loggers were downloaded.

Generally, the mean of the forward and backward runs is input into a least squares adjustment, as was the case for the pre-1993 campaigns. It was decided, however, in the

1993 and subsequent campaigns, to input both runs into the adjustment. The reasons for this change were: (i) the adjustment software used, derived the section weights from the number of setups per section, which caused a problem when single- and double-runs were included in the same adjustment; (ii) the network redundancy resulting from only two loops rendered the statistical tests associated with the adjustment meaningless; and (iii) the *a posteriori* variance of unit weight (reference variance) now provided a measure of both the random and systematic errors of the section misclosures. This resulted in more realistic *a posteriori* standard deviations. An investigation into the correlation between forward and backward levelling runs is presented, within the context of the 1994 levelling campaign, in Chapter 4.

2.2 Traversing

Horizontal monitoring of the PCS mine surface was plagued by the frequent lack of inter-visibility between monuments, resulting in numerous short traverse legs being introduced into the traverse network. This, combined with the numerous "hanging" traverses of the network (see Figures 2.2 and 2.3), resulted in local orientation anomalies.

A second major problem with the horizontal monitoring scheme was, that it started out in 1989 as a simple "coordination of monuments for plotting purposes" in support of the levelling campaign and evolved out of a series of experiments in data collection. The increasing popularity of GPS (improved satellite constellation, observation efficiency and

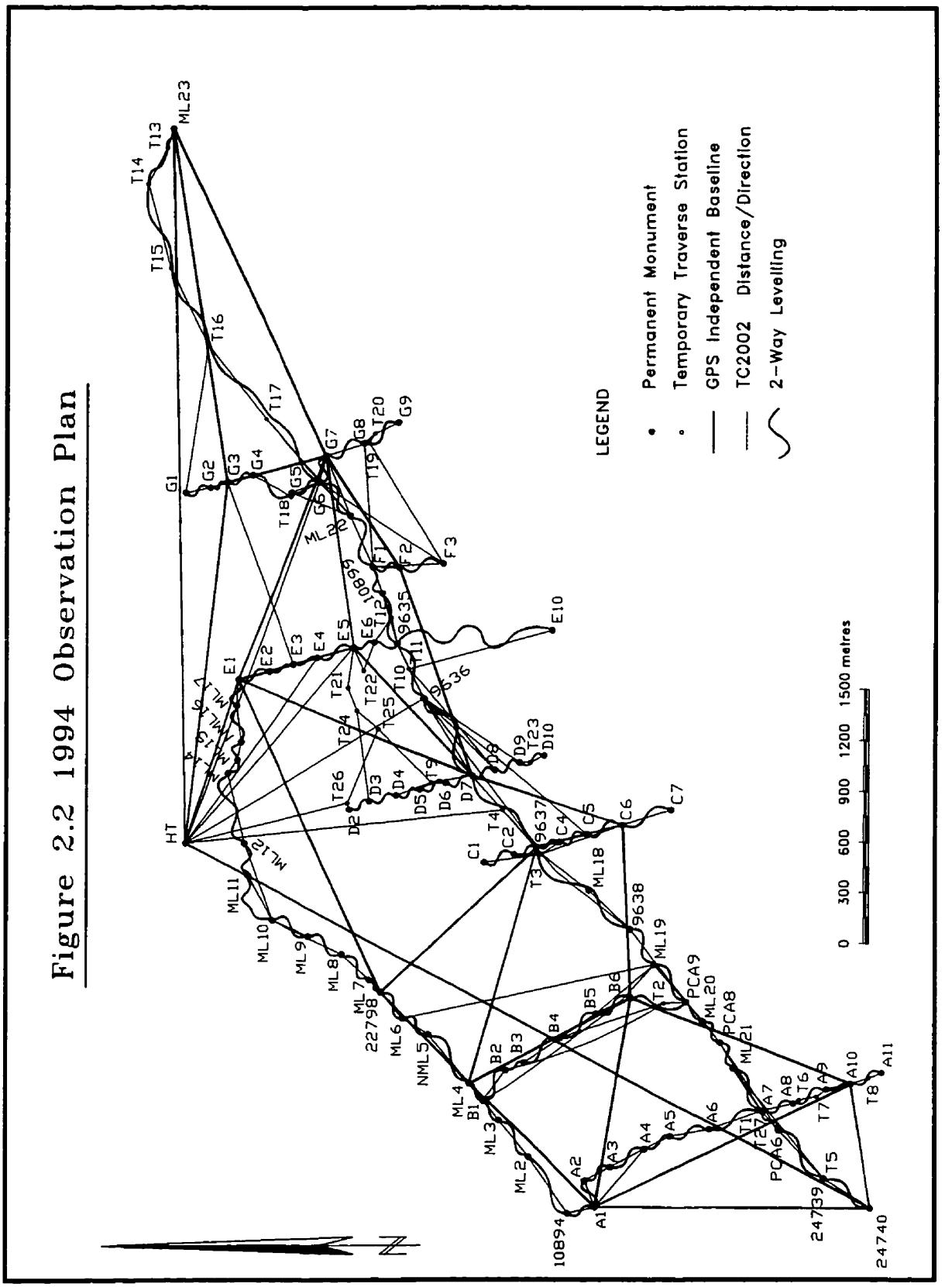
Figure 2.2 1994 Observation Plan
LEGEND
Permanent Monument
Temporary Traverse Station
GPS Independent Baseline
TC2002 Distance/Direction
2-Way Levelling
0 300 600 900 1200 1500 metres
N

Figure 2.3 1992 Traverse Observation Plan

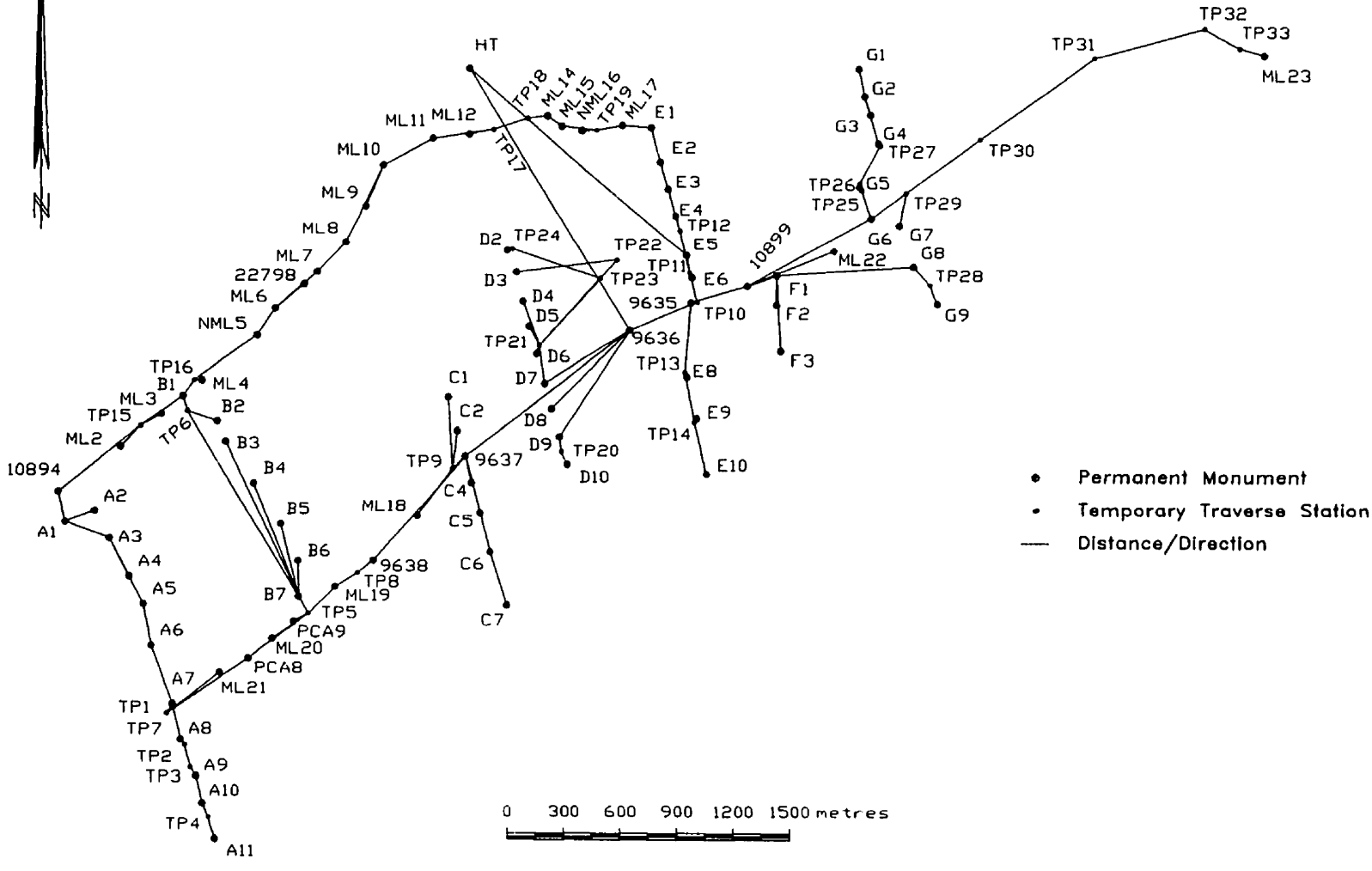

results) was seen as a means of overcoming some of the terrestrial network shortcomings. Trial projects of GPS with traversing were attempted between 1989 and 1992, where, due to the aforementioned network shortcomings, monitoring via the "observation differences" approach [Lazzarini et al., 1976] was attempted.

The implication of the "observation differences" approach was a de-emphasis on network redundancy. This monitoring approach was eventually thwarted by numerous instrument problems (mainly Electronic Distance Measurer (EDM) scale) and inconsistency in the observation schemes (due to changing field conditions, as well as the loss and replacement of several monuments). The third major problem, therefore, was a lack of strength and redundancy when reverting to the "coordinate differences" approach.

In 1992, a major extension to the monitoring network occurred, where 15 additional monuments were added to cover the region of new mining activity east of the E-line. Consequently, the horizontal monitoring discussed in this report covers, predominantly, the period 1992 to 1996 during which this "full" network existed. During this period, five different EDMs were used, which resulted in considerable attention being given to the problem of scale (both between EDMs and with regards to GPS).

The two major observables discussed in terms of traverse data collection and pre-processing are those of distance and direction. However, in the case of distances, several ancillary observations were required for reduction purposes, namely: instrument and reflector heights; meteorological data; monument elevations; and zenith angles. Some of the problems encountered in the collection of this data are discussed below.

2.2.1 Traverse Equipment

Instruments used over the years included two Kern E2 electronic theodolites, three Kern DM503 EDMs, one Tellurometer MA200 precision EDM, and one Leica TC2002 Total Station. In 1993 a CMT (Corvallis MicroTechnology Inc.) MC-V data logger was first introduced to facilitate traverse data collection and assessment in the field.

Table 2.1 Horizontal Survey Equipment List: 1992 to 1996.

Instrument	Serial No.	1992	1993	1994	1995	1996
Distances:						
Kern DM503	*325147*	*				
Kern DM503	*325207*		*			
Kern DM503	*348158*	*	*			
Tellurometer MA200	*216*	*	*			
Leica TC2002	*357992*			*	*	*
Directions:						
Kern E2	*342058*		*			
Kern E2	*345392*	*	*			
Leica TC2002	*357992*			*	*	*
GPS Receivers:						
Ashtech L-XII	*700047C0199*	*	*	*	*	*
Ashtech L-XII	*700047C0209*	*	*	*	*	
Ashtech L-XII	*700047C0297*	*	*	*	*	*
Ashtech Z-XII	*01837U*				*	*
Ashtech Z-XII	*02141U*				*	*

2.2.2 Traverse Data Collection

In the early horizontal campaigns (1989 to 1991) two Kern E2 electronic theodolites, coupled with Kern DM503 EDMs were used. In 1992 and 1993, a Tellurometer MA200 precision EDM was used to increase the strength, and redundancy, of the network through the observation of several longer distances. In the 1994 to 1996 campaigns, the Leica TC2002 total station was used exclusively for traversing purposes. However, the extent of the traverse network was reduced in favour of more dense GPS networks. Table 2.1 indicates the variety of traversing equipment used, between 1992 and 1996, for the horizontal campaigns.

2.2.2.1 Directions

Generally, spatial directions were observed as three sets of "face left" (FL) and "face right" (FR) horizontal circle readings with either gons or sexagesimal units used. Due to the number of available targets and reflectors, the necessity of interchanging targets with reflectors, a two-person traverse crew and the geometry of the network no more than four targets were observed at any one setup.

The method of recording has varied from year to year and was generally that preferred by whoever was responsible for the field work. Earlier campaigns were manually entered into fieldbooks (giving greater leeway to individual preferences), while later campaigns were "regularised" to some extent via the use of the MC-V data logger software.

2.2.2.2 Zenith Angles

The role of zenith angles in this project had been confined to that of distance reduction, i.e., they were not used in the determination of elevations for monitoring purposes. Even then, they were only used for those distances which involved temporary traverse stations (which had not been included in the levelling network). They were, however, occasionally called upon to determine missing, or erroneous, "height of EDM" or "height of reflector" data during spatial distance reductions.

The zenith angles were observed simultaneously with the directions, with three arcs (except in 1993, only one arc) in both telescope positions. Introduction of the TC2002, with its coaxial EDM, led to a duplication of the zenith angles as a result of EDM distance measurement. However, as they represented only a single pointing (i.e., one telescope position), they were rarely consulted.

2.2.2.3 Spatial Distances

The collection of EDM distances was the most time consuming of the traverse data collection activities, due mainly to the necessary collection of meteorological data and the changing of targets and reflectors between observing directions and distances. Additionally, the distance for each traverse leg was measured in both directions so as to increase its reliability. This was particularly important in lieu of the numerous "hanging" traverses.

The Tellurometer MA200 operated independently of any angle measuring equipment and required greater attention in both the setup and measuring stages. It was used in 1992 and 1993 for gathering a few long, highly accurate, network strengthening distances. This role was taken over by the TC2002 in 1994 and abandoned in later campaigns in favour of additional GPS baselines.

A major problem encountered with the Kern DM503 EDMs in the 1991 and 1992 campaigns was that of unrecorded atmospheric corrections applied by the EDM in the field. This is a common problem amongst inexperienced surveyors and shared equipment. Precise traversing procedures have always been to collect EDM distances with a "zero atmospheric correction" applied by the EDM. Atmospheric corrections are subsequently computed, and applied, on the basis of the observed meteorological data.

2.2.3 Traverse Data Pre-processing

The decision to use a three-dimensional method for the horizontal adjustment removed a considerable amount of traverse data pre-processing (as the data was to be entered into the adjustment as spatial observations). Preparation of directions for the final adjustment was minimal, as only the mean of the three, or more, observed arcs was required: to which *a priori* standard deviations were later attached (see Chapter 4). The observed EDM distances, however, still required some pre-processing so as to remove instrument and atmospheric errors.

As a result of the above decision, and as a means of ensuring consistency in the data (especially after the discovery of several bugs in the data logger software), all traverse data from 1992 to 1996 was reprocessed from source (i.e., field books and "raw" data logger files). This involved writing various FORTRAN routines and, in the case of the 1992 survey, the manual transfer of data from field books to computer. This manual data transfer was checked via the same methods prescribed for field collection.

The observed EDM distances were first corrected for atmospheric conditions through the application of a first velocity correction. Secondly, the calibrated "zero error" was removed, and finally, the distance was geometrically reduced to the required "mark-to-mark" distance. The availability of levelled heights for the permanent monuments, together with a lack of information as to the heights of temporary monuments, resulted in two options for the reduction of an "EDM-to-reflector" distance to the required mark-to-mark distance. Where levelled heights for the two monuments were available they were used; however, in their absence, the observed zenith angles (Z_{TH}) collected simultaneously with the directions were used.

2.2.3.1 First Velocity Correction , "Zero Error" and Scale.

All of the observed spatial distances were collected, together with instrument and reflector heights, mean zenith angles, wet and dry temperature readings and atmospheric pressure. The meteorological data was only collected at the instrument station, with the exception of the Tellurometer MA200 for which data was collected at both stations.

The first velocity correction accounts for the variation between the atmospheric refractive index, n, and the reference refractive index of the EDM, n_{REF} , selected by the EDM manufacturer to represent average atmospheric conditions. This correction, K′, to the observed distance, d′, is

$$K' = \left(\frac{n_{REF} - n}{n}\right) \cdot d' \approx (n_{REF} - n) \cdot d' \qquad (2.1)$$

where the approximation leads to errors of less than 0.02 ppm [Rüeger, 1990]. The above equation requires the determination of the atmospheric refractive index, n. Most EDM manufacturers provide appropriate formulae for the evaluation of the atmospheric correction based on observed meteorological readings. Consequently, the distance reduction software used on this project (DIST_RED) required the identity of the EDM prior to the computation of K′. For example, Leica [1993b] provided the following correction for their TC2002,

$$\Delta d_1 = 281.8 - \left[\frac{0.29065 \cdot P}{(1+\alpha \cdot t)} - \frac{4.126 \cdot 10^{-4} \cdot h}{(1+\alpha \cdot t)} \cdot 10^{\left(\frac{7.5 \cdot t}{237.3+t} + 0.7857\right)}\right] \qquad (2.2)$$

so that $K' = \Delta d_1 \cdot d'$, $n_{REF} = 1 - 281.8 \cdot 10^{-6}$ and

Δd_1 = atmospheric correction in ppm ;
P = atmospheric pressure (mb) ;
t = ambient (dry bulb) temperature (°C) ;
h = relative humidity (%) ; and
α = 1/273.16 .

Leica, goes on to state that its default value of 60% relative humidity will lead to a maximum error of 2 ppm. However, dry temperature and relative humidity should be observed when higher precision is required. As wet and dry bulb psychrometer readings were collected on this project, instead of relative humidity, and recognising the Magnus-

Tetens equation for the saturation water vapour pressure at (dry) temperature, T_D , as [Rüeger, 1990]

$$E'_W = 10^{((7.5 \cdot T_D/(237.3+T_D))+0.7857)}$$

together with the relationship,

$$h = \frac{e}{E'_W} \cdot 100$$

then equation (2.1) can be re-written in the more suitable form,

$$K' = \left[281.8 - \frac{79.3940 \cdot P}{(273.16+t)} - \frac{11.2706 \cdot e}{(273.16+t)} \right] \cdot d' \qquad (2.3)$$

with the partial water vapour pressure,

$$e = E'_W - 6.62 \cdot 10^{-4} \cdot P \cdot (T_D - T_W)$$

for which a more accurate saturation water vapour pressure, evaluated at wet bulb temperature, was published by Buck in 1981 as [Rüeger, 1990]

$$E'_w = \left[1.0007 + 3.46 \cdot 10^{-6} \cdot P \right] \cdot 6.1121 \cdot 10^{\left(\frac{17.502 \cdot T_w}{240.97+T_w} \right)}$$

Following the first velocity correction, were corrections for "zero error" and scale, both of which had to be pre-determined for each EDM via calibration procedures. The "zero error" was determined on a six pillar, 1.6 km baseline at Mactaquac. The EDM scale factor could have been determined on the same baseline had accurate positions of the pillars been known; unfortunately, they were not.

In 1995, an attempt was made at resolving the relative scale factors of the DM503s (used in Sussex, between 1991 and 1993) with respect to the more precise

MA200 and TC2002 EDMs via a "combined least squares adjustment with auxiliary scale parameters" of the annual calibration data. Also, the annual calibrations of the two more precise EDMs were investigated with respect to a selected EDM baseline epoch, and found to remain within 2 ppm. Unfortunately, the "Mactaquac Baseline" estimated DM503 (relative) scale factors did not appear to match those determined in the combined adjustment of terrestrial (with auxiliary scale parameters, see equation (5.8)) and GPS data. As the latter approach was deemed to be the "better" of the two, no scale factors were applied during pre-adjustment distance reductions.

2.2.3.2 Distance Reduction with Observed Zenith Angles.

This approach was restricted to distances involving temporary stations for which levelled heights were not available. It was, additionally, restricted to "short distances". The reduction is an iterative one and is outlined by Rüeger [1990], a summary of which follows.

The algorithm presented by Rüeger [1990] presupposes the separate measurement of zenith angle and EDM distance, as well as the reduction of the observed EDM distance to the straight line distance between EDM and reflector (d_2). Consequently, the measured "height above monument" of the EDM (h_{EDM}), the theodolite (h_{TH}), the target (h_T), and the EDM reflector (h_R) were required. As an initial approximation, Rüeger suggested that the mark-to-mark distance, d_{MK}, be set equal to the reduced EDM-to-Reflector distance, d_2, and that the mark-to-mark zenith angle Z_{MK} be set equal to the observed zenith angle, Z_{TH}.

The initial value of d_{MK} was then used to compute an updated value for Z_{MK} via Rüeger [1990] :

$$Z_{MK} = Z_{TH} + \Omega \tag{2.4}$$

where the correction Ω was approximated by

$$\Omega \approx \frac{h_T - h_{TH}}{d_{MK}} \cdot \sin Z_{TH} \tag{2.5}$$

Thereafter, the updated value for Z_{MK} was used to update d_{MK} from

$$d_{MK} = d_2 - \frac{(h_{EDM} - h_R)^2}{2 \cdot d_{MK}^2} \cdot d_2 + \frac{(h_{EDM} - h_R)}{d_{MK}} \cdot d_2 \cdot \cos(Z_{MK} + \delta) + \ldots \tag{2.6}$$

where δ is the refraction angle computed from the coefficient of refraction (K) and the radius of curvature of the spheroid (R) along the line of the observed distance, corrected for the first velocity error (d_1), as [Rüeger, 1990] :

$$\delta = \frac{d_1 \cdot K}{2 \cdot R} \tag{2.7}$$

2.2.3.3 Distance Reduction with Known Elevations.

This approach was given preference, as the height information for permanent monuments was accurately determined from precise levelling, as opposed to the less accurate trigonometric heighting. The algorithm used for this reduction was derived as

$$d_{MK} = \sqrt{(R+H_1)^2 + (R+H_2)^2 - \frac{(R+H_1)\cdot(R+H_2)\cdot\left[(R+H_1+h_{EDM})^2 + (R+H_2+h_R)^2 - d_2^2\right]}{(R+H_1+h_{EDM})\cdot(R+H_2+h_R)}} \tag{2.8}$$

where H_1 and H_2 are ellipsoidal heights, which were approximated by the adjusted levelling network heights.

2.3 GPS Positioning

Static differential GPS surveys have been performed since 1989. However, with increased success, the survey has gradually extended from four monuments and four independent baselines in 1989 [Secord, 1989], to 16 monuments and 36 independent baselines in 1994.

In 1995, the GPS observation scheme changed drastically: the terrestrial "densification" scheme was replaced by a "GPS trilateration" sub-network (involving fewer monuments). Additionally, two Ashtech Z-XII receivers were introduced which brought the number of stations per session to five and challenged the GPS observation logistics. Consequently, the network was divided into primary and secondary components, where the primary network comprised the previously used GPS monuments and nominal 1¼ hour static observations, while the secondary network comprised the newer GPS monuments and spatial distances extracted from 30 minute static observations.

In 1996, with only four of the five Ashtech receivers available, the GPS campaign was altered again. The primary network remained the same, but the secondary network was observed in a pseudo-static mode. The primary and secondary networks were observed simultaneously with three receivers operating in the static mode (primary) and one operating in a roving pseudo-static mode (secondary). The rapid-static technique was

not used due to its requirement for dual-frequency phase observations and the availability of only two dual-frequency receivers.

The following subsection describes the general equipment, observation schemes, and data preparation employed with the GPS data.

2.3.1 GPS Equipment

Three Ashtech L-XIIs were available for the collection of GPS data from the outset of the monitoring project. In 1995, two Ashtech Z-XII receivers became available. The L-XII models were single frequency receivers capable of collecting both phase and code (C/A and P code) observables on the L1 GPS frequency. The Z-XII models, however, were dual frequency receivers capable of collecting both phase and code observables on both the L1 and L2 GPS frequencies. The Z-XII had the added capability of extracting the code and phase observations under conditions of Anti-Spoofing (AS), which was permanently activated on 31st January, 1994 [United States Naval Observatory, 1994].

2.3.2 GPS Data Collection

Preparation of the GPS observation schedule was the most challenging aspect of the GPS survey. The objectives to be satisfied by the network design were to:

a) enable the computation of all GPS monuments with respect to the "horizontal control point" HT;

b) permit only non-trivial baselines;

c) occupy each GPS monument at least twice;

d) permit quality checks via common baseline and triangle loop misclosures;

e) observe the short lines directly connecting neighbouring monuments;

f) use nominal 1 hour 15 minute observation sessions;

g) adhere to a maximum 30 minute session intermission;

h) permit the use of only two vehicles for relocation between sessions;

i) assume that radio communication was unavailable; and

j) limit sessions to the interval (working day) 8 AM to 7 PM.

During the actual GPS survey, one operator was assigned to each receiver. Their responsibilities included: antenna setup (via a tripod and optical-plummet tribrach); antenna orientation (to magnetic north); receiver setup (site identification, sampling interval, session number, etc.); measurement of the antenna heights (at the start and end of each session); logging any technical or environmental problems (e.g., power outages, temporary obstructions, etc.); preparing or updating site locality sketches; instrument dismount and relocation; and the collection of meteorological data (wet and dry temperatures and pressure). Additionally, where a receiver was to remain at the same point for two, or more, consecutive sessions, the field operative was required to rotate the tribrach and re-set the antenna. This last action was an attempt at randomising the centring error and was strongly recommended in the Canadian "Guidelines and Specifications for GPS Surveys" [1992, p20].

The receivers were set to sample at 10 second intervals, using a mask angle of 10° (even though processing was to use a 15° mask angle). Each operator was then responsible for downloading their receiver at the end of each day. Irrespective of the receiver memory capability, the observations were downloaded each day as experience showed that certain technical problems resulted in the erasure of all stored data.

In 1995 GPS was used, in favour of extensive traversing, to survey 15 additional stations. It was decided (by others) that the way to minimise the data collection time while maintaining suitable accuracy was to use only the spatial distance component of the GPS baseline, which was reported to have a higher precision than the combination of ΔX, ΔY, ΔZ components (presumably due to unknown correlations). These observation sessions were collected via a 30 minute static mode. As this technique was significantly different from that of the main GPS network, and the accuracy expectations lower, it was designated the secondary network for this project.

In 1996, the numerous "secondary observations" required by the 1995 method, led to an attempt at using the pseudo-static (also called pseudo-kinematic) mode. Here three receivers were to cover the primary network using nominal 1¼ hour static sessions, while two receivers were scheduled to operate, simultaneously, in the pseudo-static mode. The 75 minute static session duration enabled each roving receiver to visit two stations per session. The pseudo-static session breakdown was as follows:

a) 10 minute at station A;
b) 10 minute relocation to station B (leaving tripod/tribrach at A);
c) 10 minute at station B;
d) 15 minute relocation to station A (leaving 2nd tripod/tribrach at B);
e) 10 minute at station A;
f) 10 minute relocation to station B;

g) 10 minute at station B;
h) 30 minute relocation to next pair of stations C and D.

The above schedule yielded a 35 minute gap in the data for stations A and B. It also required two sets of tripod and tribrach for each rover receiver as the antenna height had to remain the same for both occupations, while the 10 minute relocation time dictated that the two rover stations be close together. Coupled with the restrictions of only two vehicles and the poor portability of the Ashtech receivers, this was a very challenging schedule; unfortunately, the breakdown of one of the receivers reduced this challenge.

2.3.3 GPS Data Pre-processing

Pre-processing of the GPS data comprised three main stages: i) computing the baseline coordinate components (single baseline solutions); ii) internal solution verification; and iii) external solution verification (including a minimum constraint least squares adjustment). These three sections are outlined below.

2.3.3.1 Single Baseline Solutions

Once downloaded from the Ashtech receivers and sorted into separate session directories, the raw GPS data (satellite observation binary files, broadcast ephemeris binary files, and site ASCII files) were "backed-up" on $3^1/_2$" floppy disks. Some editing was generally required on the raw data files in preparation for baseline processing, most common of which was the merging of "dummy sessions" created as a result of power outages.

Ashtech's post processing software GPPS™ (and later PRISM™) was used for all (including trivial) single-baseline solutions. Antenna slant heights, from site log sheets, were entered; a mask angle of 15° was set; and default meteorological readings of 20°C, 50% relative humidity and 1010 mbar were invoked with the option to apply tropospheric corrections.

A "seeding" process, emanating from the "control" monument HT, was employed for all campaigns, where HT was held fixed at its predetermined WGS84 coordinates (ϕ: N 45° 47′ 06.62521" ; λ: W 65° 23′ 44.55982" ; h: 78.8208m). No rigorous guidelines were available for the seeding process (thus it was not a unique process). A record of the seeding procedure used was maintained, together with solution comments and any remedial actions undertaken.

2.3.3.2 Internal Verification

Baseline solutions emanating from the GPPS™ software were checked for consistency and reliability via an examination of "quality indicators" within the solution files. The most important quality indicator of the "fixed" double difference solution was the "ratio" (of the "best" solution to the "next best" solution). This "ratio" quickly identified the overall success level attained in resolving phase ambiguities.

A more specific analysis, was the examination of the estimated ambiguities from the "float" double difference solutions, which should align closely with integer values. Jivall [1992], based on experiences obtained from the provision of geodetic control in Sweden using the Ashtech GPPS™ software, suggested that for short baselines (0 to

10 km) the ambiguities had to be resolved to within 0.20 cycles and a "ratio" in excess of 3 be attained before accepting a baseline solution.

Another "quality indicator" of the ambiguity resolution problem was that of the coordinate differences estimated by the "float" and "fixed" double difference solutions. Jivall [1992] recommended a maximum deviation, in any component, of 5 cm for short baselines; however, the data collected in Sussex indicated that deviations in excess of 2 cm deserved attention.

The last major baseline solution "quality indicator" was the root-mean-square (rms) value of the fixed double difference residuals. Ashtech's GPPS™ processing software provided a graphic plot of these residuals as cycles against epochs. This plot could show any undetected cycle slips as well as the possible presence of systematic errors [Ashtech Inc., 1993].

2.3.3.2 External Verification

This stage of the data verification generally involved the comparison of baseline solutions from different sessions. However, the first verification procedure was a "session specific" check†, based on the expectation that the loop closure of baselines from the same session should be zero. These loop closures were investigated using, separately, the "float" and "fixed" double difference solutions.

---

† As at least one of the baselines would be dependent, this could have been classed as an internal check; however, as all baselines were processed separately and therefore had independent estimates of the ambiguities, (some even had different reference SV's) it was classified as an external verification.

The logical extension of this test, was to use baselines from independent sessions. Table 2.2 shows a sample of the 1994 triangle loop misclosures, for which each side represents a different observation session. Naturally, baselines common to more than one session were also checked. Guidelines for the acceptance of the loop, and common-baseline, misclosures were obtained from Table 5 of "Geometric Geodetic Accuracy Standards and Specifications for Using GPS Relative Positioning Techniques", [Hull, 1989]. The selection of loops, generally, was such that all baselines were part of at least one loop. Additional loops were then generated when attempting to isolate a baseline responsible for a poor misclosure. Poor quality baselines were generally excluded, without loss of "degrees of freedom", during selection of the non-trivial baselines.

The loop misclosures were essential in detecting the use of "incorrect antenna heights" in the baseline solution. They also simplified the identification of outliers in the minimum constraints least squares adjustment of the GPS baselines, which was the last data verification procedure prior to the final, combined adjustment.

Table 2.2 PCS 1994 GPS Loop Misclosures (Linecomp ver 5.0.00)

Day	Ses	Stn1	Stn2	Length m	Δφ "	Δλ "	ΔH m	εΔφ mm	εΔλ mm	εΔH mm
					TRIANGLE MISCLOSURES					
179	4	A1	A10	1611.7	-46.9345	-32.6443	11.490			
179	1	A10	24740		-3.3428	33.9587	9.292			
181	4	A1	24740	1552.7	-50.2778	1.3141	20.784	15.4	6.5	-2.0
			Total	**3164.4**			**ppm**	**4.9**	**2.0**	
179	2	A1	B6	1253.6	-7.1612	-57.1031	-0.069			
179	4	B6	A10	1337.0	-39.7732	24.4591	11.564			
179	1	A1	A10	1611.7	-46.9347	-32.6448	11.472	9.3	17.3	23.0
			Total	**4202.3**			**ppm**	**2.2**	**4.1**	
179	4	B6	A1	1253.6	7.1612	57.1034	0.074			
179	1	A1	A10	1611.7	-46.9347	-32.6448	11.472			
179	3	B6	A10	1337.0	-39.7734	24.4591	11.568	-3.1	-10.8	-22.0
			Total	**4202.3**			**ppm**	**-0.7**	**-2.6**	

Continued on Next Page.

Table 2.2 PCS 1994 GPS Loop Misclosures (Linecomp ver 5.0.00)

Day	Ses	Stn1	Stn2	Length m	Δφ "	Δλ "	ΔH m	εΔφ mm	εΔλ mm	εΔH mm
179	2	ML4	B6	1062.2	-30.4207	-22.9586	-6.632			
179	4	B6	A1	1253.6	7.1612	57.1034	0.074			
181	4	ML4	A1	1029.6	-23.2588	34.1446	-6.561	-21.6	4.3	3.0
			Total	**3345.4**			**ppm**	**-6.5**	**1.3**	
180	1	ML4	9637	1447.1	-12.9362	-64.3678	18.275			
182	2	9637	B6	1045.3	-17.4846	41.4099	-24.913			
179	2	ML4	B6	1062.2	-30.4207	-22.9586	-6.632	-3.1	15.1	-6.0
			Total	**3554.6**			**ppm**	**-0.9**	**4.3**	
182	2	C6	B6	1020.6	-1.1047	47.1894	-23.677			
179	4	B6	A10	1337.0	-39.7732	24.4591	11.564			
179	3	C6	A10	1997.7	-40.8780	71.6478	-12.117	3.1	15.1	4.0
			Total	**4355.3**			**ppm**	**0.7**	**3.5**	
180	6	22798	D7	1371.1	-16.9626	-58.6487	7.269			
180	2	D7	9637	559.9	-11.7338	19.7546	7.966			
182	3	22798	9637	1221.2	-28.6971	-38.8939	15.246	21.6	-4.3	-11.0
			Total	**3152.2**			**ppm**	**6.9**	**-1.4**	
180	2	D7	9637	559.9	-11.7338	19.7546	7.966			
182	2	9637	C6	520.9	-16.3799	-5.7795	-1.238			
180	4	D7	C6	919.0	-28.1137	13.9757	6.732	0.0	-13.0	-4.0
			Total	**1999.8**			**ppm**	**0.0**	**-6.5**	
181	5	E1	E5	691.2	-21.6154	-8.3252	8.358			
180	3	E5	D7	1003.0	-21.0706	35.3359	0.941			
180	6	E1	D7	1441.3	-42.6859	27.0106	9.294	-3.1	2.2	5.0
			Total	**3135.5**			**ppm**	**-1.0**	**0.7**	
181	2	HT	E1	1006.9	-10.0519	-44.2871	-49.058			
181	5	E1	G3	1166.4	1.5996	-53.9454	0.926			
181	1	HT	G3	2138.5	-8.4520	-98.2335	-48.140	-9.3	21.6	8.0
			Total	**4311.8**			**ppm**	**-2.1**	**5.0**	
182	1	E5	G7	1145.0	3.8718	-52.7554	-5.562			
181	6	G7	F2	777.2	-12.7394	31.0279	-0.298			
180	3	E5	F2	543.4	-8.8679	-21.7269	-5.868	9.3	-13.0	8.0
			Total	**2466.6**			**ppm**	**3.8**	**-5.3**	
182	1	E5	G7	1145.0	3.8718	-52.7554	-5.562			
181	6	G7	G3	616.8	19.3429	7.1343	-1.870			
181	5	E5	G3	1218.6	23.2150	-45.6202	-7.432	-9.3	-19.5	0.0
			Total	**2980.4**			**ppm**	**-3.1**	**-6.5**	
181	6	G7	G3	616.8	19.3429	7.1343	-1.870			
181	1	G3	ML23	2108.4	8.8892	-96.7693	25.804			
182	1	G7	ML23	2123.6	28.2322	-89.6348	23.928	-3.1	-4.3	6.0
			Total	**4848.8**			**ppm**	**-0.6**	**-0.9**	
181	5	E5	G3	1218.6	23.2150	-45.6202	-7.432			
181	1	G3	ML23	2108.4	8.8892	-96.7693	25.804			
182	1	E5	ML23	3231.8	32.1040	-142.3902	18.364	6.2	15.1	8.0
			Total	**6558.8**			**ppm**	**0.9**	**2.3**	

Chapter 3

The Sussex Datum

The horizontal datum in Sussex was selected to coincide with the WGS84 (World Geodetic System 1984) datum of the GPS. Two primary reasons dictated this selection. Firstly, the satellite ephemerides were broadcast in the WGS84 datum, hence by selecting the project datum to coincide with the WGS84 datum no further baseline processing was required. Secondly, the baseline solutions each contained information as to the datum scale and orientation (i.e., three rotations about the geocentric coordinate system). Consequently, only three datum defects had to be accounted for, compared to six datum defects (3 rotations and 3 translations) associated with the traverse data.

The three datum defects (3 translations) remaining in the GPS data were accounted for through constraining the coordinates of station HT to its 1990 estimated WGS84 coordinates. Station HT was considered the most suitable "fixed" point as it was located on a small hill just outside the suspected influence area of the underground

workings. However, due to the limited capabilities of the GPS at that time and the findings that a bias in the initial coordinates of the fixed point caused systematic error in the baseline solutions [Santerre, 1989], it was decided to check the previously determined WGS84 coordinates of station HT using the dual-frequency Ashtech Z-XII receivers and the Active Control System of the IGS.

This chapter summarises the re-calculation of the WGS84(G730) coordinates of station HT, including a description of the WGS84 and WGS84(G730) datums. Also presented, is the realisation of the "orthometric height" system used for the levelling campaigns and the reconciliation of the two (GPS and levelling) height systems via modelling of local "geoidal undulations".

3.1 WGS84 Datum Definition

The World Geodetic System 1984 was defined by the U.S. Department of Defence (DoD) as an Earth-centred, Earth-fixed (ECEF), Conventional Terrestrial (CT) system [Defense Mapping Agency, 1993]. The WGS84 datum was initially realised through a global network of more than 1500 Transit Doppler stations with an absolute positioning accuracy of $\pm$ 2 m [Decker, 1986]. Since its conception, the WGS84 has been refined, in terms of both its definition and realisation. In 1994, the latest realisation was undertaken, based on 10 DoD, and 22 IGS (International GPS Service for Geodynamics), GPS tracking stations

and an updated geocentric constant of gravitation (GM) value [Swift, 1994]. Eight of the above IGS stations were constrained by their ITRF91 (International Terrestrial Reference Frame 1991) coordinates, thus aligning the DoD (responsible for broadcast GPS data) and IGS (responsible for scientific GPS data) systems. The new GPS-realised datum, designated WGS84(G730) and accurate to $\pm$ 10 cm, was implemented by the U.S. Defense Mapping Agency (DMA) in the first full week of 1994 (GPS week 730) [Swift, 1994]. Ephemerides broadcast by the GPS satellites have benefited from the refined WGS84(G730) coordinates of the satellite tracking stations since 29th June, 1994 [Malys and Slater, 1994].

The reference ellipsoid adopted by the DMA for the WGS84 horizontal datum was defined via four parameters: the semi-major axis, a = 6 378 137 m; the normalised second degree zonal harmonic coefficient of the gravitational potential, C^{*}_{20} = -484.16685 x 10^{-6}; the angular velocity of the earth, ω = 7 292 115 x 10^{-11} rad.s^{-1}; and the earth's gravitational constant (mass of atmosphere included), GM = 3 986 005 x 10^{8} m^{3}s^{-2} [Defense Mapping Agency, 1993]. The semi-minor axis, b = 6 356 752.314 2 m, flattening, f = 1/298.257 223 563, and the first eccentricity, e = 0.081 819 190 842 6, were all subsequently derived from the defining parameters [Defense Mapping Agency, 1993]. The new WGS84(G730) datum varies only in a revised gravitational constant of GM = 3 986 004.418 x 10^{8} m^{3}s^{-2} [Malys and Slater, 1994].

3.2 WGS84(G730) Coordinates of Station HT

In 1990, the position of station HT, near Sussex, was established with respect to the outdated NBGIC published grid coordinates (on the ATS77 datum). By 1995, however, dual frequency GPS receivers were available, and the IGS Active Control Point (ACP) system was fully operational. It was, therefore, possible to determine the coordinates of station HT with respect to the ACPs Algonquin, St. John's and Westford in the ITRF coordinate systems. These values were then transformed into the WGS84(G730) datum via the transformation parameters given by Malys and Slater [1994].

3.2.1 Data Collection and Preparation

As the establishment of absolute coordinates for station HT was not a separate field exercise, the data collected during the 1995 and 1996 GPS observation campaigns had to be used. This was a problem, as the accuracy of these very long (640 to 990 km) baseline solutions depended, to a large extent, on the length of the observation session. Each individual session in Sussex was of a nominal 75 minute duration, with a 15 minute gap between sessions. Merging three consecutive sessions could then span about 4 ½ hours; however, in 1995, the tripod was reset at the start of each session which resulted in different antenna heights, thus precluding the above merging scheme. Nevertheless, it was

decided to process the individual session data, which provided additional redundancy and a measure of precision. This same procedure was also used for the 1996 GPS data, for which an option to merge three consecutive sessions into one was also tested. In all, ten dual frequency sessions were available, five at ML23 (1995 only) and five at HT (two in 1995 and three in 1996), of which two sessions in 1995 were collected simultaneously at ML23 and HT.

Rinex data for GPS days 190 and 191 of 1995, were obtained from the IGS Central Bureau for sites Algonquin (ALGO), Westford (WES2) and St. John's (STJO). In 1996, on GPS day 213, the receiver at St. John's was down, so that only data from ALGO and WES2 were obtained. Precise orbits were also obtained from the IGS Central Bureau for the above days, with the 1995 orbits presented in the ITRF93 reference frame and the 1996 orbits presented in the ITRF94 reference frame. The coordinates and station velocities of the three ACPs were also obtained from the IGS Central Bureau in both the ITRF93 (epoch 1993.0) and the ITRF94 (epoch 1993.0) reference frames.

As Prism™ was to be used to process the baselines and due to incompatibilities between the IGS and Sussex data, all of the data had to be prepared so as to conform and match the Prism™ input formats. Thus, the dual frequency data collected at Sussex stations HT (1995 and 1996) and ML23 (1995 only) were thinned to match the 30 second sampling rate of the IGS ACP receivers. Meanwhile, the IGS Rinex data was split into nominal 75 minute segments, corresponding to the Sussex session times and converted, via Prism™, into Ashtech binary data files. The precise orbit data was also thinned and converted from the IGS SP3 format to the Ashtech binary format. Finally, the published

station velocities were used to transform the given ITRF coordinates from their published epochs (both given at 1993.0) to the observation epochs (1995.518823 and 1996.578371).

Table 3.1 Residuals from the Prism™ ACP to WES2 baseline solutions.

YEAR	DAY	START	SPAN	ACP	δφ	δλ	δh
	[GPS]	[hh:mm]	[hh:mm]			[metres]	
1995	190	14:50	1:10	ALGO	-0.087	-0.103	-0.181
		16:25	1:19		-0.010	-0.011	-0.066
		18:05	1:15		-0.038	-0.041	-0.089
1995	191	11:17	1:23	ALGO	0.033	0.054	0.153
		14:55	1:15		-0.017	-0.018	0.177
		13:05	1:15		-0.009	0.043	0.156
1996	213	11:07	1:14	ALGO	0.004	0.087	0.170
		12:31	1:36		-0.066	-0.007	**0.221**
		14:28	1:33		-0.101	-0.010	**0.392**
1995	190	14:50	1:10	STJO	-0.009	0.096	0.010
		16:25	1:19		-0.141	0.105	-0.088
		18:05	1:15		0.025	0.103	0.005
1995	191	11:17	1:23	STJO	-0.074	**-0.630**	-0.195
		14:55	1:15		-0.037	0.086	0.000
		13:05	1:15		-0.047	**0.317**	-0.175
				AVG	**-0.038**	**0.005**	**0.033**
				RMS	**0.060**	**0.193**	**0.170**

3.2.2 Processing the IGS Rinex data with precise orbits.

Individual baseline solutions were obtained via Ashtech's Prism™ GPS software, using their ionosphere free L1C algorithm (which made no attempt at fixing the carrier phase

ambiguities) [Ashtech Inc., 1994]. All available baselines (i.e., 27) between the ACP and Sussex stations were processed, as well as the STJO-WES2 (1995), and the ALGO-WES2 (1995 and 1996) baselines. Table 3.1 shows the residuals achieved on the 643 km (ALGO) and 1572 km (STJO) long baselines to the ACP WES2 (considered known to approximately 2 cm).

The mean ITRF93(1995.518823) and ITRF94(1996.578371) coordinates of station HT, from the ACP solutions of 1995 and 1996, were separately transformed into the ITRF92(1988.0) coordinate system (see McCarthy, [1996]). A mean ITRF92(1988.0) coordinate was then determined and transformed into the WGS84(G730) coordinate system using the ITRF92 to WGS84(G730) transformation parameters given by Malys and Slater [1994, Table 6A]. The newly realised coordinates of station HT are presented in Table 3.2, together with the "old" values actually used in the Sussex project. Inconsistencies of approximately 11 m in longitude and 22 m in elevation were revealed, which will affect the single epoch baseline solutions. It remains to be seen, however, whether the effects remain constant from epoch to epoch, and thus cancel out in the monitoring of displacements, or not.

Table 3.2 Station HT absolute coordinates.

	OLD	NEW(WGS84)	DIFF. [m]
ϕ	45° 47' 06.6252"	45° 47' 06.6065"	0.58 m
λ	-65° 23' 44.5598"	-65° 23' 44.0326"	-11.39 m
h	78.82 m	57.06 m	21.76 m

3.3 Orthometric Height of Station HT

The absolute height of the levelling network was not as critical as that of the horizontal network. Consequently, the NBGIC published "orthometric" heights were used; however, the published "geoidal heights" referred to the ATS77 datum and so they were not used.

Selection of a stable point for the realisation of the vertical datum has fluctuated from year to year as the number of observing campaigns increased. Currently, station 10894 is used as it not only appears to be stable but also spans all of the observing campaigns. The orthometric height assigned to this station was 22.230 m. In 1994, reciprocal zenith angles were observed between station HT and stations E4 and E5. The elevation of station HT was thus determined from the 1994 levelling adjusted heights of stations E4 and E5 (station 10894 fixed) as 78.408 m.

3.4 Local Geoidal Undulations

The different height systems used by the GPS (ellipsoidal, h) and the levelling systems (orthometric, H) are reconciled through knowledge of the geoidal undulations. Such knowledge is now available from various agencies in the form of global, or regional, geoidal models, for which decimetre level relative accuracies (over 100 to 1000 km) have been reported (see, for example, Dodson [1995], Sideris [1993], and Forsberg and

Madsen [1990]). In the case of small networks (<10 km), local corrections to a regional, or global, geoidal model can be estimated using the differences between GPS and levelled heights. Simple interpolation schemes would then be used to obtain local "geoidal undulations" at the required stations (for example, Fiedler [1992]).

Due to an error in processing the GPS baselines with "orthometric" heights, use could not be made of the OSU89 (Ohio State University 1989) geoidal model (for example) for a first approximation of the local geoidal undulations. Consequently, the combination of GPS height differences, Δh_{GPS} , and levelled height differences, ΔH_{LEV} , were used to estimate local project corrections between the GPS and levelling height systems from the misclosures

$$\varepsilon_{\Delta N} = \Delta h_{GPS} - \Delta H_{LEV} \quad . \tag{3.1}$$

The differences between levelled and GPS heights on the same points will be practically invariant with respect to any slow deformation occurring at that point. Consequently, the differences between the levelling and GPS estimated heights, from 1992 to 1996, were used to model local (project) errors to the "geoidal" heights as linear functions of the grid northings and eastings (n_i , e_i) about a local origin (n_o , e_o) located at station A1, i.e.,

$$\varepsilon_{\Delta N} = a_0 + a_1 \cdot (n_i - n_o) + a_2 \cdot (e_i - e_o) \tag{3.2}$$

In this simplified model, all station height differences (GPS minus levelling) were considered to have equal weight. Initial results with all of the 1992 to 1996 campaigns revealed noticeable biases for some of the campaigns. Consequently, additional "offset" parameters were added to equation (3.2) to model the biases of the 1993 and 1994

campaigns (modelled via one parameter) and the 1996 campaign. Corrections for all monuments were then estimated from the final "local geoid" correction model, i.e.,

$$\varepsilon_{\Delta N} = a_0 + a_1 \cdot (n_i - n_o) + a_2 \cdot (e_i - e_o) + \delta N_{93.94} + \delta N_{96} \quad , \tag{3.3}$$

where the offsets $\delta N_{93.94}$ and δN_{96} were applicable to the designated campaigns, only. Table 3.3 lists the regression parameters resulting from the above modelling, for which an *a posteriori* standard deviation of 6 mm and a range in residuals of 26 mm, was obtained.

Table 3.3 Estimated parameters of the local geoid correction model.

Estimated Parameters.				
a_0	a_1	a_2	$\delta N_{93.94}$	δN_{96}
-0.162 m	-3.1062×10^{-6}	$+2.7113 \times 10^{-5}$	+0.007 m	-0.011 m
	-0.64 arcseconds	+5.59 arcseconds		

It should be noted that the a_0 parameter in equation (3.3) was to be interpreted as the (average from 1992 to 1996) geoidal height at station A1 and, consequently, should have been around -20.1 m (according to the OSU89 model). Instead, it is an average difference between the levelled and GPS height systems at station A1.

Chapter 4

Variance-Covariance Estimation

The outcome of any least squares adjustment is influenced by the *a priori* variance-covariance matrix assigned to the observations. The integration of several different observation types into an analysis of deformations, as well as the need to monitor deformations with magnitudes approaching the observation accuracies themselves, has produced a requirement for more detail as to the structure and magnitude of the *a priori* variance-covariance matrices of the observations. The stochastic models play several important roles in the processing and analysis of survey data, and consequently, in deformation monitoring. The most notable include:

1. the assessment of observation quality (i.e., the decision to include or exclude);
2. the assignment of relative weights (i.e., the influence of an observable on the estimated parameters); and, in the case of deformation analyses; and
3. the provision of a basis for the assessment of monument "stability".

The first, and last of these roles carry with them assumptions of normality, i.e., that the observation errors follow a normal distribution.

This chapter outlines the preparation of the *a priori* variance-covariances associated with the observables collected as part of the Sussex project, namely: spirit levelled height differences; traverse directions and distances; and GPS baseline components. Generally, one method has been adopted for each observable type; however, the results of several investigations into alternative methods are presented and briefly discussed.

The "tools" available for variance-covariance estimation on this project were limited to: a one-way Analysis of Variance (ANOVA) technique (see Hamilton, [1964] and Searle, [1971], for details); empirical models describing the standard error associated with different observables; and a limited version of the Iterated Minimum Norm Quadratic Estimation (IMINQE) algorithm [Chrzanowski et al., 1994] (Also, see Chen, [1983], and Chen et al., [1990a], for theoretical development and applications).

4.1 Levelled Height Differences

All levelling network adjustments were performed with weights assigned on the basis of the number of setups required for the measurement of a section height difference. This would have resulted in a cofactor matrix of the estimated heights from the least squares

adjustment, rather than the required covariance matrix. To correctly scale the cofactor matrix a standard error of 0.3 mm was assigned to a single setup. This approach is adequate for homogeneous data; however, with the levelling data collected via two crews (with two very different instruments), together with highly variable ground conditions, this presumption of homogeneity was not correct.

The more conventional approach to levelling, is to assign weights on the basis of the standard deviation per square root kilometre of section length. This may be more appropriate for road work but probably not for off-road levelling across rugged terrain. Nevertheless, both weighting schemes were applied to the 1994 levelling campaign (collected exclusively with the Leica NA3000 digital level, from which actual run lengths were available). A change in the estimated elevation of station ML23 (farthest from "fixed station" 10894) of only 0.1 mm was noticed, with standard deviations of 2.7 mm and 2.4 mm recorded for the "square root kilometre" and "number of setups" weighting schemes, respectively. Consequently, the "number of setups" scheme was not changed.

While using the "setups" weighting scheme, a conflict arose when "meaned" section height differences (from forward and backward runs) were mixed with "single" run height differences. Correct weighting required the meaned sections to have "half as many setups" as their single section counterparts, which led to confusion in the physical meaning of the "standard error per setup" reference variance. Considering also, the very low redundancy attained with meaned section height differences (only one to three loops available), it was decided to enter all single section observables into the adjustment. This approach, however, also had a major drawback, namely that of correlation between

forward and backward runs. Any systematic error between these runs tended to amplify the standard deviations of the final estimated elevations. Also, correlation between the observables was in violation of the "independent" observations presumption resulting from a diagonal *a priori* cofactor matrix. Consequently, an analysis of the 1994 levelling data was performed to assess this problem.

4.1.1 Forward versus Backward Section Correlation.

Investigation of the correlation between forward and backward runs was performed only on the 1994 data, with a view to establishing the severity of the problem. Firstly, a rough estimate of the correlation between the forward and backward section height differences was obtained via separate least squares adjustments using the "single", and the "meaned", section height differences. The weighting scheme used in both cases was $1/\sqrt{L}$, where L was the section run length in kilometres. The resulting *a posteriori* standard errors per square root kilometre were 1.39 mm and 0.32 mm for the single and meaned runs, respectively. Assuming that the variances of the forward ($\sigma^2_{\Delta H\_F}$) and backward ($\sigma^2_{\Delta H\_B}$) runs were equal (i.e., $\sigma^2_{\Delta H\_F} = \sigma^2_{\Delta H\_B} = \sigma^2_{\Delta Ho} = 1.39^2$ mm^2), and using the relationship,

$$\rho_{F.B} = 1 - 2\left(\frac{\sigma_{\Delta H}}{\sigma_{\Delta Ho}}\right)^2 , \qquad (4.1)$$

where $\sigma_{\Delta H}$ is the standard error of a meaned height difference (i.e., $\sigma_{\Delta H}$ = 0.32 mm), $\rho_{F.B}$ is the correlation between the forward and backward runs. Then, an estimated correlation of

+0.89 was obtained for the 1994 data. This indicated that the least squares estimated variance-covariance matrix of the adjusted elevations, derived from single run input data, was contaminated with systematic error.

A second estimate of the correlation was obtained using a technique outlined by Schmidt [1994]. This was a more detailed analysis in that it also estimated the correlation between the low- and high-scale section height differences of a single run. Noting that, for a double-run section, four observed height differences were collected:

ΔH_{FL}	from Forward run, Low-scale readings;
ΔH_{FH}	from Forward run, High-scale readings;
ΔH_{BL}	from Backward run, Low-scale readings;
ΔH_{BH}	from Backward run, High -scale readings,

from which three linear combinations, per section, were available for analysis, namely:

$$\overline{\Delta H} = \left(\Delta H_{FL} + \Delta H_{FH} - \Delta H_{BL} - \Delta H_{BH}\right)/4 \qquad (4.2a)$$

$$R = \left(\Delta H_{FL} + \Delta H_{FH} + \Delta H_{BL} + \Delta H_{BH}\right)/2 \qquad (4.2b)$$

$$D = \left(\Delta H_{FL} - \Delta H_{FH} + \Delta H_{BL} - \Delta H_{BH}\right)/2 \quad , \qquad (4.2c)$$

where the mean section height difference is given by $\overline{\Delta H}$. R then represents the discrepancy between the mean forward and mean backward height differences, and D the discrepancy between the mean low-scale and mean high-scale height differences. The R and D discrepancies above are biased according to section length, L, hence they were normalised, by dividing by $\sqrt{L}$, prior to analysis. Figure 4.1 shows the resulting histograms (double-runs with unacceptable misclosures, which were re-levelled, are excluded), from which the R discrepancies appear to have a non-central normal distribution (mean = +0.80,

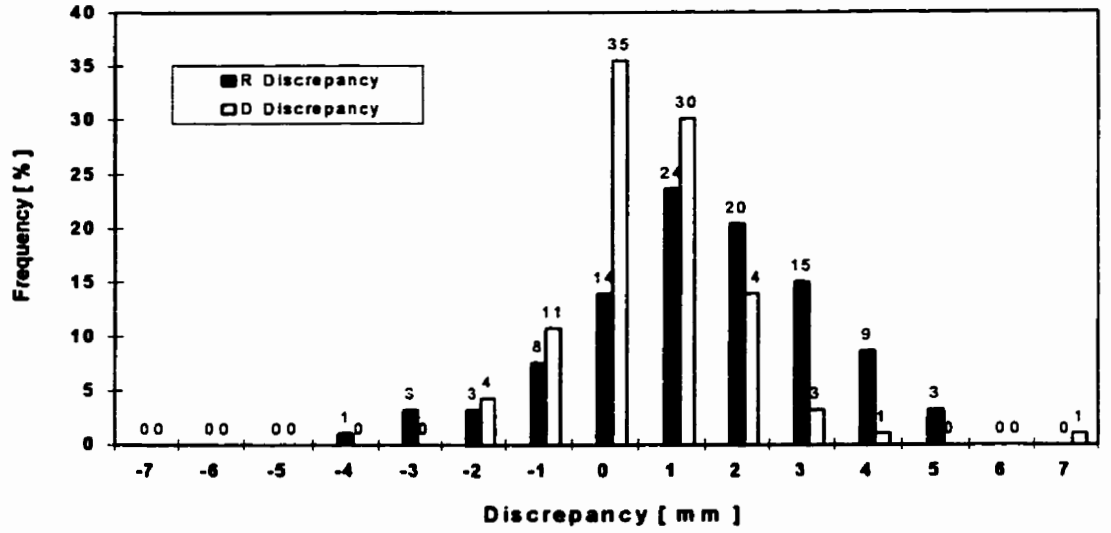

Figure 4.1 Histogram of Normalised Discrepancies from the 1994 Levelling Data.

skewness = -0.36 and kurtosis = +0.04) and the D discrepancies are non-normal (mean = +0.11, skewness = +1.01 and kurtosis = +4.06).

The application of Schmidt's algorithm to the 1994 Sussex levelling data resulted in a strong correlation, +0.84, between the forward and backward mean height differences, and almost no correlation, -0.02, between the low- and high-scale mean height differences. The very low correlation between the low- and high-scale observations could have been a result of the alternating observing sequence used, i.e., BS-FS-FS-BS, FS-BS-BS-FS (see Chapter 2). Evidence of the systematic error is presented by way of graphs of the levelling lines, showing the accumulative normalised discrepancies, R, in millimetres against the accumulative line length in kilometres (see Figure 4.2). It should be noted, however, that

none of the levelling lines analysed were observed from end-to-end, but rather, as disjointed sets of three to four consecutive sections, i.e., no chronological order is implied.

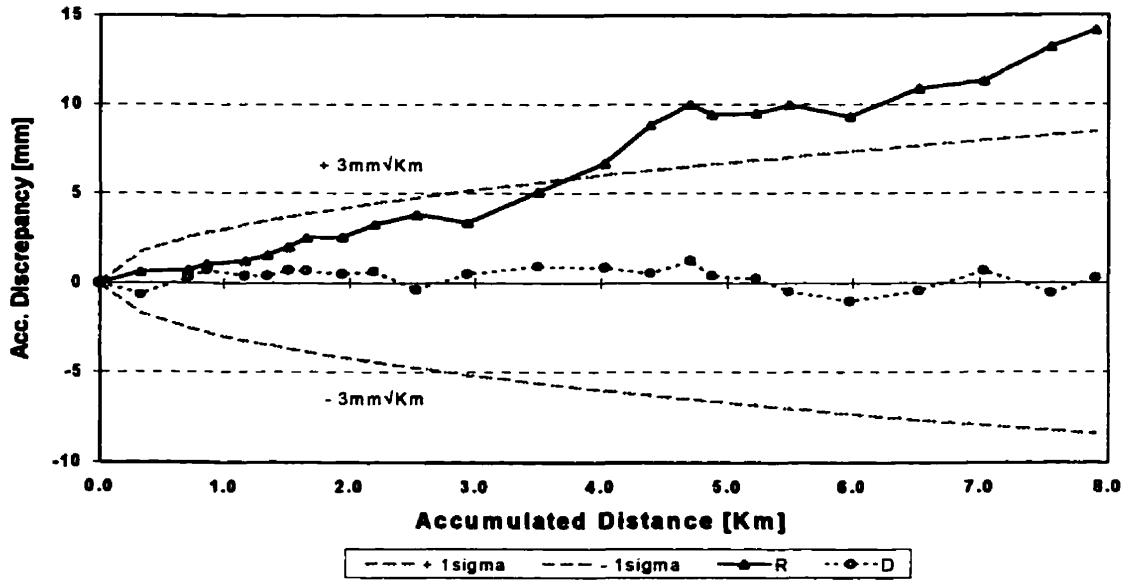

Figure 4.2 PCS 1994 Accumulated normalised discrepancies along the Trans-Canada Highway.

Having established that correlation was present, an evaluation of the extent of the correlation, i.e., whether it was common to all sections, or just specific sections, was required. This final analysis was performed using the R discrepancies of equation (4.2b) and a one-way ANOVA (see Wassef [1987], Ebong [1985] and Chiarini and Pieri [1971] for examples of the use of the one-way Analysis of Variance (ANOVA) technique with levelling discrepancies).

The null hypothesis, that all "class" discrepancy means were equal was tested via the ratio of the "between-classes" mean square error to the "within-classes" mean square error, MS_b/MS_w, which has a Fisher distribution (see Hamilton [1964] for details). The

Table 4.1 Sussex 1994 Levelling Line Discrepancies .

NORMALISED [mm/√ km] R DISCREPANCIES BY LINE.								
	A	B	C	D	E	G	TCH	BR
	1.51	-2.07	0.08	1.79	1.23	-0.74	1.04	-0.16
	2.60	-3.42	0.40	2.14	0.36	-0.69	0.18	-1.23
	1.26	-1.05	2.07	1.40	2.36	-0.60	0.85	-2.34
	0.41	-2.82	3.69	0.79	3.53	-1.21	0.34	-0.17
	-1.65	-1.97	0.28	-0.03	1.32	2.93	0.75	2.37
	0.70	-3.12	1.43	1.68	3.01	2.77	1.11	2.64
	0.13			0.45	-3.38	0.91	1.39	1.83
	-4.20			-1.46	0.01	1.78	0.06	0.24
	0.33				-0.18		1.39	4.11
	0.00				-0.63		1.02	3.17
	1.16						-0.74	3.62
							2.29	3.84
							2.21	4.15
							3.57	4.03
							2.03	1.26
							-1.37	-0.08
							0.15	1.69
							0.91	0.00
							-0.91	
							2.09	
							0.57	
							2.65	
							1.59	
No.	**11**	**6**	**6**	**8**	**10**	**8**	**23**	**18**
Mean	**0.20**	**-2.41**	**1.33**	**0.85**	**0.76**	**0.64**	**1.01**	**1.61**
Variance	**3.26**	**0.77**	**1.93**	**1.41**	**4.06**	**2.83**	**1.40**	**4.06**

null hypothesis, that all "class" discrepancy variances were equal was tested via Bartlett's Test [Hamilton, 1964]. The ANOVA Tables, presented in Table 4.2, show the results of three different classifications, where the first two are according to the levelled lines (see

profiles of Figure 2.1) while the last was according to the section terrain type, i.e., paved or unpaved.

Table 4.2 ANOVA Tables of the 1994 Levelling Discrepancies (R).

Source	SS	DF	MS	RMS	F_Test
ANOVA with All Levelling Lines.					
Between-Lines	80.96	8	10.120	3.18 mm	$F = 3.90$
Within-Lines	215.67	83	2.599	1.61 mm	$F_{(0.05,\ 8,83)} = 2.05$
Total	296.64	91	3.260	1.81 mm	**Fail**
ANOVA without B- Line.					
Between-Lines	16.35	7	2.331	1.53 mm	$F = 0.86$
Within-Lines	211.82	78	2.716	1.65 mm	$F_{(0.05,\ 7,78)} = 2.13$
Total	228.16	85	2.684	1.64 mm	**Pass**
ANOVA of Paved and Unpaved Section Discrepancies.					
Between-Surfaces	53.35	1	53.348	7.30 mm	$F = 19.21$
Within-Surfaces	252.69	91	2.777	1.67 mm	$F_{(0.05,\ 1,91)} = 3.95$
Total	364.94	92	3.967	1.99 mm	**Fail**

The F-Test on the levelling line "class means" failed at a 95% confidence level, which indicated that not all line discrepancy means were equal. Inspection of Table 4.1 clearly indicated Line B was different (in both magnitude and sign). To test the homogeneity of the remaining lines, the ANOVA was re-computed without the B-line.

The F-Test now concluded that the null hypothesis of equal class means could not be rejected at a 95% confidence level. In both cases, however, the Bartlett test concluded that the homogeneity of variances could not be rejected at a 95% level of confidence. It is noted that the levelling line classification resulted in small sample sizes, which reduced the efficiency of the tests, particularly Bartlett's test.

Closer inspection of Table 4.1, and Figure 4.2, together with local knowledge of the area, indicated that the levelling line sections along paved roads tended to exhibit the more dominant trends (notably large, positive discrepancies). Consequently, the section discrepancies were re-classified according to their terrain surfaces. Initially this classification comprised three classes: pavement, gravel and grass, for which gravel and grass (with 20 and 16 degrees of freedom, respectively) were very similar. The final classification was then reduced to two classes: paved and unpaved, with 54 and 37 degrees of freedom, respectively. The results of the ANOVA (Table 4.2) concluded that the "paved" and "unpaved" discrepancy means were different, but that their variances could not be considered different (both conclusions taken at a 95% confidence level).

A visual inspection of the distribution of the two class residuals, against both absolute section height difference and section length, did not reveal any systematic effect attributable to either of these two factors. It was concluded, that the 1994 levelling data from paved sections suffered from significant systematic effects. The exact cause of this systematic error was not determined, nor was its presence in other campaigns established (although a preponderance of positive misclosure suggested its presence).

4.2 Traverse Data.

Due to problems encountered while using IMINQE with the traverse data, the traverse variances were estimated via the traditional empirical models, using manufacturers estimates where available. The empirical models and comments on the failure of the IMINQE to resolve direction and distance variances are presented below.

4.2.1 Direction Variances.

The conventional practice of estimating the *a priori* direction variances based on an empirical model of independent component error variances has been used on this project. The variance of a direction, σ_δ^2 , was determined from

$$\sigma_\delta^2 = \sigma_{\delta r}^2 + \sigma_{\delta p}^2 + \sigma_{\delta l}^2 + \sigma_{\delta c}^2 \quad , \tag{4.3}$$

where $\sigma_{\delta r}^2$, $\sigma_{\delta p}^2$, $\sigma_{\delta l}^2$ and $\sigma_{\delta c}^2$ are the variance components attributed to reading, pointing, levelling, and centring (instrument and target) errors, respectively.

The Kern E2 and Leica TC2002 instruments used in Sussex both employed electronic reading systems, with display resolutions of 0.1 mgon (0.3") and 0.1", respectively. The empirical evaluation of the reading (only) accuracy associated with electronic theodolites is not as extensive as for their optic-mechanical counterparts. Leica [1993b] claims a reading resolution of 0.03", although Wilkins [1989] reported that laboratory testing of the T2000 (predecessor to the TC2002) by Katowski and Salzmann

[1983] resulted in a reading resolution of 0.05 mgon (0.15"). Santala and Parm [1994] used a "multiangle collimator" to also obtain a reading accuracy of 0.05 mgon for the T2000. In this analysis, a value of 0.25" was used as the *a priori* standard error component (of the total direction error) due to reading, which appears to err on the pessimistic side.

The standard error component due to pointing is mostly characterised by an instrument's optical capabilities, i.e., its resolving power, but also includes the effects of target design, focusing errors, and refraction. The pointing error component is generally given as the range

$$\frac{30''}{M \cdot \sqrt{2 \cdot n}} \leq \sigma_{\delta p} \leq \frac{60''}{M \cdot \sqrt{2 \cdot n}} , \tag{4.4}$$

where M is the instrument magnification (32x and 30x for Kern E2 and Leica TC2002, respectively) and n is the number of arcs observed. Based on the bulk of observed directions having lengths between 100 m and 500 m, as well as the generally hostile (summer) observing conditions, the upper limit of this range was used on this project.

The standard error component due to a levelling error, ε_v, was practically negligible for two reasons. First, the dual-axis compensator used by both the Kern E2 and the Leica TC2002 (setting accuracy of 0.1") was set to automatically correct the horizontal directions for mislevellment error. Secondly, the contribution of this error is a function of the zenith angle, Z, to the target, i.e.,

$$\sigma_{\delta l} = \varepsilon_v \cdot \mathrm{Sin}\,\theta \cdot \mathrm{Cot}\,Z , \tag{4.5}$$

where θ is the horizontal angle between the telescope and mislevellment planes. Apart from the slightly elevated station HT all others lay fairly close to a flat surface, resulting in a Cot Z very close to zero.

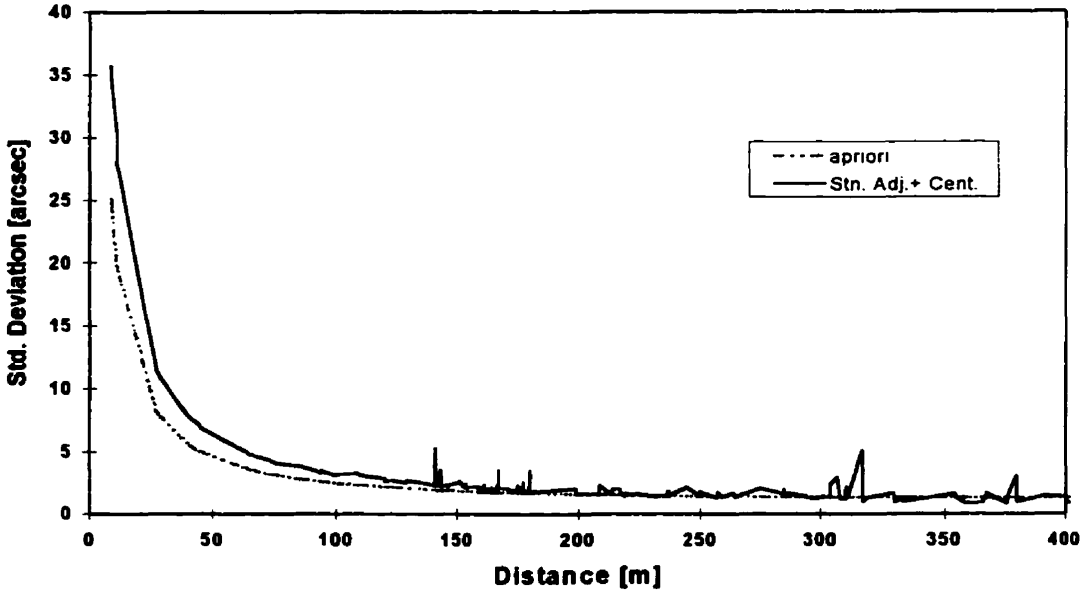

Figure 4.3 *a priori* and station adjustment estimated standard deviations of direction.

The most dominant of the standard error components were those of instrument and target centring errors. The contribution of these errors (in metres) to the direction error is

$$\sigma_{\delta c} = \frac{\rho''}{D_t} \cdot \sqrt{\sigma_{c\_i}^2 + \sigma_{c\_t}^2} \qquad (4.6)$$

for which $\rho'' = 206264.8$ and D_t is the distance (in metres) between the instrument and target (t). However, Blachut et al. [1979] show that the standard error component of centring on an angle β, obtained from two directions (to targets t1 and t2), would then be

$$\sigma_{\beta c} = \rho'' \cdot \sqrt{\frac{\sigma^2_{c\_t1}}{D^2_{t1}} + \frac{\sigma^2_{c\_t2}}{D^2_{t2}} + \frac{D^2_{t1\_t2} \cdot \sigma^2_{c\_i}}{D^2_{t1} \cdot D^2_{t1}}} \tag{4.7}$$

where D_{t1_t2} is the distance between the two targets.

Blachut et al. [1979] indicated that 0.5 mm per metre of tripod height can be expected for optical plumbing systems, which, given a setup height of 1.5 m, translates into a 0.75 mm centring error. While forced centring was employed wherever possible, not all monuments were occupied by the instrument, additionally each day of traversing required independent setups. Consequently, this error was included in the estimation of the directional standard errors.

As a comparison, the *a priori* estimated direction accuracies are plotted against sight lengths in Figure 4.3 together with the conventional "station adjustment" estimates [see Rüeger, 1994]. The same centring error contribution, at both instrument and target, used for the *a priori* estimates has been added to the station adjustment estimates. Spikes in the "station adjustment" estimates highlight potential problem directions.

4.2.2 Distance Variances

The general form of an observed EDM distance, S_{obs}, taken from Blachut et al. [1979], with some notational changes based on Rüeger [1990], is

$$S_{obs} = \frac{\Delta\Phi}{2\pi} \cdot \left(\frac{n_{ref}}{n}\right) + m\left(\frac{c_0}{2 \cdot f_{mod}} \cdot \frac{1}{n}\right) + Z_0 + \Delta S \tag{4.8}$$

where $\Delta\Phi$ is the measured phase lead in radians;

n, is the refractive index of air;

n_{ref} is an instrument reference refractive index (set by the manufacturer);

c_0 is the velocity of light in a vacuum (299 792 458 ms^{-1});

f_{mod} is the modulation frequency;

m is an integer number of full wavelengths over the measuring path;

Z_0 is a zero correction (calibrated by user); and

ΔS is a compound correction attributed to distance geometric reductions.

Blachut et al. [1979], show that the variance of the observed distance can be decomposed into three components, having the general form

$$\sigma_S^2 = a^2 + b^2 \cdot S^2 + \sigma_{\Delta S}^2 \quad , \tag{4.9}$$

for which

$$a^2 = \sigma_\Phi^2 + \sigma_{Zo}^2 \qquad , \qquad b^2 = \left(\frac{\sigma_c}{c_0}\right)^2 + \left(\frac{\sigma_f}{f_{mod}}\right)^2 + \left(\frac{\sigma_n}{n}\right)^2 \quad , \tag{4.10}$$

and $\sigma_{\Delta S}$ is the distance reduction error (formulated separately, as it is not directly part of the measurement). The sub-component errors comprise: σ_c, an uncertainty in the propagation of light in a vacuum; σ_f, the error in the modulation frequency; σ_n, the uncertainty associated with the refractive index of air (at the time of observation); σ_Φ, an error in the phase-difference determination; and σ_{Zo}, the "zero correction" calibration error.

Each of these errors is discussed in detail in Blachut et al. [1979], to which the interested reader is referred (see also Rüeger [1990] for an extensive coverage of EDMs). However, the components a and b are generally given by the manufacturer's as values in

millimetres and in parts-per-million (ppm), respectively. The "distance reduction error" is dependent on the geometric reductions performed and thus the responsibility of the user to determine. Similarly, the "zero correction" should be calibrated by the user, from which an estimate of its error should be made.

4.2.3 IMINQE

It was hoped that the shortcomings associated with the empirical model variance estimates could be overcome through implementation of the IMINQE algorithm. The observation equations of existing software [Chrzanowski et al., 1994], were formulated in a local horizon coordinate system, having its origin at the projection of the network centroid down onto the ellipsoid. This required that the "spatial distances" (for three-dimensional adjustments) had to be separately reduced to the ellipsoid, and that a two-dimensional network adjustment be performed for quality assurance. Consequently, only the 1993 and 1994 traverse data were reprocessed for the IMINQE variance-covariance analysis.

The IMINQE error structure models were [Chrzanowski et al., 1994],

$$\sigma_S^2 = a^2 \cdot \begin{pmatrix} 1 & \cdots & 0 \\ \vdots & \ddots & \vdots \\ 0 & \cdots & 1 \end{pmatrix} + b^2 \cdot \begin{pmatrix} S_1^2 & \cdots & 0 \\ \vdots & \ddots & \vdots \\ 0 & \cdots & S_k^2 \end{pmatrix} \equiv \theta_1 \cdot T_1 + \theta_2 \cdot T_2 \quad , \tag{4.11}$$

for the k distances measured with EDMs, and

$$\sigma_\delta^2 = a^2 \cdot \begin{pmatrix} 1 & \cdots & 0 \\ \vdots & \ddots & \vdots \\ 0 & \cdots & 1 \end{pmatrix} \equiv \theta_3 \cdot T_3 \quad , \tag{4.12}$$

for the observed directions.

Despite repeated attempts, the use of estimated coordinates from a successful horizontal least squares adjustment (of the same data set), the removal of outliers and the use of appropriate *a priori* estimates for the variance components (recommendations of Caissy, [1994]), the distance and direction (both individually and combined) processing via IMINQE failed to converge. This was most unfortunate as IMINQE was to be used, not only to corroborate the distance and direction variances, but also as the basis upon which to integrate the traverse and GPS stochastic models into a combined least squares adjustment.

Speculation on the above failure focused on data inconsistency and poor network configuration. Also, the direction error structure model used by IMINQE (see equation (4.12)) did not permit distance dependency. A few very short sightings (<10m) were removed from the data set, but this did not resolve the IMINQE divergence.

4.3 GPS Baselines.

As described in Chapter 2, the primary GPS baselines were processed using Ashtech's L1 solution, i.e., single frequency static double differences (see Ashtech Inc., [1992], [1993], and [1994]). Part of their solution was a correlation matrix and standard deviations for the ΔX, ΔY and ΔZ baseline components. These "Ashtech estimates" were used throughout

this project for *a priori* estimation of the GPS variances-covariances. Where the "GPS only" least squares adjustment failed the χ^2 Test on the variance factor on the "too optimistic" side (i.e., *a posteriori* variance factor greater than one), and all "blunders" had been resolved, then the *a posteriori* variance factor was used to scale the "Ashtech" covariances in preparation for the final combined (traverse and GPS) adjustment. This action was taken under the assumption that the Ashtech "error structure" was correct but that its magnitude was not. As an independent check, the GPS observables were submitted to the IMINQE algorithm. Results of the two approaches are briefly discussed below.

4.3.1 Ashtech Estimated Covariances.

While the algorithm behind Ashtech's LINECOMP (versions 4.5 and 5.0) solution differences [Ashtech Inc., (1992) and Ashtech Inc., (1994)] was not known, the magnitudes of the baseline component standard deviations appeared to be reasonable and were therefore used in the first "quality control" runs (also based on the experiences of Walford [1995]). This appearance was later justified by the acceptance of the χ^2 Tests on the *a posteriori* variance factors resulting from the "GPS only" adjustments (see Table 4.3, for the *a posteriori* variance factors from 1992 to 1996, inclusive). The 1992 χ^2 Test on the variance factor failed due to over-optimistic *a priori* estimates, while epochs 1993 to 1995 all passed, and 1996 also failed, but this time due to over-pessimistic estimates.

Table 4.3 Results of the "GPS only" three-dimensional network adjustments.

	1992	1993	1994	1995	1996
Variance Factor	1.5507	1.0094	0.9485	0.7371	0.6170
Degrees Of Freedom	54	33	42	108	66
χ^2 Test on V. F.	Fail	Pass	Pass	Pass	Fail

4.3.2 IMINQE Covariances.

An independent analysis of the GPS covariances was conducted using IMINQE. The error structure model used by the IMINQE algorithm was [Chrzanowski, et al., 1994]

$$\begin{pmatrix}\sigma^2_{\Delta\varphi}\\ \sigma^2_{\Delta\lambda}\\ \sigma^2_{\Delta h}\end{pmatrix} = a^2_{\Delta\varphi}\cdot\begin{pmatrix}1&0&0\\0&0&0\\0&0&0\end{pmatrix} + b^2_{\Delta\varphi}\cdot\begin{pmatrix}S^2&0&0\\0&0&0\\0&0&0\end{pmatrix} + a^2_{\Delta\lambda}\cdot\begin{pmatrix}0&0&0\\0&1&0\\0&0&0\end{pmatrix} + b^2_{\Delta\lambda}\cdot\begin{pmatrix}0&0&0\\0&S^2&0\\0&0&0\end{pmatrix} + \cdots$$
$$+ \rho_{\Delta\varphi\Delta\lambda}\cdot\begin{pmatrix}0&\beta_{\Delta\varphi\Delta\lambda}&0\\ \beta_{\Delta\lambda\Delta\varphi}&0&0\\0&0&0\end{pmatrix} + \cdots + \rho_{\Delta\lambda\Delta h}\cdot\begin{pmatrix}0&0&0\\0&0&\beta_{\Delta\lambda\Delta h}\\0&\beta_{\Delta h\Delta\lambda}&0\end{pmatrix} \qquad (4.13)$$

where S was the baseline length, the off-diagonal elements were calculated as,

$$\beta_{\Delta\varphi\Delta\lambda} = \sqrt{a^2_{\Delta\varphi} + b^2_{\Delta\varphi}\cdot S^2}\cdot\sqrt{a^2_{\Delta\lambda} + b^2_{\Delta\lambda}\cdot S^2}\quad ,\ \text{etc.} \qquad (4.14)$$

and the final covariance matrix was then obtained from,

$$\begin{pmatrix}\sigma^2_{\Delta\varphi}&\sigma_{\Delta\varphi\Delta\lambda}&\sigma_{\Delta\varphi\Delta h}\\ \sigma_{\Delta\lambda\Delta\varphi}&\sigma^2_{\Delta\lambda}&\sigma_{\Delta\lambda\Delta h}\\ \sigma_{\Delta h\Delta\varphi}&\sigma_{\Delta h\Delta\lambda}&\sigma^2_{\Delta h}\end{pmatrix} = \begin{pmatrix}a^2_{\Delta\varphi}+b^2_{\Delta\varphi}S^2&\rho_{\Delta\varphi\Delta\lambda}\cdot\beta_{\Delta\varphi\Delta\lambda}&\rho_{\Delta\varphi\Delta h}\cdot\beta_{\Delta\varphi\Delta h}\\ \rho_{\Delta\lambda\Delta\varphi}\cdot\beta_{\Delta\lambda\Delta\varphi}&a^2_{\Delta\lambda}+b^2_{\Delta\lambda}S^2&\rho_{\Delta\lambda\Delta h}\cdot\beta_{\Delta\lambda\Delta h}\\ \rho_{\Delta h\Delta\varphi}\cdot\beta_{\Delta h\Delta\varphi}&\rho_{\Delta h\Delta\lambda}\cdot\beta_{\Delta h\Delta\lambda}&a^2_{\Delta h}+b^2_{\Delta h}S^2\end{pmatrix} . \qquad (4.15)$$

Conversion from Cartesian to curvilinear coordinate components was performed by the IMINQE software prior to the above error modelling [Chrzanowski, et al., 1994].

In all, up to nine variance components could be accounted for; however, not all of them were appropriate. A final set of estimated components was obtained by starting with all nine and sequentially removing the most insignificant (see Chrzanowski et al. [1994]), until only significant † (at 5% or less) components remained. The "significant" components were then used to formulate the *a priori* GPS baseline variance-covariance matrices.

4.3.3 Comments on Ashtech and IMINQE Covariances.

In order to make a comparison between the Ashtech and IMINQE covariances, an "average covariance matrix" was computed from all of the Ashtech correlation matrices of the non-trivial primary GPS baseline solutions. Similarly, "average standard deviations" for the ΔX, ΔY and ΔZ baseline components were computed. The "average covariances" from each campaign were in a Cartesian geocentric coordinate system, hence they were transformed into a local geodetic coordinate system with its origin at D7 (centrally located within the network).

For analysis purposes, the covariance matrices were decomposed into three parts: a scalar; a diagonal matrix of normalised standard deviations ($\sigma^{\bullet}_{\Delta\varphi}$, $\sigma^{\bullet}_{\Delta\lambda}$, $\sigma^{\bullet}_{\Delta h}$); and a

---

† The term "significance", in statistics, is synonymous with the phrase "significance level of a test" and refers to the probability of a Type I error. It is commonly designated as either, the probability α, or the percentage $100\alpha\%$. The term "confidence", is then either, $(1-\alpha)$, or $100(1-\alpha)\%$ [Hamilton, 1964].

correlation matrix, such that,

$$\begin{pmatrix} \sigma^2_{\Delta\varphi} & \sigma_{\Delta\varphi\Delta\lambda} & \sigma_{\Delta\varphi\Delta h} \\ \sigma_{\Delta\lambda\Delta\varphi} & \sigma^2_{\Delta\lambda} & \sigma_{\Delta\lambda\Delta h} \\ \sigma_{\Delta h\Delta\varphi} & \sigma_{\Delta h\Delta\lambda} & \sigma^2_{\Delta h} \end{pmatrix} = \gamma^2 \cdot \begin{pmatrix} \sigma^{\bullet}_{\Delta\varphi} & 0 & 0 \\ 0 & \sigma^{\bullet}_{\Delta\lambda} & 0 \\ 0 & 0 & \sigma^{\bullet}_{\Delta h} \end{pmatrix} \begin{pmatrix} 1 & \rho_{\Delta\varphi\Delta\lambda} & \rho_{\Delta\varphi\Delta h} \\ \rho_{\Delta\varphi\Delta\lambda} & 1 & \rho_{\Delta\lambda\Delta h} \\ \rho_{\Delta\varphi\Delta h} & \rho_{\Delta\lambda\Delta h} & 1 \end{pmatrix} \begin{pmatrix} \sigma^{\bullet}_{\Delta\varphi} & 0 & 0 \\ 0 & \sigma^{\bullet}_{\Delta\lambda} & 0 \\ 0 & 0 & \sigma^{\bullet}_{\Delta h} \end{pmatrix} \tag{4.16}$$

from which, for example,

$$\sigma^2_{\Delta\varphi} = \gamma^2 \cdot \left(\sigma^{\bullet}_{\Delta\varphi}\right)^2 \quad , \quad \text{and} \quad \sigma_{\Delta\varphi\Delta\lambda} = \gamma^2 \cdot \sigma^{\bullet}_{\Delta\varphi} \cdot \sigma^{\bullet}_{\Delta\lambda} \cdot \rho_{\Delta\varphi\Delta\lambda} \ . \tag{4.17}$$

A rough indicator of the magnitude of the various three-dimensional covariances is now represented by the scalar γ (converted to millimetres), while the relative contributions of the baseline component standard errors are represented by $\sigma^{\bullet}_{\Delta\varphi}$, $\sigma^{\bullet}_{\Delta\lambda}$, $\sigma^{\bullet}_{\Delta h}$. As usual, the correlation between the baseline components is represented by, $\rho_{\Delta\varphi\Delta\lambda}$, for example. The above elements, from both the Ashtech (type - A) and IMINQE (type - I) covariances, are presented in Table 4.4. Similarly, the standard deviations of the baseline components, in millimetres, are presented in Table 4.5.

The reader is reminded that the Ashtech covariances presented here are network averages, calculated for the sake of comparison, and were not those used with any particular baseline. One of the advantages of the Ashtech estimates were that they varied in accordance with the strength of the baseline solution, i.e., weakly resolved ambiguities in the L1 double difference solution were represented by larger variances and covariances. While IMINQE, due most probably to a limited variation in the magnitudes of the baseline components, resulted in the same covariance matrix for each baseline, insensitive to any

difficulties encountered in the baseline solution (e.g., power outages, obstructed satellite visibility, etc.).

Table 4.4 Structure of Ashtech and IMINQE Covariance Matrices.

(A = Ashtech, I = IMINQE, derived values)

Estimate	γ [mm]	$\sigma^{\bullet}_{\Delta\phi}$	$\sigma^{\bullet}_{\Delta\lambda}$	$\sigma^{\bullet}_{\Delta h}$	$\rho_{\Delta\phi}$	$\rho_{\Delta\lambda}$	$\rho_{\Delta h}$
1992 - A	10.5	0.43	0.30	0.85	0.03	0.13	-0.04
- I	***8.4***	***0.67***	***0.44***	***0.60***	***0.54***	***0.57***	
1993 - A	8.1	0.40	0.32	0.86	-0.01	-0.05	-0.07
- I	***6.5***	***0.38***	***0.44***	***0.81***	***0.58***		
1994 - A	8.4	0.41	0.32	0.85	0.01	-0.08	-0.02
- I	***7.3***	***0.55***	***0.33***	***0.76***			***-0.45***
1995 - A	13.3	0.40	0.27	0.87	0.09	-0.05	0.03
- I	***10.7***	***0.39***	***0.33***	***0.86***	***0.44***	***-0.53***	
1996 - A	11.3	0.47	0.31	0.83	-0.11	-0.07	0.09
- I	***8.7***	***0.42***	***0.36***	***0.83***	***0.35***		

With the exception of the 1992 height component (5.0 ppm) and the 1995 longitude component (2.4 mm and 1.7 ppm), the IMINQE variance components were all resolved as "constants", which resulted in the same *a priori* covariance matrix for each of the GPS baselines. The values shown in Table 4.4 for the 1992 height, and 1995 longitude components, were based on a 1.5 km long baseline, typical of the Sussex GPS networks.

Table 4.5 Ashtech and IMINQE Standard Deviations.

(A = Ashtech, I = IMINQE, derived values)

YEAR	Type	$\sigma_{\Delta\phi}$	$\sigma_{\Delta\lambda}$	$\sigma_{\Delta h}$
1992	- A	4.6 mm	3.2 mm	8.9 mm
	- *I*	*5.6* mm	*3.7* mm	*5.0* mm
1993	- A	3.2 mm	2.6 mm	7.0 mm
	- *I*	*2.5* mm	*2.9* mm	*5.3* mm
1994	- A	3.4 mm	2.7 mm	7.1 mm
	- *I*	*4.1* mm	*2.4* mm	*5.6* mm
1995	- A	5.3 mm	3.7 mm	11.7 mm
	- *I*	*4.1* mm	*3.6* mm	*9.2* mm
1996	- A	5.2 mm	3.5 mm	9.3 mm
	- *I*	*3.7* mm	*3.1* mm	*7.2* mm

Inspection of Table 4.4 shows that the Ashtech "average" estimates are very consistent in structure from year to year, despite quite different network geometries and observation numbers. Also, the Ashtech average covariances indicate zero correlation between the three baseline components in the local geodetic coordinate system. The IMINQE structure, on the other hand, shows a similar structure for the baseline component variances, but variable structure in the correlations. It does, however, consistently indicate minor correlation between the two horizontal components (causing a rotation of the absolute (point) error ellipses away from the typical North-South orientation resulting from $\sigma_{\Delta\varphi} > \sigma_{\Delta\lambda}$). Finally, the magnitudes of the IMINQE covariances (partially due to the correlations) are consistently smaller than the average Ashtech magnitudes (which, with the exception of 1992, produced variance factors less than unity).

Based on the above, there did not seem to be any advantage gained through the use of the IMINQE covariances in favour of the Ashtech estimates. Use of the Ashtech estimates enabled any subsequent least squares adjustments to stay "in tune" with the single baseline solution "ambiguity fixing" results. Thus, they provided the covariance "structure", but occasionally had to be "re-scaled" (e.g., by the GPS only minimum constraints *a posteriori* variance factor) if they caused the failure of the χ^2 Test.

4.4 Scaling of Heterogeneous Covariances.

Failure of the IMINQE algorithm to converge during the estimation of traverse covariance components, necessitated an alternative technique for "relatively scaling" the observation group covariances in the combined adjustment. The technique used was that of iterated least squares. Gruendig [1985] shows that, assuming gross errors have been removed in previous minimum constraint solutions, the reference variance may be estimated by a group (k) of observations (numbering n_k for the k^{th} group) as,

$$\hat{\sigma}^2_{ko} = \frac{\left(v_k^T \cdot P_k \cdot v_k\right)}{r_k} \quad , \qquad \text{for} \quad r_k = \sum_{j=1}^{n_K} r_j \quad , \tag{4.18}$$

where v_k , P_k are the vector of residuals and *a priori* weight matrix, respectively, for the k^{th} group of observations. The group redundancy is represented by the scalar r_k , which is the sum of the redundancy numbers, r_j , of the individual observations in group k. The j^{th}

redundancy number is, in turn, the j^{th} diagonal element of the product, $C_{\hat{v}\hat{v}} \cdot C_{\ell\ell}^{-1}$. If the group estimated reference variance, $\hat{\sigma}_{ko}^2$, differs from the global reference variance, $\hat{\sigma}_o^2$, then the respective observation weights are pre-multiplied by $\hat{\sigma}_{ko}^2/\hat{\sigma}_o^2$ and re-adjusted.

Unfortunately, the redundancy numbers are difficult to obtain as the covariance matrix of the estimated residuals, $C_{\hat{v}\hat{v}}$, is computationally expensive and was not available from GeoLab™ [BitWise Ideas Inc., 1993]. However, an estimated standard deviation of the j^{th} estimated residual, $\hat{\sigma}_{\hat{v}_j}$, was available, hence, for n_k observations in group k, the quantity

$$r_k = \sum_{j=1}^{n_k} \left(\frac{\hat{\sigma}_{\hat{v}_j}^2}{\sigma_{\ell_j}^2} \right) , \tag{4.19}$$

was computed as an approximate redundancy number, assuming mutually independent observations within the group [Snay, 1989]. An estimate of the reference variance could then be obtained from the k^{th} observation group as [Snay, 1989]

$$S_k^2 = \frac{1}{r_k} \cdot \sum_{j=1}^{n_k} \left(v_j^* \right)^2 \quad , \qquad \text{where} \qquad v_j^* = \frac{v_j}{\sigma_{\ell_j}} \quad , \tag{4.20}$$

(note that the residual is normalised via the *a priori* standard error of the observation, and not the more usual standard error of the residual). Snay [1989] points out that if the *a priori* variances of the k^{th} group observables differ from their true values by a common factor, then S_k^2 has been shown [Horn et al., 1975] to provide an "Almost Unbiased Estimate" of this factor.

As considerable effort had been put into the *a priori* group variances, particularly in terms of separate minimum constraints adjustments, it was expected that only relative group weights would be required to correctly scale the group variances in the combined adjustment. Consequently, a routine was written which would compute the approximate group redundancy numbers, equation (4.19), and estimated variance factors, S^2_k, from the GeoLab™ output data. These values were then used to re-scale the group (directions, distances by EDM type, primary GPS baselines, and secondary GPS observations) *a priori* variances for a subsequent adjustment, of which only one was ever needed. Results of this procedure, as applied to the 1992 to 1996, campaigns are reported in Chapter 5.

Chapter 5

Integrated, Single Epoch Adjustments

The classical approach to the adjustment of terrestrial networks has been to separate the observations for either a vertical (trigonometric- and spirit-levelling) or horizontal (angles, directions, azimuths and distances) adjustment. Horizontal observations were "reduced" to a reference ellipsoid or mapping plane, while vertical observations were "reduced" to a local horizontal plane or the geoid. This approach was used to simplify the mathematics and (manual) numerical processing. Additionally, the nature of the observations tended to support this approach as the correlation between horizontal and vertical dimensions was minimal, leading to the equivalence of the separate and combined adjustment approaches.

The introduction of three-dimensional extraterrestrial observations, most notably GPS, together with an international move towards global datums (and the subsequent re-adjustment of national networks thereon), has conferred greater recognition on the three-dimensional least squares adjustment.

A three-dimensional adjustment of terrestrial observations has three major

advantages over the classical separate adjustment approach. Firstly, no geometrical reductions to the ellipsoid are required [Vincenty, 1980; Vaníček and Krakiwsky, 1986], secondly, "It is ... theoretically more accurate because it does not impose any restrictions on the lengths of the lines nor on the extent of the network" [Vincenty, 1980], and finally, the concept is more " ... perspicous, particularly when applied in combination with three-dimensional observations" [Vincenty, 1982].

A drawback of the three-dimensional "horizontal" adjustment is in the case of weakly determined heights, and how to deal with them in the adjustment. Vincenty [1980] presents several options for a "height-controlled three-dimensional adjustment" in either the X,Y,Z Conventional Terrestrial (C.T.) coordinate system or the u,v,w Local Astronomic (L.A.) system. Additionally, Bowring [1980], Vincenty [1982] and Steeves [1984] present the three-dimensional "height-controlled" adjustment in the x, y, z local geodetic coordinate system. This latter method appears to be that used by the three-dimensional least squares adjustment software, GeoLab™, which was used exclusively in this project. Appropriately, a review of the local geodetic observation equations follows.

5.1 Observation Equations in the Local Geodetic System

Steeves [1984] states that it is simpler to formulate the observation equations in either the local astronomic or local geodetic coordinate systems, than in the geodetic coordinate system. As terrestrial observations are collected in a local astronomical system, it seems logical to use this system in preference to a local geodetic system. However, Steeves

[1984] shows a preference for the local geodetic system where a "height-controlled" adjustment is required.

Preference for the selection of the local geodetic system (over the local astronomic system) in which to form the observation equations is provided via reference to Figure 5.1. It can be seen that incremental (horizontal) adjustment corrections (δu, δv) in a local

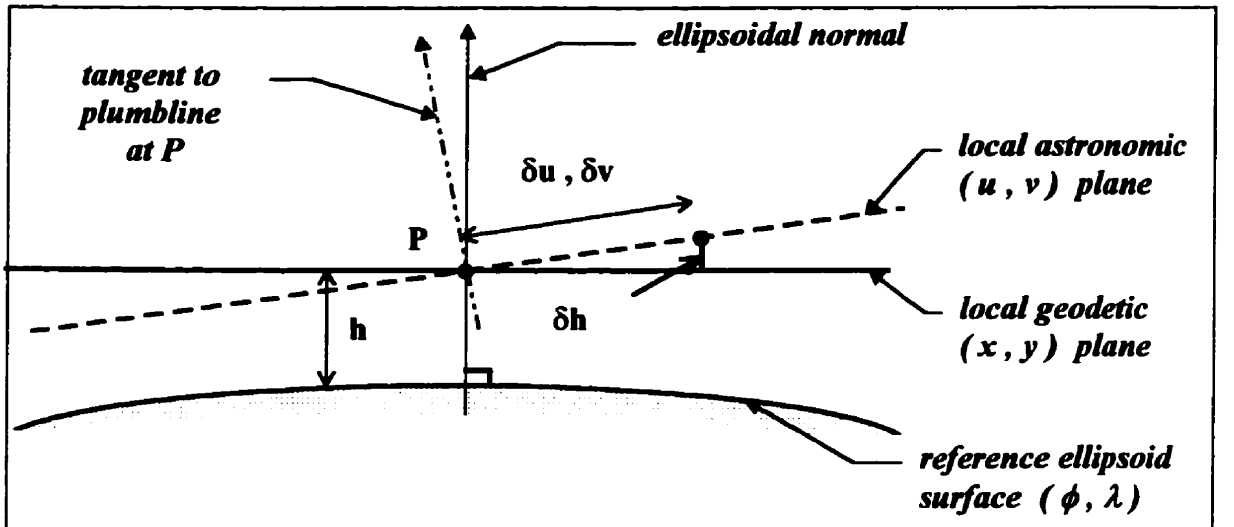

Figure 5.1 Change in h due to a shift in the L.A. system (after Steeves [1984]).

astronomical system theoretically leads to a change, δh, in ellipsoidal height (proportional to the deflection of the vertical at P). The corresponding corrections in a local geodetic system, however, induce insignificant change (provided the initial position of P is known to within a few tens of metres). Bowring [1980] provides an example where an inclination of 60" between the local astronomic and local geodetic planes could lead to a height separation in excess of 0.5 mm for only a 2 m horizontal shift while an 80 m shift in the

local geodetic plane would be required to produce a similar height displacement.

As the local geodetic system is defined separately at each station in the network, the estimated "horizontal" corrections (δx, δy) have to be transformed into their corresponding geodetic coordinate corrections ($\delta\phi$, $\delta\lambda$) via [Steeves, 1984]

$$\delta\phi_i = \delta x_i / (\rho_i + h_i) \quad , \qquad \delta\lambda_i = \delta y_i / ((\nu_i + h_i) \cdot \cos\phi_i) \tag{5.1}$$

where ρ_i and ν_i are the radii of curvature of the reference ellipsoid in the meridian and prime vertical, respectively, at station i. Additionally, coefficients for the terrestrial observation equations are formulated in terms of C.T. Cartesian coordinates (X, Y, Z) and astronomical coordinates (Φ, Λ). These coordinates are computed from the initial geodetic coordinates for each station in the network (with the exception of those stations at which Φ, Λ are observed). Figure 5.2 shows a general procedure for the three-dimensional "height-controlled" adjustment of terrestrial observations.

Derivations for spatial distance, azimuth, unoriented direction and three-dimensional coordinate difference observation equations, including a review of the coordinate systems involved, can be found in Steeves [1984]. A summary of these observation equations, together with comments as to the use (in this project) of any "auxiliary" parameters is presented below and in the following subsections.

The functional model of the least squares adjustment can be written in the parametric form

$$v = A \cdot \delta + f \tag{5.1}$$

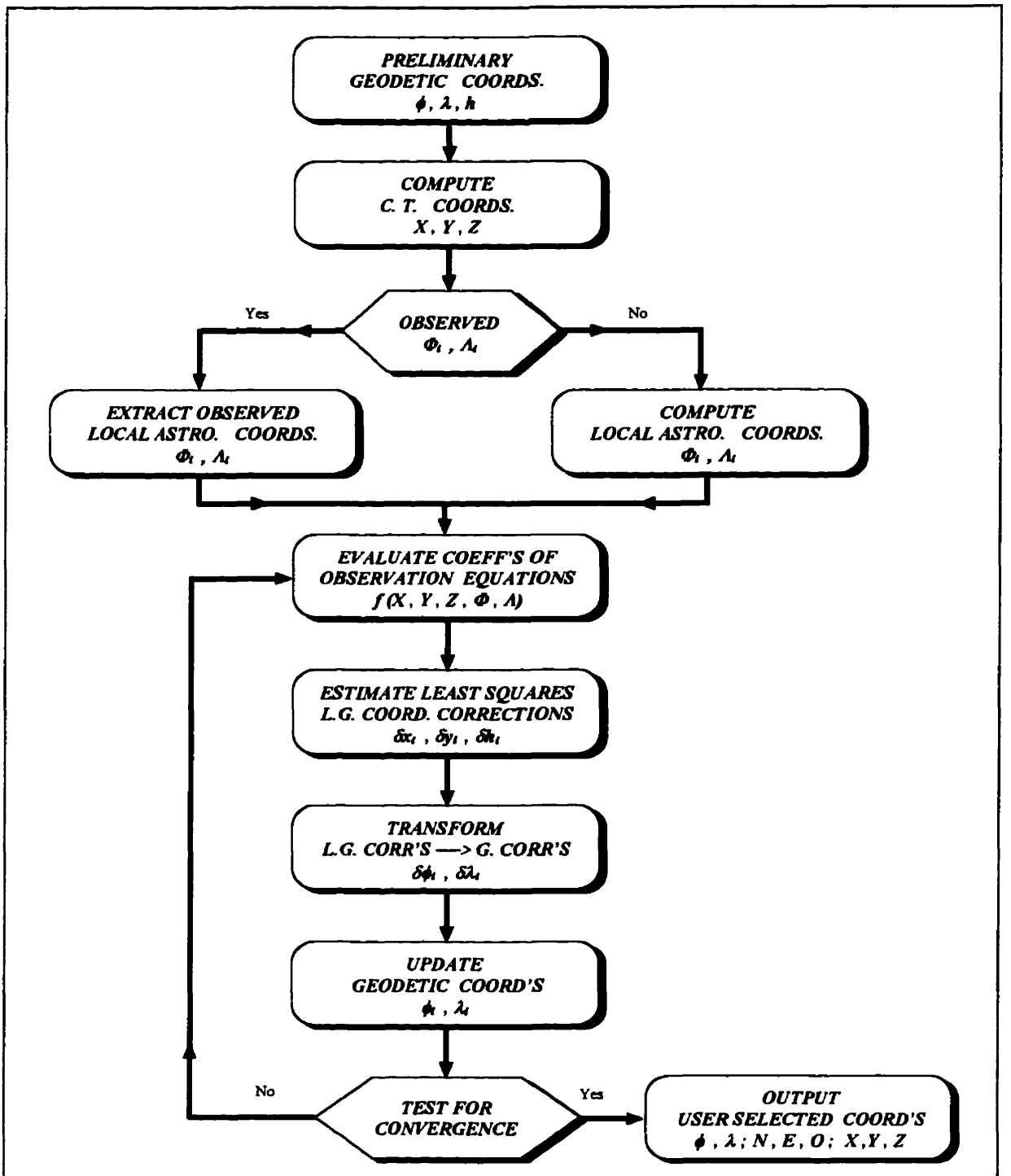

Figure 5.2 Flow chart for a three-dimensional height-controlled terrestrial adjustment.

where the elements of the design matrix A (coefficients of the observation equations) are formulated as functions of the C.T. Cartesian and astronomic coordinates using the following quantities [Steeves, 1984][†]:

$$c_i = -\sin\Phi_i \cdot \left(\cos\Lambda_i \cdot \Delta X_{ij} + \sin\Lambda_i \cdot \Delta Y_{ij}\right) + \cos\Phi_i \cdot \Delta Z_{ij} \quad ; \tag{5.2}$$

$$d_i = -\sin\Lambda_i \cdot \Delta X_{ij} + \cos\Lambda_i \cdot \Delta Y_{ij} \quad ; \tag{5.3}$$

$$m_i = \sin\Phi_i \cdot \left(\sin\Lambda_i \cdot X_i - \cos\Lambda_i \cdot Y_i\right)/p_i \quad ; \tag{5.4}$$

$$S_{ij}^2 = \Delta X_{ij}^2 + \Delta Y_{ij}^2 + \Delta Z_{ij}^2 \quad ; \tag{5.5}$$

$$\Delta X_{ij} = X_j - X_i \quad , \quad \Delta Y_{ij} = Y_j - Y_i \quad , \quad \Delta Z_{ij} = Z_j - Z_i \quad ; \text{ and} \tag{5.6}$$

$$p_i = \sqrt{X_i^2 + Y_i^2} \quad . \tag{5.7}$$

The subscripts i and j refer to the "from" and "to" stations, respectively, of an observation and p_i is the "equatorial distance" [Steeves, 1984] of station i. The misclosure vector, f, is the difference between the input observation and its computed (via prior estimates) counterpart.

5.1.1 Spatial Distance Observation Equations

Observation data input to the three-dimensional adjustment (GeoLab™) had to be reduced to the straight line distance between the two station markers (referred to as spatial, or mark-to-mark, distances). In the context of this project, two sources of spatial distances

---

[†] c_i and d_i are the horizontal coordinate components (u, v) of station j in the L. A. system of station i.

were used: EDM and GPS, where the latter has only been used in the 1995 campaign. In the case of EDM measurements, the raw observations had to be corrected for atmospheric and instrument errors, as well as for the offset heights of the instrument and reflector above their respective station markers (see Chapter 2).

EDMs were used in all campaigns, with two or more used in the earlier campaigns. Calibration of these instruments included only the instruments "zero error" but not its scale factor. Consequently, the issue of datum scale was tackled in the combined GPS and terrestrial adjustment through the inclusion of an "auxiliary" scale parameter (k) in the terrestrial distance observation equations. In a similar manner, an "auxiliary" constant parameter (c) was available in GeoLab™ for the modelling of an "offset" error [BitWise Ideas Inc., 1993].

The linearised observation equation for an observed spatial distance (S_{obs}), as a function of: local geodetic coordinate corrections (δx, δy); corrections to the scale auxiliary parameter (δk); and corrections to the constant auxiliary parameter (δc), was presented by Steeves [1984] as:

$$v_s = a_1 \cdot \delta x_i + a_2 \cdot \delta y_i + a_3 \cdot \delta x_j + a_4 \cdot \delta y_j - S^o \cdot \delta k - \delta c + f_s \tag{5.8}$$

where v_s is the distance residual and f_s the distance misclosure. The coefficients a_i (elements of the design matrix A) are evaluated from

$$\begin{aligned} a_1 &= -\left(c_i + m_i \cdot d_i\right)/S^o & a_2 &= -\left(d_i - m_i \cdot c_i\right)/S^o \\ a_3 &= -\left(c_j + m_j \cdot d_j\right)/S^o & a_4 &= -\left(d_j - m_j \cdot c_j\right)/S^o \end{aligned} \tag{5.9}$$

where

$$S^{\circ} = \frac{1}{2} \cdot \left(\frac{S_{ij}^2}{S_{obs}} + S_{obs} \right) \tag{5.10}$$

from which the misclosure is computed, using the updated values, c^0 and k^0, of the constant and scale auxiliary parameters, as:

$$f_s = S^{\circ} - S_{obs} - (1 + k^{\circ}) \cdot c^{\circ} - k^{\circ} \cdot S^{\circ} \tag{5.11}$$

It is noted that the scale, k, is treated in the observation equations as a "parts per million" (ppm) factor for numerical reasons, i.e., absolute scale is $1 + k \cdot 10^{-6}$.

5.1.2 Spatial Direction Observation Equations

The direction observation equation is analogous to that of the azimuth equation, to which an unknown "auxiliary" orientation parameter is attached. An auxiliary orientation parameter is assigned to each "set" of directions emanating from the same instrument setup. This process was performed automatically by GeoLab™, based on the identification of direction sets at data input [BitWise Ideas Inc., 1993]. The GeoLab™ adjustment, however, did not permit output of the orientation unknowns as they were considered "nuisance" parameters [BitWise Ideas Inc., 1993].

The linearised equation for an observed spatial direction (d_{obs}) is given [Steeves, 1984] by

$$v_d = a_1 \cdot \delta x_i + a_2 \cdot \delta y_i + a_3 \cdot \delta x_j + a_4 \cdot \delta y_j - \rho'' \cdot \delta\Omega + f_d \tag{5.12}$$

where v_d is the direction residual; f_d is the direction misclosure; $\delta\Omega$ is the correction to the direction orientation Ω; and $\rho'' = 206264.806$. The coefficients a_i are then evaluated from

$$a_1 = \left(d_i - m_i \cdot c_i\right)/D_i^2 \qquad a_2 = -\left(c_i + m_i \cdot d_i\right)/D_i^2$$
$$a_3 = \left(q_1 + m_j \cdot q_2\right)/D_i^2 \qquad a_4 = \left(q_2 - m_j \cdot q_1\right)/D_i^2 \tag{5.13}$$

where

$$D_i^2 = c_i^2 + d_i^2 \tag{5.14}$$

and the new quantities q_1 , q_2 are evaluated from

$$q_1 = -d_i \cdot \left(\cos\Phi_i \cdot \cos\Phi_j + \sin\Phi_i \cdot \sin\Phi_j \cdot \cos\Delta\Lambda\right) - c_i \cdot \sin\Phi_j \cdot \sin\Delta\Lambda \tag{5.15}$$

$$q_2 = c_i \cdot \cos\Delta\Lambda - d_i \cdot \sin\Phi_i \cdot \sin\Delta\Lambda \tag{5.16}$$

using

$$\Delta\Lambda_i = \Lambda_j - \Lambda_i \quad . \tag{5.17}$$

Steeves [1984] suggests that the initial value of the orientation unknown, Ω^0, be computed using the (numerically) smallest "observed direction" as the "reference origin" direction, d_{RO}, i.e.,

$$\Omega^o = \arctan\left(d_i/c_i\right) - d_{RO} \tag{5.18}$$

where the quantities c_i and d_i are the "horizontal coordinates" (North and East, respectively) of the observed station (referred to by the direction) in the local astronomic coordinate system of station i. The direction misclosure, f_d, would then be determined from

$$f_d = \arctan\left(d_i/c_i\right) - d_{obs} - \Omega^o \tag{5.19}$$

5.1.3 GPS Coordinate Difference Observation Equations

GPS observations do not suffer from as weak a vertical dimension as their terrestrial counterparts, consequently their observation equations do not need the special treatment rendered to the terrestrial observations. Their observation equations could be formed in the global C.T. Cartesian coordinate system. However, when integrated with terrestrial observations in a "height-controlled" three-dimensional adjustment, it is necessary to formulate the observation equations in the same local geodetic coordinate system.

Vincenty [1982, with notation altered] derives the equation for the observed three-dimensional coordinate differences (ΔX_{obs}, ΔY_{obs}, ΔZ_{obs}), as

$$\begin{pmatrix} v_{\Delta X} \\ v_{\Delta Y} \\ v_{\Delta Z} \end{pmatrix} = -\mathbf{R}_i^T \cdot \begin{pmatrix} \delta x_i \\ \delta y_i \\ \delta h_i \end{pmatrix} + \mathbf{R}_j^T \cdot \begin{pmatrix} \delta x_j \\ \delta y_j \\ \delta h_j \end{pmatrix} - \Delta U_{ij} \cdot \begin{pmatrix} \omega_X \\ \omega_Y \\ \omega_Z \end{pmatrix} - k \cdot \begin{pmatrix} \Delta X_{ij} \\ \Delta Y_{ij} \\ \Delta Z_{ij} \end{pmatrix} + \begin{pmatrix} \Delta X_{ij} - \Delta X_{obs} \\ \Delta Y_{ij} - \Delta Y_{obs} \\ \Delta Z_{ij} - \Delta Z_{obs} \end{pmatrix} \tag{5.20}$$

where $R_{(.)}$ is the point transformation matrix from geodetic to local geodetic coordinates, e.g., at station i

$$\mathbf{R}_i = \begin{pmatrix} -\sin\phi_i \cdot \cos\lambda_i & -\sin\phi_i \cdot \sin\lambda_i & \cos\phi_i \\ -\sin\lambda_i & \cos\lambda_i & 0 \\ \cos\phi_i \cdot \cos\lambda_i & \cos\phi_i \cdot \sin\lambda_i & \sin\phi_i \end{pmatrix} ; \tag{5.21}$$

ω_X, ω_Y, ω_Z are auxiliary "rotation" parameters around the X, Y, Z axes, respectively, having the configuration matrix,

$$\Delta U_{ij} = \begin{pmatrix} 0 & -\Delta Z_{ij} & \Delta Y_{ij} \\ \Delta Z_{ij} & 0 & -\Delta X_{ij} \\ -\Delta Y_{ij} & \Delta X_{ij} & 0 \end{pmatrix} , \tag{5.22}$$

for which the computed coordinated differences are as per equation (5.6); and the scale difference, k, is analogous to that described in the spatial distance observation equations.

GeoLab™ [BitWise Inc., 1993] permitted the inclusion of the geocentric-rotations and scale auxiliary parameters into the adjustment; however, the size of the monitoring network (approximately 7.5 km x 2.5 km) was far too small to resolve these "global" rotation parameters (Vincenty [1982, p.240], reports problems even on a continental extent). Also, the GPS observations had been selected (see Chapter 3) to realise the datum scale hence, no auxiliary scale (difference) parameter was used (although it could have been used to investigate scale consistency between GPS observation sessions).

5.2 Algebraic Review of the Single Epoch Adjustment

"The classical way of defining (realising) the datum of a geodetic network is to delete those columns of the design matrix A ... which refer to the parameters being kept fixed" [Caspary, 1987]; often referred to as a "zero-variance computational base", since all variances are estimated relative to those of the fixed points. More often, though, the network is constrained to a particular azimuth, rather than to the coordinates of two points. In this case the azimuth is entered as an observation with infinite weight - rather than being tagged as a "constraint equation" by GeoLab™. This is just an extended case of the "zero-variance computational base", i.e., with pseudo-observations. A short review of the "zero-variance computational base" algorithm based on that of Caspary [1987] is

presented below as a link between the observation equations of section 5.1 above and the trend analysis of the next Chapter.

If the d "fixed" parameters (coordinates in this case) of the full model are sorted so as to reside in the last d positions of the parameter vector, then the partitioned parametric model is of the linear form, cf. equation (5.3),

$$v = \begin{pmatrix} A_1 & A_2 \end{pmatrix} \cdot \begin{pmatrix} \delta_1 \\ \delta_2 \end{pmatrix} - \ell \tag{5.23}$$

where δ_1 and δ_2 represent the estimated corrections to the free and fixed parameters, respectively; ℓ is the observation vector; v is the vector of residuals; and A_i are the respective design matrices for δ_1 and δ_2. Since A_2 covers the datum deficiency, d, of the network (after pseudo-observations have been considered), then if A_1 is of full column rank the columns of A_2 will be linear combinations of the columns of A_1. Hence,

$$A_1 \cdot L = A_2 \tag{5.24}$$

for some matrix L, which after substitution into equation (5.23) yields

$$v + \ell - A_1 \cdot L \cdot \delta_2 = A_1 \cdot \delta_1 \tag{5.25}$$

which is now a model of full rank. The general solution of the free parameters is then,

$$\begin{aligned} \delta_1 &= \left(A_1^T \cdot P \cdot A_1\right)^{-1} \cdot A_1^T \cdot P \cdot \left(\ell - A_1 \cdot L \cdot \delta_2\right) = N_{11}^{-1} \cdot (u_1 - N_{12} \cdot \delta_2) \\ \delta_2 &= \delta_2 \end{aligned} \tag{5.26}$$

which implies that the "fixed" parameters are undefined and consequently their corrections from each iteration remain the same. Generally, however, these parameters are only coordinates and are defined to be equal to their *a priori* coordinate values, which implies that the $\hat{x}_2$ corrections equate to zero. This more specific case reduces equation (5.26) to

the more familiar form:

$$\begin{aligned} \delta_1 &= \left(\mathbf{A}_1^T \cdot \mathbf{P} \cdot \mathbf{A}_1\right)^{-1} \cdot \mathbf{A}_1^T \cdot \mathbf{P} \cdot \ell = \mathbf{N}_{11}^{-1} \cdot \mathbf{u}_1 \\ \delta_2 &= 0 \end{aligned} \tag{5.27}$$

In both cases, Caspary [1987] gives the cofactor matrix as

$$\mathbf{Q}_{\hat{x}} = \begin{pmatrix} \mathbf{Q}\hat{\mathbf{x}}_{11} & \mathbf{Q}\hat{\mathbf{x}}_{12} \\ \mathbf{Q}\hat{\mathbf{x}}_{21} & \mathbf{Q}\hat{\mathbf{x}}_{22} \end{pmatrix} = \begin{pmatrix} \mathbf{N}_{11}^{-1} & 0 \\ 0 & 0 \end{pmatrix} \tag{5.28}$$

from which the algorithms' name derives (i.e., $\mathbf{Q}\hat{\mathbf{x}}_{22} = 0$ implies the computational base, or datum constraints, has "zero variance"). Interpretation, therefore, of the subsequent variances is of a relative nature, i.e., with respect to the computational base.

The cofactor matrix output by GeoLab™ is equivalent to $\mathbf{Q}\hat{\mathbf{x}}_{11}$ of (5.28), which excludes any uncertainties associated with the fixed station(s). As a full network cofactor matrix was required for subsequent processing (trend analysis and displacement modelling) the GeoLab™ cofactor matrix had to be expanded through the inclusion of rows and columns of zeros equal to the number of fixed coordinates.

In practice, considerably more effort then simply adding rows and columns of zeroes was required in the preparation of the GeoLab™ data for subsequent analysis. Most notably, for the two-dimensional horizontal analyses, the geodetic coordinates (φ, λ) and their local geodetic covariances[‡] (m^2), had to be rigorously transformed onto a "project" mapping plane; for which the New Brunswick Stereographic Double Projection was used (see Thomson et al. [1977], for projection definitions and algorithms). The

---

[‡] GeoLab™ produces curvilinear geodetic coordinate (φ, λ) variances-covariances in a local geodetic coordinate system using linear (metres or feet) units [BitWise Inc., 1993, p.4-15].

"project" mapping plane, however, was not the official "New Brunswick mapping plane".

5.3 The Integrated Terrestrial and GPS Adjustments.

While the traverse data was integrated with the GPS observed baselines in a combined network adjustment, predominantly of the horizontal components, the levelling data was adjusted separately. This section presents the procedures used and the results obtained from the campaign adjustments.

Table 5.1 95% Point standard deviations estimated via Levelling and GPS.

1994 1-D 95% Standard Deviations [m]		
STATION	[LEV]	[GPS]
10894 / HT	*0.0000*	*0.0000*
9637	0.0029	0.0128
22798	0.0025	0.0126
24740	0.0028	0.0109
A1	0.0009	0.0127
A10	0.0028	0.0140
B6	0.0022	0.0130
C6	0.0033	0.0127
D7	0.0030	0.0107
E1	0.0032	0.0079
E5	0.0032	0.0102
F2	0.0037	0.0114
G3	0.0042	0.0083
G7	0.0042	0.0087
ML4	0.0019	0.0131
ML23	0.0047	0.0088

5.3.1 Levelling and GPS.

The small extent of the Sussex network (only 7.5 km x 2.5 km), together with tripod setups for the GPS antennae, were not conducive to an improvement in the levelling-only estimated elevations via an integration of the two. Table 5.1 shows the 95% confidence intervals for the 1994 levelling and GPS estimated heights. Although both systems are referred to different minimum constraints, the magnitudes of the GPS estimates are consistently larger than their levelling counterparts.

Table 5.2 Annual biases in the Local Geoidal Undulation models.

Year	P. C. S.	Potacan
1992	+ 0.000 m	-
1993	+ 0.007 m	+ 0.008 m
1994	+ 0.007 m	+ 0.000 m
1995	+ 0.000 m	+ 0.000 m
1996	- 0.011 m	- 0.007 m

While attempting to model the local geoid corrections using the levelled and GPS determined heights from campaigns 1992 to 1996, inclusive, a systematic trend was noticed in the campaign residuals. Table 5.2 shows the "relative vertical offsets" for the annual GPS-Levelling differences, estimated for each campaign with respect to the first campaign. Also shown in Table 5.2 are the equivalent vertical offsets obtained at a nearby salt and potash mine, Potacan Mining Co. (located approximately 30 km SW of P.C.S. and always observed after the P.C.S. campaigns). While the two trends appeared to be suspiciously similar in nature, no further investigation has as yet been performed.

It was concluded, from the above, that integrating the levelling and GPS data for analysing vertical displacements on this project was unlikely to improve upon the levelling data. Instead, effort was directed towards horizontal integration.

5.3.2 Traversing and GPS.

Integration of the traverse and GPS data into a least squares network adjustment was not a one step operation, even after the data pre-processing of Chapter 2, but rather a sequence of several adjustment stages.

Stage one was in fact the least squares adjustment of the levelling data, this had to precede the "horizontal" adjustment as it was the primary source of height information (i.e., the most complete source). These heights, despite remaining fixed in the "horizontal" adjustments played a significant role in the final solution as poor "fixed heights" led to erroneous distance reduction within the three-dimensional height controlled system. The heights required for temporary stations were determined separately through the combination of the final levelled heights and the zenith distance derived height differences.

Stage two of the process involved the separate adjustments of the traverse and GPS data. The primary purpose of these adjustments was to check the internal consistency of the data, i.e., to search for and correct, where possible, blunders. In the case of traversing this second stage was also used to generate and check the approximate horizontal coordinates of temporary stations (where approximate coordinates for the permanent stations were obtained from the previous years' final estimates). In the case of

GPS baseline adjustments, for which the Prism™/GPPS™ assigned covariances were adopted, the estimated variance factor was used to scale the *a priori* variances if the χ^2 Test on the variance factor failed. Table 4.3 shows a steady decline in the variance factor estimated for the 1992 through 1996 primary GPS network adjustments, with 1992 and 1996 failing the χ^2 Test due to "too optimistic" and "too pessimistic" *a priori* estimates, respectively.

Stage three of the adjustment process involved the determination of "local geoidal undulations" for all stations used in the "horizontal" network, based on the modelling outlined in Chapter 3. Only the primary GPS network stations were used for this purpose. Results of the combined 1992 to 1996 modelling of the "local geoidal undulations" indicated different campaign specific vertical offsets of the order of 1 cm were required, which precluded the adoption of a single "local geoidal model", applicable for all campaigns: past, present and future.

Stage four involved the merging of the traverse, GPS primary (and secondary for the 1995 and 1996 campaigns) and the "local geoidal undulations" data into the first combined adjustment. Auxiliary scale factors were, at this stage, assigned to all distance observations, including the GPS derived distances of 1995. This left the GPS coordinate difference observations to realise the scale of the network. The difference between this and the final adjustment was that the *a priori* variances for the different observation types were used, as outlined in Chapter 4. Again, the detection of outliers was performed but generally, at this stage, those found tended to be more a result of inappropriate weighting than blunders and were predominantly associated with directions. Also, as the fixed

traverse heights were from the levelling adjustment, the "orthometric" height of the fixed station, HT, was held fixed rather than its ellipsoidal counterpart. This permitted the ellipsoidal estimate to change in the adjustment in a manner similar to those of the other GPS occupied stations.

Table 5.3 Statistical Summary of the Final Horizontal Network Adjustments.

	1992	1993	1994	1995	1996
Residual Critical Value Type	Tau Max	Tau Max	Tau Max	Tau Max	Tau Max
Residual Critical Value	3.8794	4.0421	4.0505	3.8407	4.0025
Number of Flagged Residuals	0	0	0	0	0
Convergence Criterion [m]	0.0005	0.0005	0.0005	0.0005	0.0005
Final Iteration Count	3	4	3	3	3
Confidence Level [%]	95.0	95.0	95.0	95.0	95.0
Estimated Variance Factor	**1.2243**	**1.0331**	**1.0891**	**1.0138**	**1.1626**
Degrees of Freedom	**93**	**258**	**267**	**152**	**253**
lower limit	0.9365	0.8757	0.9257	0.8195	0.9839
χ^2 **Test on Variance Factor**	**Pass**	**Pass**	**Pass**	**Pass**	**Pass**
upper limit	1.6692	1.2375	1.3004	1.2867	1.3951

The final stage comprised a re-adjustment with scaled group *a priori* variances. The basis for the re-assignment of group weights (via scaling group variances) was the analysis of the residuals, normalised by the *a priori* standard deviations of the associated observations (not the standardised residuals output by the adjustment and used for data snooping purposes). This technique, while not rigorous in the presence of correlated observations, was outlined in Chapter 4. The estimated group scale factors used are presented in Tables 5.4-5.6. In all cases, 1992 to 1996, the re-weighted adjustment passed the χ^2 Test on the variance factor, so that no iterative re-weighting was required. Table

5.4 gives the statistical summaries resulting from each of the final, combined adjustments, where the number of flagged residuals does not include those observations removed from, or individually re-weighted within, the adjustment. It does, however, indicate that all outliers were accounted for.

Table 5.4 Synopsis of Horizontal Network Direction Residuals

Year	Instrument	No.	Re-weight	RN	rms	min.	max.
1992	Kern E2	135 / 74	2.422	16.9	4.2 "	-16.9 "	+ 21.7 "
1993	Kern E2	255 / 26	3.034	80.5	1.8 "	- 04.9 "	+ 06.2 "
1994	Leica TC2002	254 / 26	1.624	84.7	2.9 "	- 05.2 "	+ 42.3 "
1995	Leica TC2002	29 / 5	1.997	2.3	0.6 "	- 01.0 "	+ 01.0 "
1996	Leica TC2002	139 / 9	1.491	46.6	1.3 "	- 05.0 "	+ 03.6 "

5.4.3 Comments on the Horizontal Adjustment.

Many items worth noting were encountered during the various "horizontal" adjustments; however, only a few of the more significant ones are commented on here. The first sub-section deals with general data problems while the second looks at the 1995 and 1996 secondary GPS schemes. As a rough indicator of the accuracies achieved by the different observables, a list of the root mean square (rms) errors of their residuals was compiled for each campaign and presented in Tables 5.4 to 5.6 (in which: No. ≡ Total/Unique number of observables; RN ≡ approximate Redundancy Number; rms ≡ root mean square; min. ≡ minimum residual; and max. ≡ maximum residual). "Normality" in the distribution of the group standardised residuals was via visual inspection of the group histograms produced

by GeoLab™, as the recommended "χ^2 Goodness of Fit" tests were not supported by GeoLab™ [BitWise Inc., 1993].

Table 5.5 Synopsis of Horizontal Network Distance Residuals

Year	EDM	No.	Re-weight	RN	rms [mm]	min. [mm]	max. [mm]
1992	DM503 # 325147	21 / 3	0.601	9.8	2.4	- 5.1	+ 5.1
	DM503 # 348158	61 / 44	2.093	9.7	3.0	- 5.6	+ 6.3
	MA200 # 216	6 / 0	1.625	2.4	3.6	- 4.7	+ 5.1
1993	DM503 # 325307	114 / 9	1.618	71.7	3.1	- 8.9	+ 8.3
	DM503 # 348158	98 / 6	1.081	58.2	2.1	- 5.6	+ 5.4
	MA200 # 216	19 / 0	2.338	10.9	4.2	- 5.6	+ 7.8
1994	TC2002 # 357992	231 / 16	0.942	129.1	1.0	- 7.6	+ 3.5
1995	TC2002 # 357992	29 / 6	0.551	14.6	0.6	- 1.0	+ 1.6
	GPS Receivers	57 / 0	0.783	23.9	2.9	- 7.4	+ 6.3
1996	TC2002 # 357992	131 / 6	0.530	71.1	0.5	- 1.6	+ 1.9

5.4.3.1 General Comments.

One of the first items worth commenting on was the relatively poor performance of the MA200. The specification given by the manufacturer [Tellumat, 1988] was for a standard deviation of $\pm$ 0.5 mm $\pm$ 0.5 ppm, which amounts to $\pm$ 0.9 mm over the longest distance (9637 to HT was 1597 m) measured by the MA200. This was considerably different from the rms errors of 3.6 mm and 4.2 mm achieved in the 1992 and 1993 campaigns, respectively. A combined "EDM-Baseline adjustment", with all MA200 and TC2002 summer calibration data, spanning the years 1992 to 1995, yielded an rms error of 0.9 mm

from 128 distance observations (ranging from 263 m to 1103 m) with the MA200 (and 233 observations with the TC2002). The primary differences between the baseline results and the field results were that:

Table 5.6 Synopsis of Horizontal Network GPS Baseline Residuals

Year	GPS Baseline	No.	Mean	Re-weight	RN	rms [mm]	min. [mm]	max. [mm]
1992	DX	28	- 0.14	0.660	18.7	3.2	- 9.8	+ 4.7
	DY	28	- 0.07	0.558	19.1	5.2	- 11.4	+ 13.7
	DZ	28	- 0.15	0.930	19.0	11.5	- 51.2	+ 8.2
	DXDYDZ	**84**	**- 0.12**	**0.716**	**56.8**	**7.5**	**- 51.2**	**+ 13.7**
1993	DX	21	- 0.21	0.948	11.8	2.1	- 4.5	+ 2.9
	DY	21	- 0.07	0.760	11.5	3.9	- 5.7	+ 11.9
	DZ	21	+ 0.03	0.536	11.4	2.8	- 5.1	+ 7.0
	DXDYDZ	**63**	**- 0.08**	**0.750**	**34.7**	**3.0**	**- 5.7**	**+ 11.9**
1994	DX	29	- 0.12	1.348	17.2	2.8	- 4.4	+ 7.0
	DY	29	+ 0.15	1.025	16.3	4.6	- 10.5	+ 12.8
	DZ	29	- 0.14	0.730	15.7	3.8	- 69.7	+ 11.4
	DXDYDZ	**87**	**- 0.04**	**1.044**	**49.2**	**3.8**	**- 10.5**	**+ 12.8**
1995	DX	52	+ 0.06	0.837	37.3	4.1	- 8.5	+ 10.5
	DY	52	+ 0.00	0.817	37.5	7.1	- 21.7	+ 19.4
	DZ	52	+ 0.09	0.574	37.7	5.5	- 13.1	+ 11.2
	DXDYDZ	**156**	**+ 0.05**	**0.743**	**112.5**	**5.7**	**- 21.7**	**+ 19.4**
1996 (Pri)	DX	38	+ 0.08	0.596	25.8	3.1	- 8.6	+ 7.2
	DY	38	- 0.07	0.423	25.0	4.6	- 14.2	+ 13.0
	DZ	38	+ 0.03	0.560	25.2	5.2	- 13.2	+ 15.3
	DXDYDZ	**114**	**+ 0.01**	**0.527**	**76.1**	**4.4**	**- 14.2**	**+ 15.3**
1996 (Sec)	DX	34	- 0.16	0.784	20.4	6.0	- 21.9	+ 9.1
	DY	34	+ 0.10	1.083	18.2	11.2	- 14.4	+ 52.4
	DZ	34	- 0.12	0.505	16.9	5.4	- 17.7	+ 12.9
	DXDYDZ	**102**	**- 0.06**	**0.797**	**55.4**	**8.0**	**- 17.7**	**+ 52.4**

1. the baseline comprised concrete pillars with grooved centring plates, while the Sussex data was collected via tripods;
2. the baseline measurements barely exceeded the 1 km range specified by the manufacturer, while 1.5 km distances were observed in Sussex; and
3. the Sussex data comprised very few measurements (only 6 in 1992 and 19 in 1993) compared with the other distance measurement types (in the Sussex networks).

Additionally, in 1993, while measuring with the MA200, centring the instrument and prism required an elaborate, iterative procedure due to damaged optical plummets. This would have resulted in considerably less accuracy than the 0.5 mm expected.

Table 5.7 Summary of Auxiliary Distance Scale Factors

YEAR	EDM	SERIAL #	SCALE	σ_o	n	RN
1992	DM503	325147	-48.0	± 6.5	24	9.8
	DM503	348158	- 3.7	± 3.5	105	9.7
	MA200	216	+ 3.6	± 4.3	6	2.4
1993	DM503	325307	+ 8.7	± 1.6	123	71.7
	DM503	348158	+ 5.4	± 1.8	104	58.2
	MA200	216	- 7.2	± 1.6	19	10.9
1994	TC2002	357992	- 3.3	± 0.5	247	129.1
1995	TC2002	357992	+ 1.7	± 1.0	35	14.6
	GPS_DIST	-	+ 1.4	± 0.8	57	23.9
1996	TC2002	357992	- 1.9	± 0.6	137	71.1

Another major problem encountered in the 1992 adjustment involved the scale of the DM503 #325147, which was used along the A-line. This particular EDM was estimated, from a combined EDM-Baseline adjustment, to have a - 106 ppm scale difference when compared to the DM503 #348158. The estimated scale factor from the

1992 combined network adjustment was - 48 ppm (± 7 ppm), compared to the - 4 ppm (± 4 ppm) estimated for the DM503 #348158, and the + 4 ppm (± 4 ppm) for the MA200. Such drastic changes, together with its erratic measurements and subsequent replacement [Engineering and Mining Surveys Research Group, 1992], render the data collected via this instrument unreliable. The final estimated auxiliary scale parameter for each EDM-epoch combination are listed in Table 5.7, together with their estimated standard deviations, sample sizes and approximate redundancy numbers (see Chapter 4 for details). There does not appear to be any consistency in the signs of the scale corrections, but then neither was there any consistency in the "traversing". Hence, the "stability" of the GPS realised scale from epoch to epoch could not be checked.

One final comment on the 1992 traverse network pertains to the very low redundancy associated with the network. As mentioned earlier, the initial intention was to monitor the horizontal displacements via observation differences which may have lead to minimal effort being placed into creating redundant data. This can be seen in Figure 2.3 which clearly shows the numerous uniquely determined stations, it can also be seen in Tables 5.4 and 5.5, where the number of observations are broken down into the number of redundant and unique observations. The 1992 unique-to-redundant ratios for distances and directions were 1:2 and 1:2, respectively, compared to the 1:14 and 1:10 achieved in 1993 and 1994. These numerous hanging lines resulted in large error ellipses which later made it difficult to separate monument displacements from observation errors.

The 1992 campaign was not the only problematic data set. In 1993 a string of directions between stations ML10 and ML14 were flagged as outliers, even after the re-

weighting scheme. Inspection of the meteorological data for the distances showed that during these setups the temperature climbed to a high of 32 °C, which would have adversely affected pointing accuracy (particularly as this section of the traverse was along paved road). This suspicion was confirmed via station adjustments of the directions collected on that day (as the original data was entered into a field book, it was not subjected to any station adjustment) and by the increase from three to four arcs of observations at stations ML10, ML11 and ML14. Based on the observed increase (approximately double) in the station adjustment variances (see Table 5.8), the *a priori* standard deviations were increased by a factor of $\sqrt{2}$.

Table 5.8 Results of Station Adjustments on directions of 93/07/14

Setup	No. Arcs	No. Tgts	Std. Dev.	Temp.
NML5	3	2	0.6 "	23 °C
ML6	3	2	0.6 "	24 °C
22798	3	2	0.1 "	26 °C
ML7	3	3	0.5 "	27 °C
ML8	3	2	0.5 "	29 °C
ML10	4	3	1.5 "	31 °C
ML11	4	2	1.2 "	31 °C
T15	3	3	0.8 "	32 °C
T16	3	2	1.0 "	30 °C
ML14	4	2	1.1 "	29 °C
ML15	3	2	0.4 "	28 °C
NML16	3	2	0.5 "	28 °C
T17	3	3	0.4 "	28 °C
E1	3	3	0.5 "	28 °C

Less successful was the resolution of several GPS coordinate difference observations flagged as outliers in the 1994 campaign. Despite an independent re-processing of all baseline solutions, no source of error could be found for these observations. These flagged baselines also appeared in, and could be held accountable for, the larger triangle loop misclosures involving independent session solutions. Due to the strong redundancy of the GPS network and the unresolved source of their errors, these observables were discarded from further processing.

5.4.3.2 The Densification Schemes.

The role of the primary GPS static observation scheme was to realise the datum and control the propagation of traverse errors. The latter is aptly demonstrated by Figure 5.3 which shows the 95% error ellipses resulting from the traverse only, and the integrated, adjustments. The improved network led to a desire to extend the GPS network, in favour of traversing, but without the necessity for long static sessions.

In 1995 a departure from the extensive traverse densification schemes of the 1992 to 1994 campaigns was made, to a less dense GPS trilateration scheme. This trilateration scheme was later substituted by a pseudo-static densification scheme in 1996 (supplemented with traverse densification in the central region of the monitoring network). The 95% error ellipses of stations common to the 1994 through 1996 densification schemes are shown in Figure 5.4 and listed in Table 5.9, where blank cells indicate a station was not part of the densification scheme.

Figure 5.3 : 1994 Traverse and GPS Error Ellipses

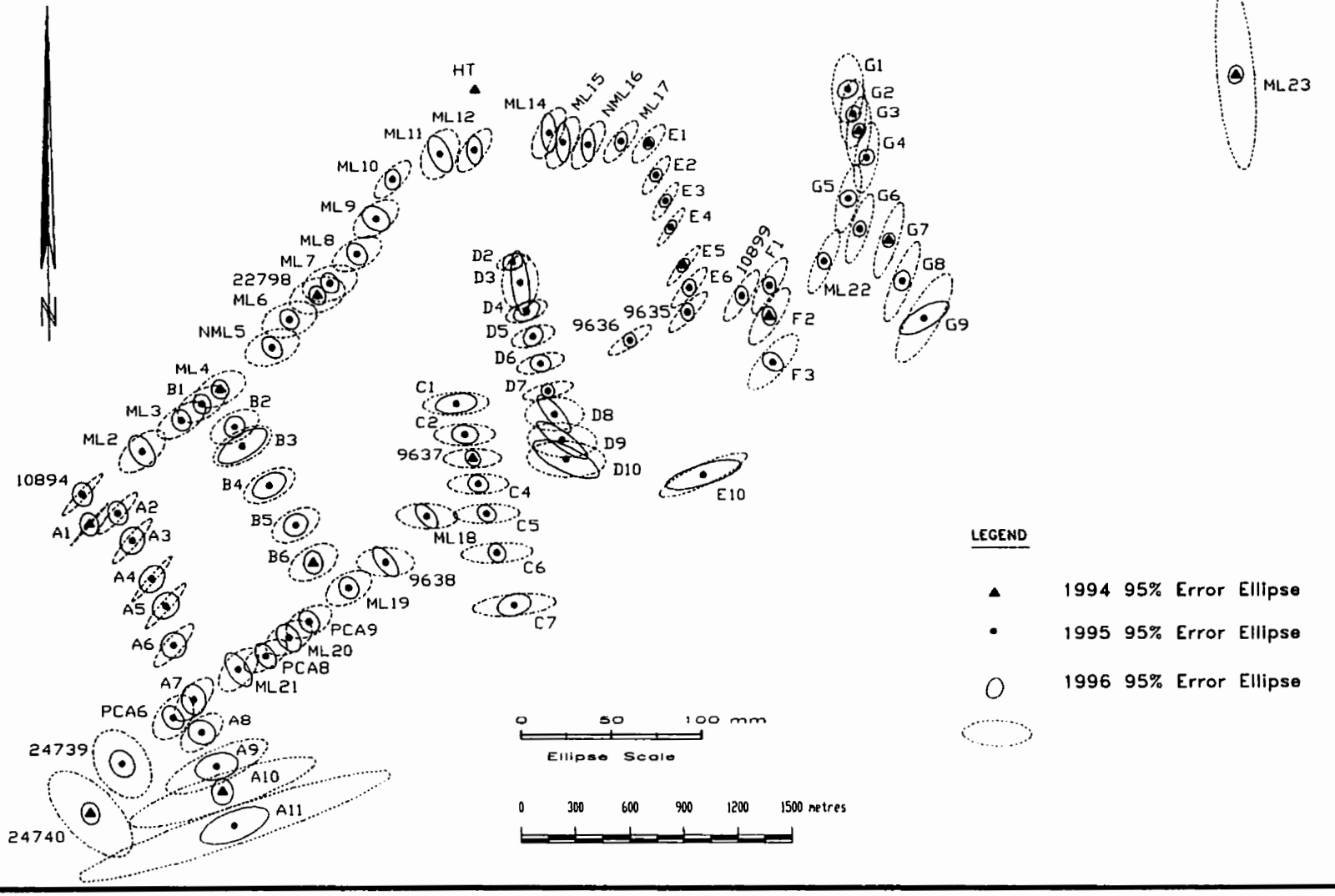

Figure 5.4 : 1994–1996 Densification Schemes

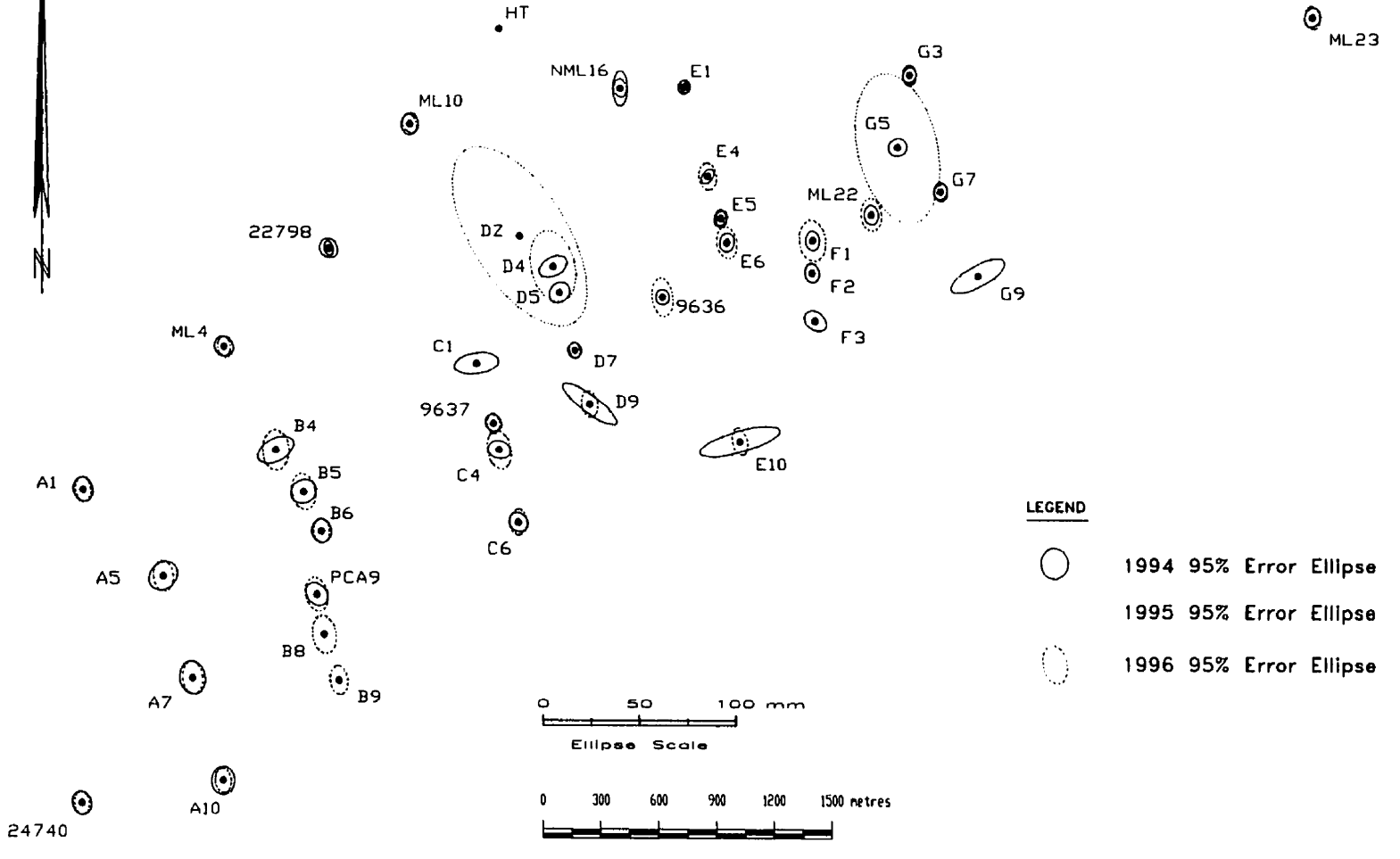

Stations C1 and G9 were both part of the 1996 densification scheme, unfortunately the ambiguities could not be resolved due to extremely poor satellite geometry which was in turn the result of severe obstructions and the short sampling time (two 10 minute sessions about 30 minute apart). The large error ellipses attributed to stations DZ, D4 and G5 were due to similar reasons; however, they were included in the adjustment as they were independently determined by traversing. It can be seen that at these particular stations the 30 minute GPS distance observations resulted in smaller error ellipses. However, considering the remainder of the unobstructed stations, it can be seen that the pseudo-static mode performed better, with semi-major axes slightly less than 1 cm. It can also be seen that the pseudo-static ellipses are strongly aligned North-South with the East-West confidence interval being almost half the magnitude of the North-South interval.

With a few exceptions, the 1994 traversing scheme outperformed both of the GPS densification schemes. This was expected within a small, geometrically strong network. The exceptions, for example D9, E10 and G9, tended to be stations on the ends of open traverses where zero redundancy was achieved.

The above observations indicated that traversing with the TC2002 was the more accurate of the three methods used for densification where closed loops were achieved, while GPS was best suited to controlling traverse nodes and terminals. Unfortunately, so many of the monuments lie within heavy vegetation that neither method can be used efficiently.

Table 5.9 95% Error Ellipses of 1994-1996 Densification Schemes.

	1994			1995			1996		
Station	a mm	b mm	Az °	a mm	b mm	Az °	a mm	b mm	Az °
24740	6.1	5.0	163	6.0	4.4	2	5.9	3.8	172
A1	6.3	5.1	164	6.7	4.8	1	6.1	4.0	172
ML23	5.0	4.1	20	5.5	4.0	4	6.1	3.8	169
9636	3.9	3.6	169				9.8	5.4	173
A5	8.0	6.5	50	10.4	9.4	66	7.6	5.2	172
A7	8.0	6.7	166	9.7	9.3	114	7.7	5.3	173
B4	10.1	5.8	62	10.6	8.3	76	10.5	6.9	177
B5	6.9	5.8	59				9.3	6.1	169
B8				12.2	8.0	110	9.7	6.2	171
C1	11.7	5.3	82	12.1	9.1	67	-	-	-
C4	5.9	4.6	107	11.1	7.8	110	10.1	6.2	168
D4	7.9	4.6	63	10.0	7.7	159	18.1	11.5	165
D9	17.1	4.4	125	11.5	7.6	126	6.7	4.2	169
DZ							51.4	24.4	146
E10	21.7	5.5	74	9.9	8.5	128	7.3	3.8	165
E4	4.2	2.6	38	12.2	7.3	73	6.9	4.5	174
E6	4.5	3.8	13				8.0	5.2	168
F1	4.8	3.6	174				10.4	6.8	172
G5	4.9	4.5	59	9.3	8.3	75	38.6	20.6	167
G9	15.6	5.3	62	11.9	9.1	0	-	-	-
ML10	5.7	4.3	7	12.5	7.0	132	4.9	3.5	164
ML22	4.7	3.7	171				8.0	5.3	173
NML16	9.0	3.8	180	11.0	7.2	31	4.8	3.1	170
PCA9	6.5	5.0	140				8.7	5.7	166

Chapter 6

Trend Analysis

Trend analysis is the precursor to deformation modelling. The identification of trends is necessary for the selection of both the model characteristics and their regions of application. Trend analysis is also used to define "normal" behaviour of the object under observation, and consequently "abnormal" behaviour, where the abnormalities may be just as important in that they would trigger alarm systems or, more poignantly, alert the analyst to potential errors, oversights, etc.

Ideally datum invariant quantities are sought, such as angles and distances, however, these quantities are not always appropriate and datum dependent coordinates have to be used instead. Minimisation of the datum effects is then of primary concern, as they tend to cloud the picture and may even mislead the analyst. The iterative weighted similarity transformation is an analytical aid in the identification of trends from biased coordinate estimates.

This Chapter looks at the iterative weighted similarity transformation (IWST) as a tool in the identification of both horizontal and vertical spatial trends in the Sussex data. The results of the IWST trend analyses of the Sussex data, together with a few, more traditional, graphic techniques, are also presented.

6.1 Iterative Weighted Similarity Transformation

This technique was presented in detail by Chen [1983], and subsequently summarised by Chrzanowski et al. [1986] and Chen et al. [1990b]. This description of the Iterative Weighted Similarity Transformation (IWST) was taken from these sources.

6.1.1 The Weighted Similarity Transformation

The algorithm was first presented by Chen [1983] as a special similarity transformation, which was considered to be a more robust solution to the datum defects problem than the inner constraints solution. It was subsequently expanded into a more general form, from which variations in the "weighting" schemes were exploited. An outline of the approach, taken from Chen [1983], follows.

Generally, the single epoch vector of estimated coordinates, $\hat{\mathbf{x}}$, can be transformed to a new datum, $\hat{\mathbf{x}}_1$, subject to new datum constraints,

$$\mathbf{D}^{\mathrm{T}} \cdot \hat{\mathbf{x}}_1 = 0 \quad , \tag{6.1}$$

via a special similarity transformation. If the vector t contains the desired transformation parameters and matrix H is the configuration matrix of the transformation, then the new coordinates can be determined from

$$\hat{\mathbf{x}}_1 = \hat{\mathbf{x}} + \mathbf{H} \cdot \mathbf{t} \quad . \tag{6.2}$$

The unknown transformation parameters, t, are required to satisfy the new datum constraints equation, hence,

$$\mathbf{D}^{\mathrm{T}} \cdot \hat{\mathbf{x}}_1 = \mathbf{D}^{\mathrm{T}} \cdot \left(\hat{\mathbf{x}} + \mathbf{H} \cdot \mathbf{t} \right) = 0 \tag{6.3}$$

from which t is determined as,

$$\mathbf{t} = -\left(\mathbf{D}^{\mathrm{T}} \cdot \mathbf{H} \right)^{-1} \cdot \mathbf{D}^{\mathrm{T}} \cdot \hat{\mathbf{x}} \quad . \tag{6.4}$$

As the transformation parameters need not be known (although they could be used to evaluate variations in orientation and scale of the reference network), they can be treated as nuisance parameters and removed from the solution. Consequently, after back-substituting for t, the new coordinates are estimated as

$$\hat{\mathbf{x}}_1 = \left(\mathbf{I} - \mathbf{H} \cdot \left(\mathbf{D}^{\mathrm{T}} \cdot \mathbf{H} \right)^{-1} \cdot \mathbf{D}^{\mathrm{T}} \right) \cdot \hat{\mathbf{x}} \quad . \tag{6.5}$$

Chen, then showed that this form of the solution could be extended, using projection theory in the parameter space, into an alternate form, namely

$$\hat{\mathbf{x}}_1 = \left(\mathbf{I} - \mathbf{H} \cdot \left(\mathbf{H}^{\mathrm{T}} \cdot \mathbf{W} \cdot \mathbf{H} \right)^{-1} \cdot \mathbf{H}^{\mathrm{T}} \cdot \mathbf{W} \right) \cdot \hat{\mathbf{x}} \quad , \tag{6.6}$$

where the "weight" matrix W is

$$\mathbf{W} = \mathbf{D} \cdot \left(\mathbf{D}^{\mathrm{T}} \cdot \mathbf{D} \right)^{-1} \cdot \mathbf{D}^{\mathrm{T}} \quad . \tag{6.7}$$

Selection of specific forms of the W matrix would then lead to different solutions. Most notably, setting W equal to the identity matrix, I, would imply that the transposed datum constraint matrix, D, is equal to the similarity configuration matrix, H, and the result would be the inner constraints solution. Better still, W could be used to permit the assignment of heavier weights to the more favourable station coordinates.

The transformed cofactor matrix of the new coordinates, $\hat{x}_1$, was then obtained by Chen [1983] as,

$$Q_{\hat{x}_1} = \left(I - H \cdot \left(H^T \cdot W \cdot H\right)^{-1} \cdot H^T \cdot W\right) \cdot Q_{\hat{x}} \cdot \left(I - H \cdot \left(H^T \cdot W \cdot H\right)^{-1} \cdot H^T \cdot W\right)^T \quad (6.8)$$

where $Q_{\hat{x}}$ is the cofactor matrix resulting from the previously adjusted coordinates.

An important attribute of the "weighted" similarity transformation, noted by Chen [1983], was that it is invariant with respect to the datum constraints of the original solution. This made the algorithm suitable for the transformation of two, or more, single epoch solutions onto a common "best" datum.

6.1.2 The IWST Applied to Displacement Analysis

Under the assumptions that no a priori variance factors are known, that the two epoch adjustments have the same geodetic datum, and that they are stochastically equivalent (i.e., the null hypothesis Ho: $\hat{\sigma}^2_{o_1} = \hat{\sigma}^2_{o_2}$ is not rejected), the pooled variance factor, $\hat{\sigma}^2_{o_p}$, is obtained with df_p degrees of freedom from [Chen et al., 1990b]

$$\hat{\sigma}^2_{o_p} = \frac{df_1 \cdot \hat{\sigma}^2_{o_1} + df_2 \cdot \hat{\sigma}^2_{o_2}}{df_p} \quad , \quad \text{where} \qquad df_p = df_1 + df_2 \quad , \tag{6.9}$$

and $\hat{\sigma}^2_{o_i}$, df_i are the estimated variance factor and degrees of freedom of the i^{th} epoch adjustment. The null hypothesis above is not rejected at a significance level α if the ratio of the two single epoch estimated variance factors lies within the confidence interval

$$\frac{1}{F(\alpha/2, df_2, df_1)} < \frac{\hat{\sigma}^2_{o_1}}{\hat{\sigma}^2_{o_2}} < F(\alpha/2, df_1, df_2) \quad . \tag{6.10}$$

The displacements, d, between two epochs and their resultant cofactor matrix, Q_d, are then obtained as

$$d = \hat{x}_2 - \hat{x}_1 \quad , \qquad Q_d = Q_{\hat{x}_1} + Q_{\hat{x}_2} \quad , \tag{6.11}$$

which may have been distorted through their respective definitions of the datum. These distortions may be reduced by transforming the biased displacement vector, d, onto a "best" common datum via an iterative weighted similarity transformation. Chen [1983] identified as "best", that datum upon which the sum of the absolute displacements was a minimum.

Chen [1983] proposed an iterative weighting procedure, based on the intuitive feeling that points exhibiting the most displacement should contribute the least to the definition of the datum. Also, in order to accommodate the tendency of some points to move in certain directions, their components should be assigned different weights (compared to weighting solely according to the magnitude of the displacement vector). As a first step, Chen proposed the inner constraint solution, which was then followed by the

iterations with re-weighting according to the inverse of the absolute value of the displacement component. Thus, the weight matrix W was defined as

$$\begin{aligned} W^0 &= I && \text{for} \quad k = 0 \\ W^{k+1} &= \text{diag}\left\{ 1 \Big/ \left|\tilde{d}_i^k\right| \right\} && \text{for} \quad k \geq 1 \end{aligned} \quad , \tag{6.12}$$

for which $\left|\tilde{d}_i^k\right|$ was the absolute value of the i^{th} element of the displacement vector from the k^{th} iteration.

A look at equation (6.12) reveals a numerical instability when $\left|\tilde{d}_i^k\right|$ approaches zero. Chen et al. [1990b] suggested that the addition of a small constant, δ, to each absolute displacement would ensure a non-zero term in the denominator (δ could, for example, be set equal to the convergence criterion, ε, used to terminate the iterations).

The iterative displacements, from the k^{th} iteration, are then estimated as

$$\tilde{d}^{k+1} = S^k \cdot \tilde{d}^k \quad , \tag{6.13}$$

where $\tilde{d}^0$ was the biased displacement vector, d, of equation (6.11), and

$$S^k = I - H\left(H^T W^k H\right)^{-1} H^T W^k \quad , \tag{6.14}$$

was the corresponding iterated weighted similarity transformation matrix.

The iterations continued until all displacement changes converged to within a given criterion (i.e., $\left|\tilde{d}^{k+1} - d^k\right| \leq \varepsilon$). Having achieved convergence, a new cofactor matrix was then obtained via the last similarity transformation matrix as,

$$Q_{\tilde{d}} = S^{k+1} \cdot Q_d \cdot \left(S^{k+1}\right)^T \quad . \tag{6.15}$$

A few comments regarding the IWST were offered by Chen [1983], and are worth repeating here. Firstly, when combining the two epochs, Chen cautions that "...the matrices H and D should consist of the appropriate columns corresponding to the union of the datum parameters of the two epochs and of the appropriate rows for the common points in the two epochs." [Chen, 1983, p.67]. Chen also emphasises that the trend analysis problem differs from the datum defect problem in that the datum equations are unknown, and that they must be realised in such a manner as to provide a clear displacement picture. In so doing, the resultant covariance matrix becomes deterministic rather than stochastic. The IWST is, therefore, to be considered a "... general tool for the purpose of preliminary identification of a deformation pattern." [Chen, 1983, p.123]. Consequently, the IWST estimated displacements, and especially their covariances, should not be used in any subsequent deformation modelling routines.

6.1.3 Stable Point Analysis

A "stable" monument has been defined by Vaníček et al. [1987] as one which "within the bounds of our ability to measure, maintains a fixed position relative to the immediate terrain upon which it sits, over a time interval exceeding the age of the geodetic network of which it is a part." In stable point analysis, the time interval alluded to above is effectively reduced to the interval spanning the observation epochs. Consequently, points identified as stable may, in the presence of new data, be tagged "unstable", so that stability

analysis is an ongoing process. The IWST algorithm was then applied to the analysis of stability spanning two epochs of observations under the assumptions that observational blunders and systematic errors had been removed, and that the null hypothesis Ho; $\hat{\sigma}^2_{o_1} = \hat{\sigma}^2_{o_2}$, had not been rejected.

The stability of a point is assessed, either visually, as a display of the transformed "displacement" vector of point j, $\tilde{d}_j$, against its 100(1-α)% confidence region, or numerically, via the quadratic form of a single point displacement with u_j degrees of freedom ($u_j = \dim\{\tilde{d}_j\}$), i.e.,

$$R_j = \tilde{d}_j^T \cdot \Sigma_{\tilde{d}_j}^{-1} \cdot \tilde{d}_j \tag{6.16}$$

for which the test statistic,

$$T = \frac{R_j}{\hat{\sigma}^2_{o_p} \cdot u_j} \tag{6.17}$$

has a Fisher distribution. The point j is considered significantly unstable, at 100α%, when $T \geq F(\alpha ; u_j , df_p)$. Each point common to both epochs is tested for stability at the 95% level of confidence and flagged if significantly unstable. In the event of relative networks the inclusion of all stations in the resolution of the datum defects may lead to biased results, in which case an iterative procedure could be adopted. For example, those stations displaying maximum displacements after the IWST would be excluded (i.e., given zero weights in W) from subsequent "realisations" of a common datum. Iterations would then continue until all "datum-realising" stations were assessed as "stable" (or, displacing equally).

6.2 Vertical Trend Analysis

Prior to any analysis, the estimated displacements between consecutive epochs were transformed into annual displacement rates, based on the time interval between levelling campaigns. These vertical displacement rates were then charted as accumulated displacement profiles and cross-sections (e.g., Figure 6.3 below), as well as single epoch displacement values on a map of the monument locations (see Chrzanowski et al., [1996]). These first views of the displacements indicated two major problems. Firstly, most of the monuments appeared to be within the influence zone[†] of the underground workings; and secondly, numerous monuments exhibited isolated and extensive upheaval in areas where subsidence was expected. The latter was generally attributed to frost action, while the former precluded the identification of a set of "stable" reference points.

6.2.1 Stable Point Analysis

The identification of "stable" (from 1989 to 1996, inclusive) monuments was unsuccessful due to the aforementioned reasons. The most obvious candidate for "stable reference point" designation was monument ML23, which was sufficiently far from the area under observation that it was unlikely to have been affected by current mining activities (although it may still have been affected by other unknown activities). Unfortunately,

---

[†] The *influence zone* of mining activity was initially assumed to be that region within which monuments were observed to be unstable.

monument ML23 has only been monitored since 1992, with no continuity between it and its predecessor, monument 10482. Consequently, for the trend analysis, monument 10894 was selected as the "stable point" which would best connect the pre- and post-1992 campaigns.

The problem with just a single reference point is that there is no means of verifying its stability. Ideally, monuments HT and 24740 could also have been used as reference points, unfortunately, levelling up the steep hill to HT was uneconomical and monument 24740 was probably too close to the underground works to be confident of its insensitivity to mining activity. On the other hand, mining has progressed away from 24740 towards ML23, hence it may eventually prove to be suitable. Also, one or more stations along the Back Road (its official name) may have been sufficiently distant to be adjudged "stable".

Table 6.1 IWST Vertical Translation Parameters.

	89-90	90-91	89-91	91-92	92-93	93-94	94-95	95-96
No. of All Stations	63	63	69	67	80	86	83	86
Datum Shift [mm]	-6.4	+1.4	-0.9	-0.4	-1.4	-2.8	-4.8	+0.6
No. of Ref. Stations	5	5	5	5	6	8	8	8
Datum Shift [mm]	-0.4	+4.0	+0.9	+1.6	+0.9	-0.3	-0.3	+1.8
Datum Bias [mm]	***-6.0***	***-2.6***	***-1.8***	***-2.0***	***-2.3***	***-2.5***	***-4.5***	***-1.2***

The lack of a set of clearly identifiable "reference points" produced a significant bias in the IWST results. The IWST analysis with all monument displacements

contributing to the resolution of the datum defect, resulted in a downward shifting of the realised datum, i.e., the expected stable points would appear to be rising. Consequently, a set of "reference" monuments exhibiting similar displacements was identified (10894, A1, A10, A11, ML12, ML23, 24740 and PCA6[‡]) and used with the IWST to realise new datums. Table 6.1 shows the IWST translation parameters based upon the above set of monuments, together with those based upon all monuments. In all cases, the set of "reference" monuments realised a datum higher than the datum realised via all monuments. The estimated datum parameters from the "all-stations" analyses were generally negative, with the exception of intervals 1990 to 1991 and 1995 to 1996. The transformations resulting from the "reference set" are generally less than 2 mm, hence the trend analysis with monument 10894 held fixed was not re-computed.

6.2.2 Vertical Trends

Six major trend sources were expected in the Sussex analysis, namely: frost heave; water table fluctuations; observation error; datum bias; direct impact; and mining activity. As the objective of this project was to monitor mining induced ground movements, the other trends had to be eliminated first. A few characteristics pertaining to these trends, together with examples from this project are presented below.

[‡] The number of reference stations in Table 6.1 refers to the left-most stations of this list.

6.2.2.1 Miscellaneous Trends

Frost heave requires: freezing temperatures; water; and soil with particle sizes less than 0.02 mm [Vaníček et al., 1987]. Monuments exhibiting frost heave were characterised by: visible protrusion of the concrete casing above ground level; continuous upward annual displacements; proximity to either the Kennebecasis river or its surrounding marshes; and reports from the monument construction crews of water inundation during monument installation. Numerous examples of frost heave were encountered, most notably on the B- and D-lines. Figure 6.1 shows the displacement rates observed for 11 monuments distributed throughout the network, including B2, B4, B6, D2, D3 and D4. The apparent correlation between the suspected "frost heave" trends indicates the possibility of some common underlying physical process.

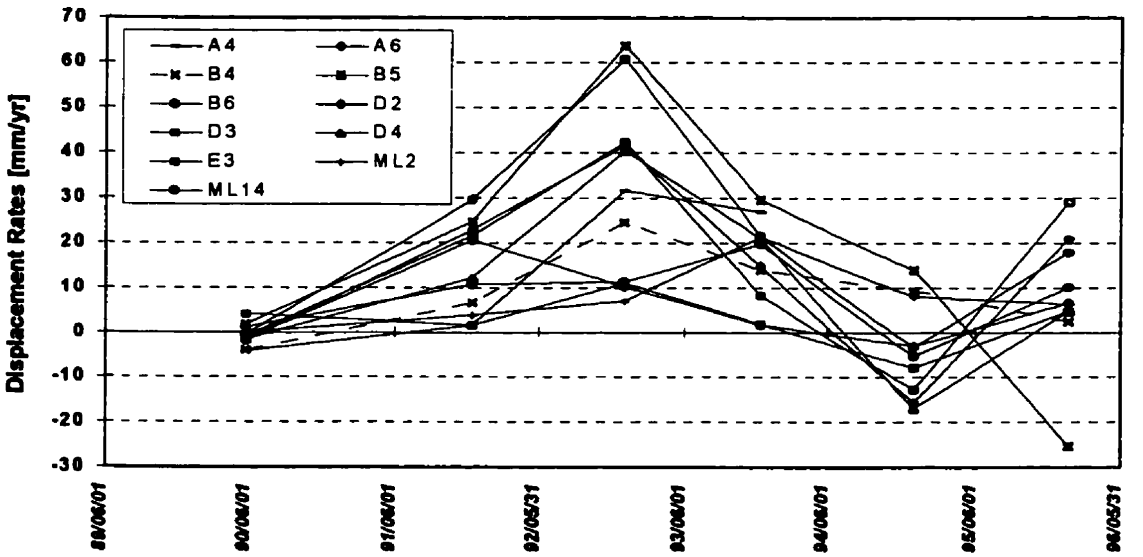

Figure 6.1 Vertical Displacement Rates of "Frost-Heaved" Stations.

Sliwa [1987], and Vaníček et al. [1987] both comment on the effect of changes in the water table level on bench mark stability. Sliwa [1987] indicated that bench marks placed in fine-grain soils may experience upward displacement due to a rising water table. Given the silt-stone in Sussex [Chrzanowski et al., 1996, Figure 43] it is suspected that, if present, the water table induced monument displacements would tend to follow the direction of the water table. It is apparent from Figure 2.1 that the water table effects are likely to peak within the low level area enclosed by the Trans-Canada Highway and the Back Road. Apart from the unusually high water levels reported in 1990 (which prevented observation of monuments D1 to D6 and B3) no information on the water table was obtained, hence no displacement trends were identified as resulting from water table fluctuation.

Some observation errors, which may have escaped detection within a single campaign, may be detected in the trend analysis. A typical trend of these errors would appear on stable, or marginally unstable monuments, as a pair of consecutive displacement rates with almost equal magnitudes but opposite signs. The 1989-1990-1991 pairs of consecutive displacement rates from the Back Road profile, see Figure 6.2, was suspected to be an example of such an error. Had this pair appeared in the opposite order, i.e., a nominal 10 mm/year rise followed by a nominal 10 mm/year fall, one may have speculated that it was due to the raised water table of 1990. The pre-1994 practice of only levelling the Back Road and TCH routes in one direction, together with the observed (from two-way levelling) systematic errors of the 1994 levelling data (see Figure 4.2), increased the probability of the observed trend being the result of observation error. Consequently, the

displacement rates between 1989 and 1991 were re-computed as a two year average, without the 1990 elevations. These values were then used in all subsequent trend analyses.

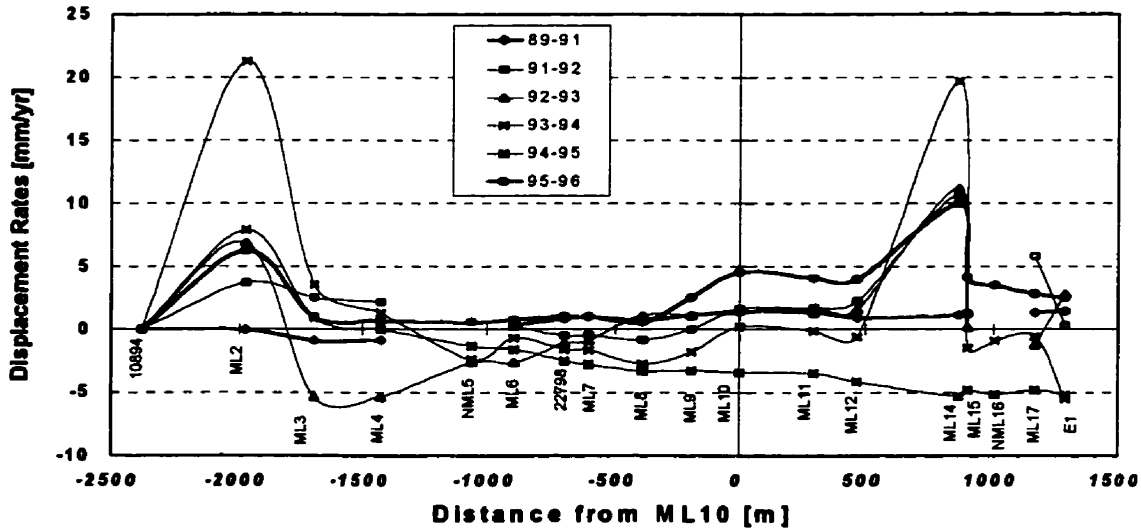

Figure 6.2a Back Road Profile: Vertical Displacement Rates, 1989-1996

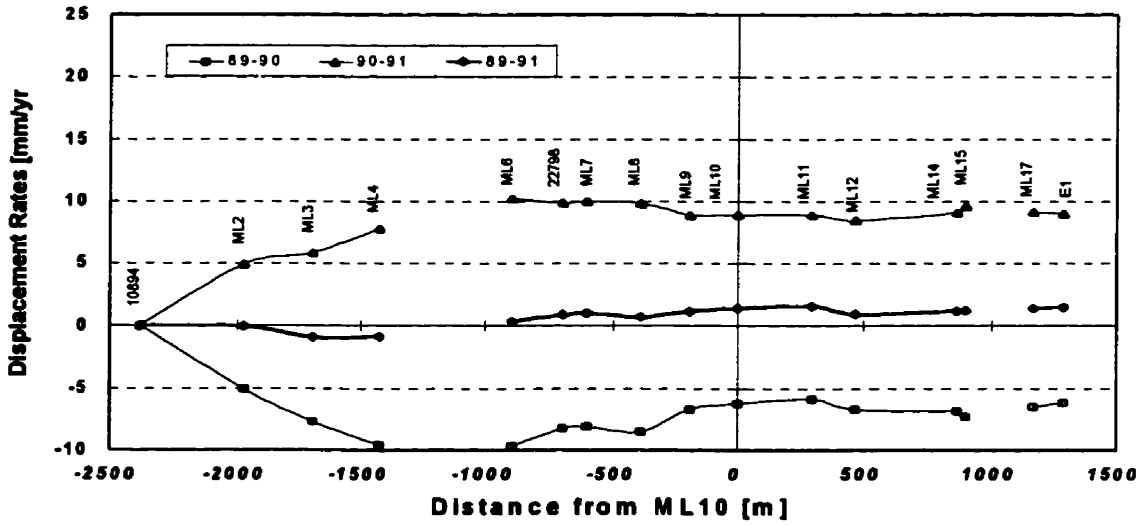

Figure 6.2b Back Road Profile: Vertical Displacement Rates, 1989-1991

Datum trends are characterised by regional or global network biases, i.e., subsidence of the "fixed" station would appear as a positive bias in the displacements of all other stations. An example of an apparent local datum bias involved the 1992 levelling from monument 9635 to ML23, including the F- and G-lines. This block of levelling was performed approximately two months after the main network. An inspection of the 1992 to 1993 displacements showed ML23 to have risen 8 mm, it also showed the G-line to have risen a similar amount north of the TCH and only marginally less south of the TCH. This was inconsistent with the subsequent displacement trends of the area. A - 8 mm correction applied to this block of 1992 data resulted in the 1992 to 1993 displacements of the F- and G-lines, as well as monument ML22, aligning closer to those observed between 1993 and 1995. A second datum-type trend was noticed in the 1995 to 1996 displacements, where a bias of between + 2 mm to + 4 mm was suspected. No corrections were applied, nor should they be unless the results of the 1997 levelling campaign support this postulation.

Direct impact on a monument is evidenced via discontinuities in the displacement trend, or, more obviously, by a mound of rubble where the monument ought to have been. Unfortunately, examples of direct impact were also available from the Sussex data set. Sometime between the end of the 1992, and beginning of the 1993, campaigns the trees and brush surrounding the E-line between the TCH and monument E9 were cleared via bulldozer. In 1993, monument E7 was noticed to have sustained major damage, but remained intact and solid. Monuments E8 and E9, however, were never found, only the scattered remnants of their concrete casings. Since 1993, E7 has been used as a temporary

point in the long levelling runs between 9635 and E10, however, the displacement trend of E7 since 1993 appears consistent with neighbouring monuments. Consequently, E7 has been restored to "full monument status" and is a valuable source of information in an important monitoring sector. Monuments ML18, A4, NC7 and C8 were the latest examples of destroyed monuments.

6.2.2.2 Mining Induced Trends

Mining induced displacements were expected to appear as a subsidence trough centred directly above the mine workings, i.e., in the vicinity of the TCH between the D- and E-lines. The subsidence trough was also expected to "travel" north-east, as per mining progress. This over-simplistic expectation was only a very rough starting point in the identification of the mining induced trends, and was not based on any predictive modelling nor on the underground observations. Nevertheless, removal of the other trends should leave a fairly smooth (since no surface cracks were reported) subsidence trough.

The TCH Profile displayed most of the effects of the mining activity in the Sussex area and was, therefore, the primary source of the vertical trend analysis. The various cross-sections tended to play supporting roles in the lateral extensions of the primary trends, with the Back Road profile indicating that it was probably the north-western extent of the mining induced vertical displacements.

As an aid to the analysis, three types of displacement tables were generated for each profile and cross-section, namely, accumulated annual displacements, annual

Table 6.2 TCH Profile: Accumulated Vertical Displacements, 1989 to 1996.

[units = mm]

BM	Dist[m]	1991	1992	1993	1994	1995	1996
24740	-3382			0.0	-0.7	1.4	5.6
24739	-3086			0.0	4.1	3.1	10.1
PCA6	-2711			0.0	0.1	-1.1	0.2
A7	-2561	-0.3	-1.0	-5.0	-4.9	-7.3	-8.9
ML21	-2264	-5.4	-7.1	-13.0	-16.7	-21.4	-27.4
PCA8	-2097	-7.7	-10.6	-16.8	-22.8	-28.8	-35.5
ML20	-1937	-9.4	-13.6	-22.5	-29.2	-36.6	-43.0
PCA9	-1794	-12.1	-18.7	-29.8	-37.6	-46.4	-52.8
ML19	-1511	-16.7	-26.2	-39.9	-47.7	-58.4	-63.5
9638	-1265	-21.4	-31.4	-45.3	-54.9	-65.8	-72.1
9637	-555	-29.7	-46.1	-65.2	-84.2	-102.5	-116.3
D7	0	-22.9	-36.8	-50.2	-66.6	-82.1	-90.3
9636	527	-14.4	-24.5	-37.8	-56.2	-76.7	-91.6
9635	877	-0.8	-6.3	-12.0	-19.8	-38.5	-54.1
10899	1173				-12.3	-28.1	-42.7
F1	1332		0.0	3.0	6.8	-5.3	-15.6
ML22	1656		0.0	-3.0	-8.2	-14.4	-15.3
G7	2017		0.0	-1.9	-5.4	-10.0	-6.1
ML23	4118		0.0	0.2	0.4	-0.2	3.2

Table 6.3 TCH Profile: Annual Vertical Displacement Rates, 1989 to 1996.

[units = mm/year]

BM	Dist[m]	89-91	91-92	92-93	93-94	94-95	95-96
24740	-3382				-0.7	2.1	4.2
24739	-3086				4.1	-0.9	7.0
PCA6	-2711				0.1	-1.3	1.3
A7	-2561	-0.1	-0.7	-4.0	0.1	-2.3	-1.7
ML21	-2264	-2.7	-1.7	-5.8	-3.7	-4.8	-5.9
PCA8	-2097	-3.8	-2.9	-6.2	-6.0	-6.1	-6.6
ML20	-1937	-4.7	-4.1	-9.0	-6.7	-7.4	-6.4
PCA9	-1794	-6.0	-6.6	-11.1	-7.8	-8.8	-6.4
ML19	-1511	-8.4	-9.5	-13.6	-7.8	-10.7	-5.1
9638	-1265	-10.7	-10.0	-14.0	-9.6	-10.9	-6.3
9637	-555	-14.8	-16.5	-19.0	-19.0	-18.3	-13.8
D7	0	-11.5	-13.8	-13.4	-16.4	-15.5	-8.2
9636	527	-7.2	-10.2	-13.2	-18.4	-20.5	-14.8
9635	877	-0.4	-5.5	-5.8	-7.8	-18.7	-15.5
10899	1173				-12.3	-15.8	-14.6
F1	1332			3.0	3.8	-12.0	-10.3
ML22	1656			-3.0	-5.3	-6.1	-1.0
G7	2017			-1.9	-3.5	-4.6	3.9
ML23	4118			0.2	0.2	-0.6	3.4

Table 6.4 TCH Profile: Vertical Displacement Rate Changes, 1989 to 1996.

[units = mm/year/year]

BM	Dist [m]	1990	1992	1993	1994	1995
24740	-3382				2.7	2.1
24739	-3086				-5.0	7.9
PCA6	-2711				-1.4	2.5
A7	-2561	-0.6	-3.2	4.0	-2.4	0.7
ML21	-2264	1.0	-4.1	2.1	-1.0	-1.2
PCA8	-2097	0.9	-3.3	0.1	0.0	-0.6
ML20	-1937	0.6	-4.8	2.2	-0.7	1.0
PCA9	-1794	-0.6	-4.4	3.3	-1.1	2.4
ML19	-1511	-1.2	-4.1	5.8	-2.9	5.6
9638	-1265	0.7	-4.0	4.4	-1.3	4.5
9637	-555	-1.7	-2.5	0.0	0.7	4.5
D7	0	-2.4	0.4	-3.0	0.9	7.4
9636	527	-3.0	-3.1	-5.2	-2.1	5.7
9635	877	-5.1	-0.2	-2.0	**-10.9**	3.2
10899	1173				-3.5	1.2
F1	1332			0.8	**-15.8**	1.7
ML22	1656			-2.3	-0.9	5.2
G7	2017			-1.6	-1.1	8.5
ML23	4118			0.0	-0.8	4.0

displacement rates, and changes (accelerations) in the displacement rates. Tables 6.2 to 6.4 are those pertaining to the TCH profile. As the identification of trends is greatly assisted by visual analysis, Figures 6.3 and 6.4 were generated to display the accumulated, and annual rates of, displacement along the TCH profile.

A word of caution is necessary when examining the "accumulated" data. Most of the data presented has been accumulated since 1989, however, monuments F1, G7, ML22 and ML23 represent accumulations since 1992, while 10894 has only been accumulated since 1993. Similarly, monuments PCA6, 24739, and 24740 have been accumulated from 1993. Their inclusion into a single data set was based on the following:

1. Monument PCA6 did not display any significant movement between 1993 and 1996, while 24740 appeared stable between 1993 and 1995 with only a recent possibility of an upward trend appearing in 1995. Hence, it was assumed that this section was stable prior to the start of monitoring, i.e., 1993.
2. Monument 9635 appeared to have been stable up to 1991, followed by a low constant subsidence rate (- 5 mm/year) between 1991 and 1993, while monument F1 appeared to be marginally heaving (+ 3 mm/year) between 1992 and 1994. This suggested that an inconsistency of only a few millimetres would be introduced through the merging of the "F1 to ML23" section to the 1989 base data.
3. Monument 10894, unfortunately, was not included in the 1992 campaign. Its inclusion in the data set was based on the consistency of its data after 1993. Its late introduction, however, may have caused the "step" visible in the trough profile of Figure 6.3. For this assumption to be correct, 10899 must have experienced moderate heave between 1992 and 1993 (possibly in a similar manner to that of monument F1). The subsidence rate observed between 1993 and 1994, - 12 mm/year, was marginally less than the nominal - 15 mm/year rates observed between 1994 and 1996, which may support the above assumption of marginal heave between 1992 and 1993.

Returning to the mining induced trends, Figure 6.3 indicates that the subsidence trough currently extends from PCA6, in the south-west, to just past G7, in the north-east, with maximum subsidence reaching -116 mm at monument 9637. It is also apparent that a "dimple" has developed around monument D7, where its accumulated subsidence lags that of its south-westerly neighbour, 9637, and was, in 1996, eventually surpassed by its north-

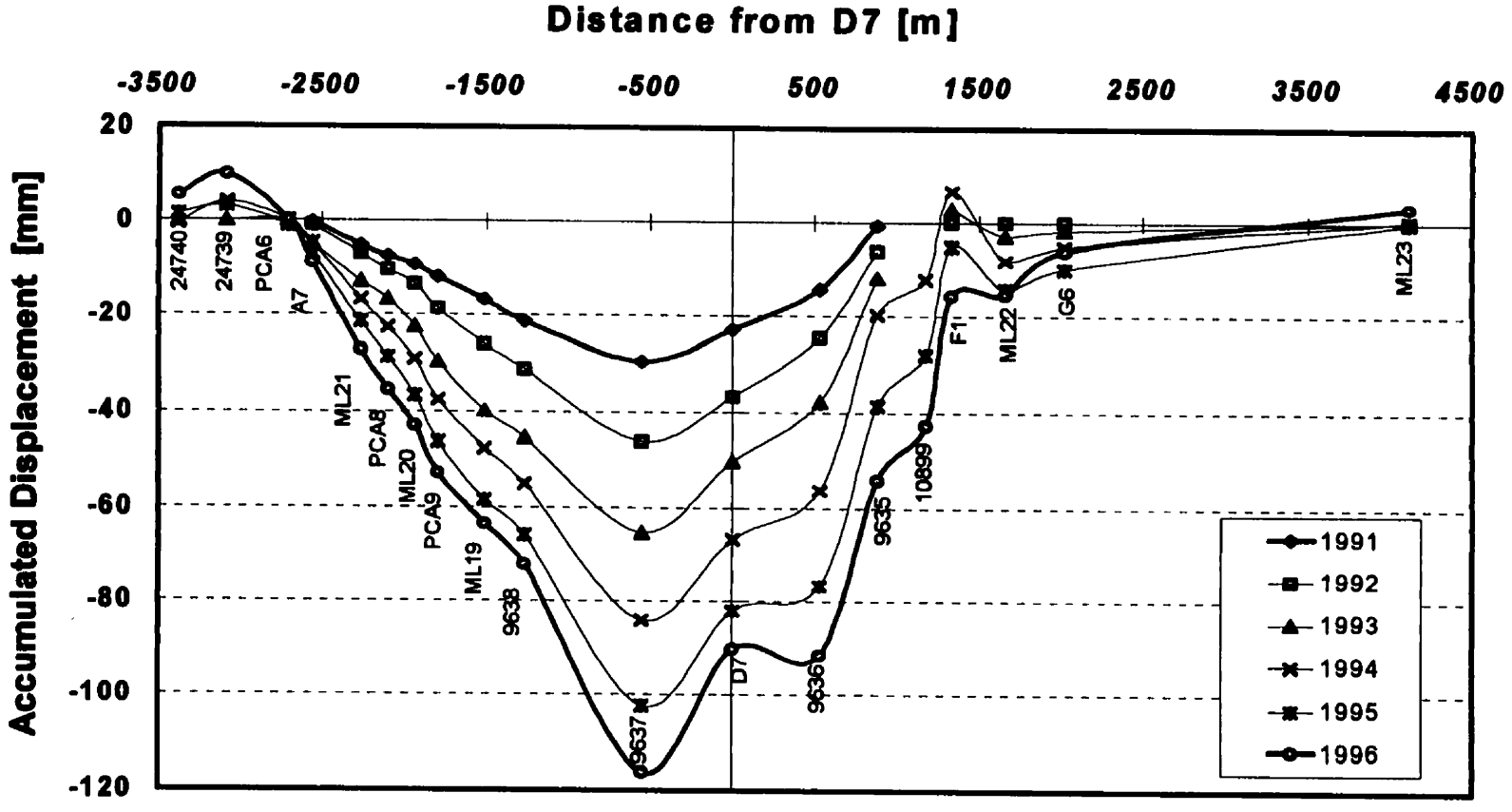

Figure 6.3 TCH Profile: Accumulated Vertical Displacements, 1989 to 1996.

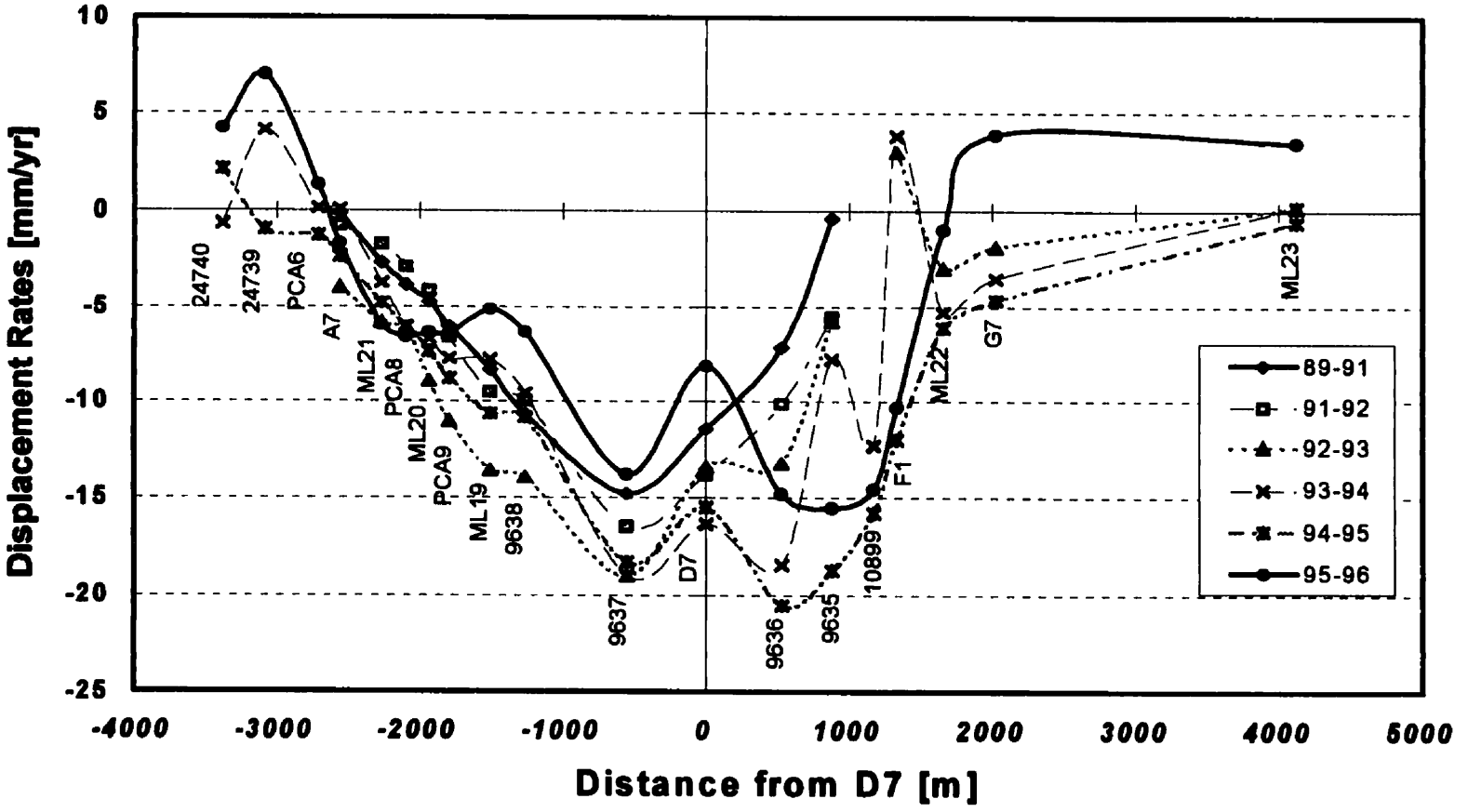

Figure 6.4 TCH Profile: Annual Vertical Displacement Rates from 1989 to 1996.

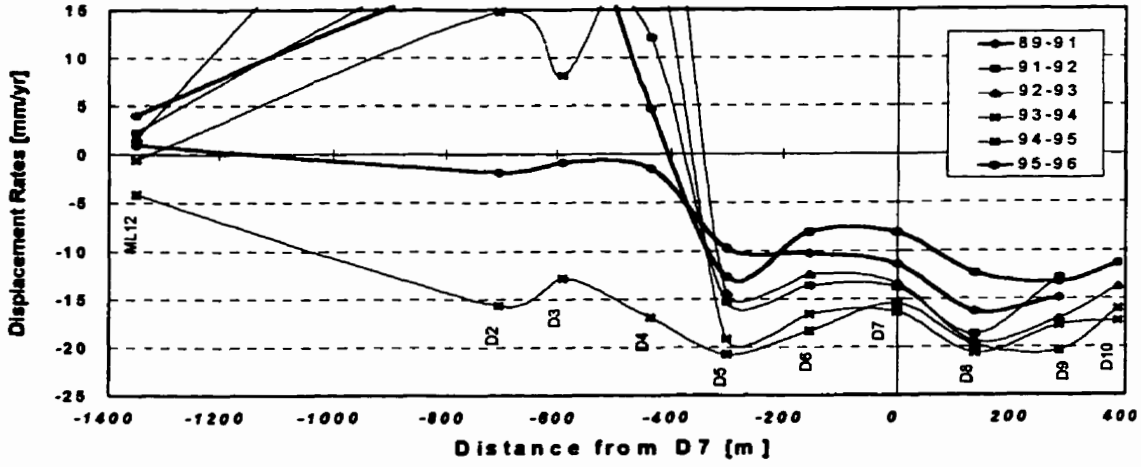

Figure 6.5 D-line Profile: Vertical Displacement Rates, 1989 to 1996.

easterly neighbour, 9636. Inspection of the D-line rates (see Figure 6.5) not only supports this local dimple anomaly, but indicates that D6 may also be a part of it.

Several trends supported the expected north-easterly progression of the trough. Firstly, Table 6.3 of the TCH displacement rates shows that 9637 had the fastest rate of subsidence up until 1994, after which it was surpassed by monument 9636, which was in turn surpassed by monument 9635 in the period 1995 to 1996. Secondly, monuments 9635, 10894, and F1 have successively progressed from stability to significant subsidence. Monument 9635 appeared to start subsiding around 1991, followed by 10894 in 1993/1994 and then F1 in 1994/1995. Thirdly, monuments 9637, D7 and 9636 appeared to have experienced periods of accelerated subsidence followed, more recently, by a decelerating subsidence (see Table 6.4 and Figure 6.6). Monument 9637 accelerated from - 15 mm/year between 1989 and 1991 to a peak of - 19 mm/year around 1993 before

decelerating[‡] to -14 mm/year in 1996. Similar trends were noted for monuments D7 and 9636, but with lags of around one and two years, respectively.

Figure 6.4 of the TCH displacement rates shows that the north-westerly progression of the subsidence trough is occasionally realised as a series of small slips, rather than a single smooth slide, as revealed by monuments 9635, F1, and (possibly)

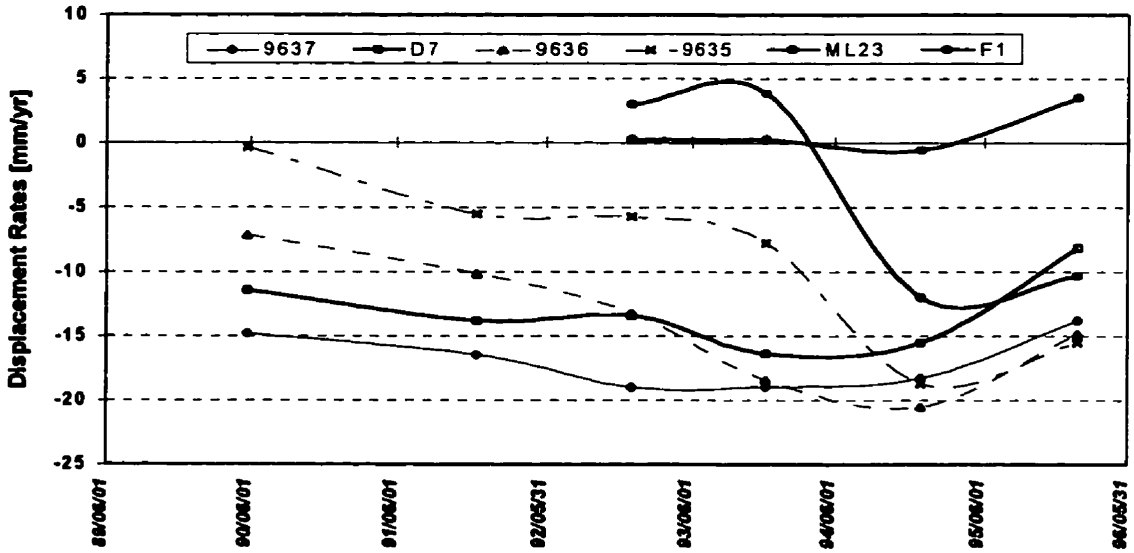

Figure 6.6 TCH Profile: Vertical displacement rates of selected stations.

10894. Figure 6.6 shows this more clearly by charting the individual monuments' displacement rates as a function of time; however, Table 6.4 demonstrates this most clearly via the relatively large "change in displacement rates" around 1994. Additional

[‡] Due partly to a suspected bias in the 1996 data, almost all of the monuments appeared to decelerate between 1995 and 1996. Absence of this bias may have reduced the decelerations to "constant" rates, but some monuments, e.g., 9636, 9637, D7, etc. would still appear to be decelerating.

evidence is provided via monuments E8 and E9 between 1991 and 1992, where they experienced "change in displacement rates" of - 11 and - 13 mm/year/year, respectively.

Another interesting trend noted on the TCH displacement rates was that there appeared to be a maximum subsidence rate of around - 21 mm/year. This value was supported by other monuments, not too far from the TCH, on the C-, D- and E-lines, namely: C4 (- 20 mm/year, 1993 to 1994); D5 (- 21 mm/year, 1994 to 1995); D8 (- 21 mm/year, 1993 to 1994); D9 (- 20 mm/year, 1994 to 1995); and E7 (- 24 mm/year, 1994 to 1995).

In conclusion, there exists a significant subsidence trough which appears to be progressing north-east with the occasional mini-slip mixed with smooth slides. The maximum accumulated subsidence (since 1989) appears at monument 9637, while the current maximum rate of subsidence appears at monument 9635. Additionally, a local anomaly appears to have formed around monuments D6 and D7. Despite all of the above it should be remembered that the magnitudes of these trends are small, compared to, for example, subsidence rates of around -70 mm/year at the nearby Potacan mine.

6.3 Horizontal Trend Analysis

The horizontal analysis was restricted to the extended networks of 1992 through 1996. Like the vertical analysis, the identification of stable reference points proved difficult,

more so with the pre-1993 campaigns where traversing errors were so predominant. A subset of all 33 stations common to each of the 1993 through 1996 horizontal campaigns was selected as the basis for the trend analysis. Inclusion of the 1992 campaign required the above subset to be reduced by one, namely station 24740.

6.3.1 Stable Point Analysis

Initial analyses of the horizontal displacements were based upon the minimum constraint solutions with station HT held fixed. A small group of stations was subsequently selected to realise the project datum, based on the following criteria:

1. the station was located at an extremity of the horizontal monitoring network;
2. the station was included in the GPS primary observation networks;
3. the station did not exhibit any large or systematic displacements (based on the IWST with all stations contributing to the datum realisation); and
4. the station monument was noted to be in good condition.

The above criteria resulted in the selection of stations HT, A1, and ML23, with stations E1 and G1 rejected on the basis of systematic displacements. Station 24740 was not included in the above set for two reasons. Firstly, it was only observed for the first time in 1993, by traverse, and in 1994, by GPS. Secondly, the 1993 to 1994 displacement of 24740 was quite large, around 65 mm. However, this displacement was consistent with an angular observation error, which would have "swung" the hanging traverse around station A7. Its inclusion, though, was primarily due to its importance to future analyses.

While not truly at a network extremity, station A1 was one of only three stations occupied by GPS in all monitoring campaigns. Its role, therefore, was to permit a link between the pre- and post-1992 monitoring campaigns.

Figure 6.7 shows the sets of annual displacements spanning the years 1992 to 1996, with the error ellipses of the 1994 to 1996 IWST analysis. The IWST estimated displacements involving 1992 or 1993 data were based on a datum realisation using stations A1, HT, and ML23, while 1994 through 1996 estimates also included station 24740. In all cases, only two datum defects were modelled, namely translations in northing and easting. The "star shaped cluster" of displacement vectors at stations HT and ML23, suggested these displacements were random (possibly the result of datum uncertainties). Station 24740, with the exception of the suspected traverse error between 1992 to 1993, also appeared to be stable. The displacements at A1 were also very small but appear to be unstable due to the overoptimistic 1994 to 1996 error ellipse.

A closer look at station HT, via Figure 6.8, shows that since 1994 it may have started to move southward (also downhill). The 1994 to 1996 IWST analysis, see Figure 6.8, clearly marks HT as unstable, while A1, ML23 and 24740 appear to be stable. Table 6.5, on the other hand indicates that the annual displacement rates of most of the monuments are still less than the 95% confidence ellipses of the horizontal surveys. The 1997 horizontal data will be needed to confirm, or refute, the stability of HT. If HT is moving, then station 24740 will obviously become a lot more important in future analyses.

Figure 6.7 : IWST Horizontal Displacements 92-93-94-95-96

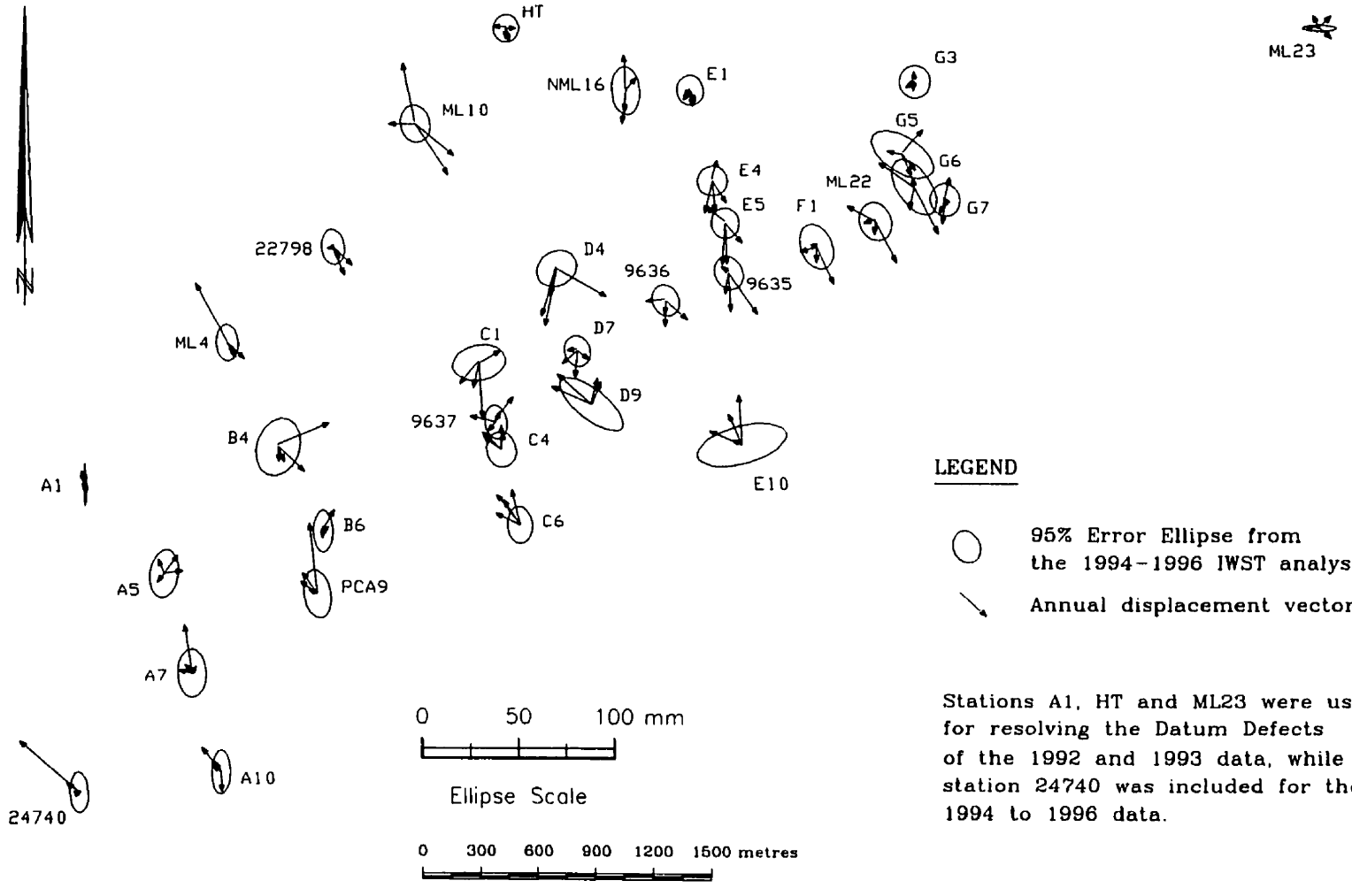

6.3.2 Horizontal Trends

Although the IWST algorithm has been applied to all stations common to consecutive epochs [Chrzanowski et al., 1996], only the 33 stations common to campaigns 1993 to1996 are reported on here. The 1994 to 1996 displacements of Figure 6.8 clearly show three sets of distinct displacements, identified as Sectors† I, II and III. Stations between the A-line and the E-line, north-west of the TCH (Sector I) are moving in a south-easterly direction. Stations F1, ML22 and those of the G-line (Sector II) are moving similarly, but in a more southerly to south-westerly direction. In strong contrast, the stations south-east of the TCH (Sector III) are moving in a north-westerly direction.

These trends are confirmed by the orientations of the "annual displacement vector clusters" shown in Figure 6.7. While the magnitudes of the annual displacements shown are only slightly larger than the 95% error ellipses of the 1994 to 1996 analysis (which is probably the most precise set achieved to date), their tendency to point in the same direction suggests the presence of systematic displacements.

Based on the 1994 to 1996 analysis, the maximum horizontal rates of displacement appeared to be in the order of 23 mm/year in a south-easterly direction at station D4. The maximum opposing displacements appeared to be in the order of 13 to 15 mm/year from stations C1, C6, and D10.

---

† Lines demarcating Sectors in Figure 6.8 are not discontinuities, but aids in the description of trends.

Figure 6.8 : 1994–1996 IWST Horizontal Displacements

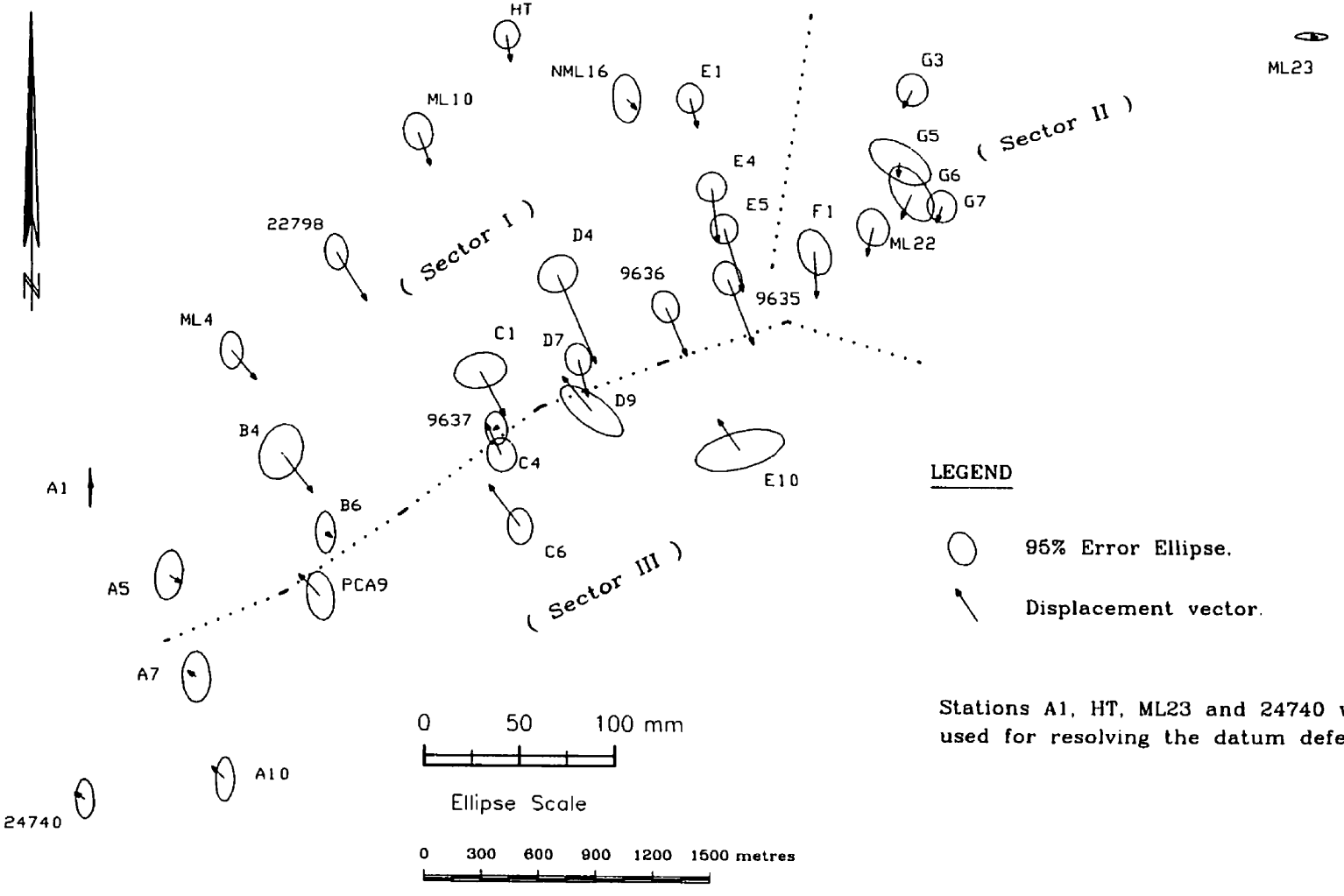

6.4 Summary

The analysis of both the vertical and horizontal trends has been hampered to some extent by the lack of a clearly identifiable set of homogeneous reference points. Nevertheless, through the selection of a set of monuments experiencing similar trends a consistent set of trends have appeared. The horizontal displacements towards the TCH between the C- and E-lines was consistent with the thalweg of the subsidence trough identified in the vertical analysis. Similarly, the south-westerly orientation of the G-line displacements was consistent with the leading edge of the trough having only recently extended this far north-east. In lieu of the above, the destruction of the south-eastern portions of the E- and F-lines has robbed us of important information in a critical monitoring section (in terms of both space and time).

A few comments of the observed trends, in relation to the major structures in the region, are in order. Firstly, the horizontal displacements in the vicinity of the Canadian National Railway (CNR) ranged from 7 mm/year in the east (E1) to 9 mm/year in the west (ML4), and may have been increasing since 1994. The vertical displacements, if at all present, have tended to be very slight and as yet not systematic. Several small road bridges exist on the A- and E-lines, however, displacements in these areas are fairly uniform. On the other hand, the longer bridge on the TCH, between D7 and 9636, may have a far more interesting stress field. The horizontal displacements observed at D7 and 9636 have the

same direction but 9636 appears to have a slightly higher rate. In the vertical, D7 was subsiding at a slightly faster rate than 9636 between 1989 and 1993. Since 1993, 9636 appears to have been subsiding at just over 5 mm/year faster than D7, which resulted in their accumulated (since 1989) subsidences being equal in 1995.

The differential movements reported above are probably considerably less than those designed for the daily expansions and contractions of the structures. It is only their long term, systematic effects that should be assessed and monitored.

Table 6.5 IWST Annual Displacement Rates based on the 1994 and 1996 Epochs.

Station	Displacement Rates [1994/1996 Avg]					95% Error Ellipse		
	ΔN	ΔE	d	α		a	b	Az
	[mm/year]			[°]		[mm]		[°]
22798	-11.2	7.5	13.5	146.1	*	8.7	6.1	353
24740	***1.5***	***-2.4***	***2.8***	***302.0***		***10.1***	***4.8***	***358***
9635	-15.3	6.4	16.6	157.4	*	8.7	7.1	328
9636	-11.5	5.3	12.6	155.5	*	8.4	6.8	330
9637	-0.4	-0.6	0.8	237.0		8.7	5.8	353
A1	***1.6***	***0.0***	***1.6***	***359.2***		***10.3***	***0.3***	***360***
A10	3.0	-3.2	4.4	312.7		11.1	4.9	1
A5	-1.9	3.1	3.6	121.6		12.3	7.3	8
A7	1.4	-2.0	2.4	304.2		12.7	7.4	358
B4	-9.9	7.8	12.6	141.6		14.8	11.1	21
B5	-4.6	7.6	8.9	120.9		12.9	8.5	0
B6	-1.2	1.5	1.9	127.2		10.4	5.1	359
C1	-11.1	6.2	12.7	150.8		14.0	9.1	80
C2	-4.4	0.9	4.5	168.4		9.9	9.1	280
C4	7.6	-3.9	8.5	333.0		8.9	7.7	344
C6	10.1	-7.7	12.7	322.7	*	9.2	6.5	355
D10	12.6	-8.2	15.0	326.9		23.0	10.5	296
D2	-14.9	8.5	17.1	150.4	*	9.6	8.6	53

continued on next page

Station	Displacement Rates [1994/1996 Avg]					95% Error Ellipse		
	ΔN	ΔE	d	α		a	b	Az
		[mm/year]		[°]		[mm]		[°]
D3	-15.5	9.8	18.3	147.7	*	19.8	9.0	353
D4	-21.1	9.6	23.2	155.6	*	10.9	8.7	64
D5	-18.0	9.9	20.6	151.2	*	9.0	8.7	29
D6	-13.6	6.4	15.0	154.8	*	9.3	8.4	303
D7	-9.0	2.5	9.3	164.7	*	8.3	6.7	341
D8	-1.5	-2.5	2.9	239.9		16.4	7.5	321
D9	8.6	-7.3	11.3	319.8		19.7	7.7	307
E1	-6.9	1.9	7.2	164.3		7.6	6.9	349
E10	7.6	-5.4	9.3	324.4		23.8	9.5	76
E2	-9.0	0.0	9.0	180.2	*	8.0	7.6	75
E3	-10.9	-1.0	11.0	185.0	*	8.3	7.6	79
E4	-13.3	1.6	13.4	173.0	*	7.9	7.5	69
E5	-14.6	4.6	15.3	162.4	*	7.6	7.3	349
E6	-13.7	4.6	14.5	161.3	*	8.3	7.5	324
F1	-10.6	0.6	10.6	176.8		11.7	8.1	334
G3	-4.1	-2.2	4.7	208.1		8.3	8.0	354
G5	-3.7	-0.3	3.7	185.2		18.1	9.0	301
G6	-5.9	-2.4	6.4	202.2		16.0	8.5	325
G7	-3.7	-1.3	3.9	199.0		8.3	7.7	337
ML10	-8.4	3.1	8.9	159.9		9.7	7.6	345
ML11	-8.0	2.7	8.4	161.5		15.9	8.4	333
ML12	-8.8	2.4	9.2	165.1		12.6	7.7	349
ML14	-9.0	1.7	9.2	169.1		14.9	7.7	355
ML15	-8.3	2.8	8.7	161.5		14.8	7.5	356
ML17	-3.7	3.4	5.0	137.3		9.3	7.2	360
ML22	-6.6	-1.5	6.8	192.5		9.8	8.2	333
ML23	***-0.1***	***1.4***	***1.4***	***95.0***		***8.7***	***1.6***	***271***
ML4	-7.1	6.2	9.4	138.8	*	9.5	5.8	356
ML6	-10.6	5.4	11.9	153.2		13.4	7.2	329
ML7	-10.5	7.4	12.8	144.7	*	9.4	7.0	341
ML8	-11.9	8.5	14.6	144.7	*	10.9	7.5	328
ML9	-11.1	7.0	13.1	147.6	*	12.8	9.2	310
NML16	-2.5	2.5	3.5	135.4		12.3	7.3	355
PCA9	5.0	-5.3	7.3	313.6		12.3	7.1	349
HT	***-6.2***	***1.0***	***6.3***	***170.7***		***7.0***	***6.6***	***17***

Chapter 7

Conclusions and Recommendations

This report has dealt extensively with the data collection and data processing aspects of the displacement monitoring project at the PCS mine, and somewhat less extensively with the analysis of those displacements. This is commensurate with the author's experience. In summation, then, these two aspects of the report have been grouped under separate headings.

7.1 Data Collection and Processing

In Chapter 2 it was concluded that use of the "three-dimensional height controlled" system resulted in fewer traverse data reduction procedures than the traditional two-dimensional "horizontal" approach. It was also concluded that the zenith distances were superfluous;

however, considering the minimal additional effort required for their collection and their potential usefulness in a combined three-dimensional adjustment of all data, my recommendation is that their collection, via three arcs, be continued.

Chapter 3 showed that the approximate position of station HT in the WGS84(G730) datum was nominally 11m west, and 22 m too high. This positioning error should be corrected, in spite of the necessity to reprocess all GPS data from all campaigns. In this regard the calculations of the fixed station HT should be checked by a more scientific GPS processing package capable of, for example, multi-station solutions, earth tide corrections, modern tropospheric models, etc.

Also in Chapter 3, biases were observed in the "1993/1994" and 1996 local geoidal corrections. This indicated that a single sub-centimetre "local geoidal correction model" for all campaigns was not achieved and that these corrections had to be applied on a single campaign basis. Also, the uncertainty introduced by this procedure precluded the integration of the GPS and levelling data for vertical displacement monitoring. This, however, was a preliminary investigation, for which the GPS and levelled heights were considered to have equal weights. If GPS and levelling are to be integrated, on such a small area, then a more rigorous investigation of the local geoid must be undertaken, with particular emphasis on its instability from year to year.

Chapter 4 highlighted the failure of the IMINQE algorithm to assess the traverse data accuracies. The recommended procedure was to use the empirical models, with the manufacturers accuracy claims, as a first approximation (which should also be conducted for detecting, and removing, outliers prior to the IMINQE analysis). Subsequently, a re-

scaling of the *a priori* variances in an iterated least squares adjustment, using the group estimated variance factors outlined in Chapter 4 and Chapter 5, should be performed. It was noted, however, that the IMINQE software used was in a preliminary stage of development. It is recommended, therefore, that data segmentation routines be added to the IMINQE software which would permit grouping within the observation types according to instrumentation, environmental conditions, dates, etc. This should be undertaken before any expansion of the initial limited set of error structure models.

Chapter 4 also showed that, in terms of the 1994 levelling data, a correlation of between +0.84 and +0.89 existed between the forward and backward runs, while no correlation was found between the low- and high-scale estimates. Further, a one-way ANOVA indicated that the "paved" and "unpaved" sections had significantly different mean discrepancies, from which the steeper "paved" sections were noted to enhance the systematic error (source unknown). Despite this, the variances for both paved and unpaved sections were found not to be different. It is recommended, therefore, that additional investigations into this systematic error be performed, initially to establish its presence in other campaigns, and subsequently into whether it cancels in the mean of two levelling runs. Consequently, it is further recommended that the current practice of double-run sections along the Trans-Canada Highway and the Back Road be continued.

Chapter 4 also concluded that the Ashtech estimated covariances for the GPS baselines, from their solution files, were preferred to the IMINQE estimate which was unable to separate the baseline covariance components into constant and scale parts. However, the Ashtech *posteriori* variance factors (from primary GPS-only adjustments)

indicated that the *a priori* estimates had been progressively more and more pessimistic, so that they should be scaled by the GPS-only *a posteriori* variance factor prior to entry into the combined adjustment. As the Ashtech covariances are closely linked to the strength of the baseline solution, their continued use is recommended.

Chapter 5 introduced the three-dimensional height controlled system as used by GeoLab™. It is strongly recommended that this system be continued. However, the integration of three-dimensional GPS data with two-dimensional traverse data requires a reconciliation of the height systems used. Such reconciliation was obtained via local geoidal corrections estimated for all monitoring stations, whether they were constrained in the vertical, or not. The inclusion of mark-to-mark zenith distances may assist in the verification of elevation consistency through an introduction of residuals into the data snooping routine. This should be investigated.

Chapter 5 also concluded that the traversing densification scheme was the most accurate, unfortunately it was also very time consuming. Also, the pseudo-static GPS densification was more appropriate in open areas than the trilateration scheme of 1995; however, static would still be required for "obstructed" sites. The pseudo-static method, unfortunately, still requires two occupations for a single solution. It is recommended, therefore, that the possibility of rapid-static, for which only a single 10 to 15 minute occupation would be required, be investigated. The feasibility of such an approach would be subject to the "portability" of the dual-frequency GPS equipment (in which category the Ashtech Z-XIIs do not rate highly).

Chapter 6 outlined the IWST and its application to trend analysis. It was also shown, with respect to the levelling data, that the "common" datum realised by the IWST, experienced a "downward shift" when all monitoring stations were used to realise the datum (despite re-weighting according to displacement magnitudes). The final IWST analysis was then performed via the selection of a set of similarly, but slowly, displacing monuments for the datum realisation. It is recommended, therefore, that not all monuments be used to realise the datum in the IWST analysis of relative networks and that, instead, a set of similarly displacing (possibly even stable) set of well distributed monuments be sought. This recommendation is also applicable to the horizontal analysis, for which the selection of stable points was equally difficult.

7.2 Horizontal and Vertical Displacements

The analysis of vertical displacements was primarily based upon the trends exhibited by the TCH profile, with cross-sections playing supporting roles. From this analysis is was concluded that commencement of monitoring of the F- and G-lines in 1992 was just in time to detect the first stages of mining induced subsidence. It was also concluded that a noticeable subsidence trough extended from monument PCA6 in the south-west, to just past G7 in the north-east, and northward as far as the Back Road. The southerly extent of the trough was not identified as it extended past all monitored stations. It is recommended

that the "destroyed' monuments south of the Trans-Canada Highway be re-established and even extended farther south (unfortunately, this will have to wait until the current construction of the new Trans-Canada Highway has been completed).

It was also noticed that the "point" of maximum subsidence, and consequently the subsidence trough itself, was progressing slowly in a north-easterly direction. Maximum subsidence rates of between -20 and -24 mm/year are currently experienced near the intersection of the TCH profile and E-line cross-section. While the maximum accumulated subsidence, since 1989, was recorded at station 9637 as -116 mm.

The epochs 1992 to 1996 and a subset of 33 monuments common to these epochs were used to analyse the horizontal trends. The conclusion was that three distinctive sectors were identified (see Figure 6.8) from which Sector I appeared to be displacing in a south-easterly direction with a maximum horizontal displacement rate of 23 mm/year at station D4. Sector III, on the other hand, appeared to be displacing in a north-westerly direction with a maximum displacement rate of around 14 mm/year at stations C1, C6 and D10. Sector II appeared to be a newly displacing region ahead of the progressing subsidence trough, consequently the displacements appeared to be oriented in a more south to south-westerly direction.

Both the horizontal and vertical displacements appeared to be consistent with the progression of underground workings in a north-easterly direction. Consequently, with surface displacements at the G-line, planning for a new cross-section (H-line) should start now so that it may be established prior to the effects of mining activities reaching the surface.

References

Ashtech Inc. (1992). "*Ashtech XII GPPS Post-Processing System Manual Covering Versions 4.4.00 and 4.4.01.*" Ashtech Inc., Sunnyvale, California, U.S.A.

Ashtech Inc. (1993). "*Ashtech XII GPPS™ Post-Processing System Manual Software Version 5.0.00.*" Ashtech Inc., Sunnyvale, California, U.S.A.

Ashtech Inc. (1994). "*PRISM Precision GPS Surveying Software.*" Ashtech Inc., Sunnyvale, California, U.S.A.

BitWise Ideas Inc. (1993). "*GeoLab™ Users Guide*", Version 2 Series, GEOsurv Inc, Ottawa, Ontario, Canada.

Blachut, T. J., A. Chrzanowski and J. H. Saastamoinen (1979). *Urban Surveying and Mapping*. Springer Verlag, New York, Berlin.

Bossler, J. D. (1984). "Standards and Specifications for Geodetic Control Networks." Federal Geodetic Control Committee, Rockville, Maryland.

Bowring, B. R. (1980). "Notes on space adjustment coefficients." *Bulletin Géodésique*, 54, pp. 191-199.

Caissy, M. (1994). Personal communication. Graduate student, Dept. of Geodesy and Geomatics Engineering.

Caspary, W. F. (1987). "Concepts of network and deformation analysis." Edt. by J.M. Rüeger, Monograph 11, School of Surveying, University of New South Wales, Kensington, N.S.W., Australia.

Chen, Y. Q. (1983). *Analysis of deformation surveys: a generalised method.* Ph.D. Thesis, Department of Surveying Engineering Technical Report No. 94, University of New Brunswick, N.B., Fredericton, Canada.

Chen, Y. Q., A. Chrzanowski and M. Kavouras (1990a). "Assessment of observations using minimum norm quadratic unbiased estimation (MINQUE)." *CISM Journal*, Vol.44, No.4, Spring, pp.39-40.

Chen, Y.Q., A. Chrzanowski and J. M. Secord (1990b). "A strategy for the analysis of the stability of reference points in deformation surveys." *CISM Journal ACSGC*, Vol. 44, No. 2, Summer, pp. 141-149.

Chiarini, A., and L. Pieri (1971). "Statistical analysis of discrepancies in high precision levelling." *Bulletin Géodésique*, No. 99, March, pp. 5-27.

Chrzanowski, A., Y. Q. Chen and J. M. Secord (1986). "Geometrical analysis of deformation surveys." *Proceedings of the Deformation Measurements Workshop*. Massachusetts Institute of Technology, Cambridge, Mass., U.S.A.

Chrzanowski, A., M. Caissy, J. Grodecki and J. Secord (1994). "Software development and training for geometrical deformation analysis." *Final contract report to Geodetic Survey Division, Department of Natural Resources*, Vol. I-VI. Engineering Surveys Research Group, Department of Geodesy and Geomatics Engineering, UNB, Fredericton.

Chrzanowski, A., A. Szostak-Chrzanowski, G. Bastin and B. Singleton (1996). "1989-1995 Ground Subsidence Study in the Mining Area of Potash Corporation of Saskatchewan - New Brunswick Division Near Sussex, N.B." Report submitted to Potash Corporation of Saskatchewan - N. B. Division. Engineering and Mining Research Group, Department of Geodesy and Geomatics Engineering, University of New Brunswick, N.B., Fredericton, Canada.

Decker, B. L. (1986). "World Geodetic System 1984." *Proceedings of the 4th International Geodetic Symposium on Satellite Positioning*. Austin, Texas, 28th April - 2nd May, Vol. 1, pp. 69-92.

Defense Mapping Agency (1993). "Department of defense World Geodetic System 1984: Its definition and relationships with local geodetic systems." DMA TR 8350.2, 2nd Edition. Reprinted from original by Navtech Seminars & Book and Software Store, Inc., due to limited availability from U.S. Geological Survey.

Dodson, A. H. (1995). "GPS for height determination." *Survey Reviews*, Vol. 33, No. 256, April, pp. 66-76.

Ebong, M. B. (1985). "On the use of multiple comparisons test for the analysis of levelling discrepancies." *Bulletin Géodésique*, Vol. 59, No. 1, pp.1-10.

Engineering and Mining Surveys Research Group (1992). "PCA Sussex 1991, 1992 Field Book." Dept. of Geodesy and Geomatics Engineering, UNB, Fredericton, N.B., 24th June, p. 119.

Fiedler, J. (1992). "Orthometric heights from Global Positioning System." *Journal of Surveying Engineering*, Vol. 118, No. 3, August, pp. 70-79.

Forsberg, R. and F. Madsen (1990). "High precision geoid heights for GPS levelling." *Proceedings of 2nd International Symposium on Precise Positioning with the GPS*. Ottawa, Canada, 3-7 September, pp. 1060-1074.

Gruendig, L. (1985). "Special adjustment tools for surveying networks." In Papers for the Precise Engineering and Deformation Surveys Workshop, Eds. W. F. Teskey and L. Gruendig, The Canadian Institute of Surveying, Calgary, Alberta, pp.52-63.

"Guidelines and Specifications for GPS Surveys" (1992). Release 2.1, Geodetic Survey Division, Canada Centre for Surveying, Surveys, Mapping and Remote Sensing Sector, December, 1992.

Hamilton, W. C. (1964). *Statistics in Physical Science: Estimation, Hypothesis Testing and Least Squares.* The Ronald Press Co., New York.

Horn, S. D., R. A. Horn and D. B. Duncan (1975). "Estimating heteroscedastic variances in linear models." *Journal of the American Statistical Association*, Vol. 70, pp. 380-385.

Hull, W. V. (1989). "Geometric Geodetic Accuracy Standards and Specifications for Using GPS Relative Positioning Techniques." Version 5.0, Reprinted with corrections August 1, 1989. *Federal Geodetic Control Committee*, Rockville, Maryland.

Jivall, L. (1992). "GPS for geodetic control surveying in Sweden." *Proceedings of the 6th International Geodetic Symposium on Satellite Positioning*, Columbus, Ohio, March 17-20, Vol. I, pp. 501-510.

Katowski, O. and W. Salzmann (1983). "The Angle-measurement System in the Wild Theomat T2000." Wild Heerbrugg Ltd., Precision Engineering, Optics, Electronics, Heerbrugg, Switzerland.

Kern, (1987). "GK2-A: The Precise Automatic One." Kern and Co. Ltd., Technical Brochure 123e 5.87.RT ., CH-5001 Aarau, Switzerland.

Lazzarini, T., R. R. Steeves and A. Chrzanowski (1976). "Lazzarini's approach to the determination of displacements and deformation of structures and their environment by geodetic means." In SE4061 Selected Papers and Lecture Notes by A. Chrzanowski, UNB, Fredericton, 1985.

Leica (1993a). "Wild NA2002, NA3000: Information about digital levels." Brochure G1 221e-IV.93, Leica AG, CH-9435 Heerbrugg, Switzerland.

Leica (1993b). *Wild T2002, T3000, TC2002 User Manual.* Leica G2 245e - I.93. Leica AG, CH-9435 Heerbrugg, Switzerland.

Malys, S. and J. Slater (1994). "Maintenance and enhancement of the World Geodetic System 1984." *Proceedings of ION GPS-94.* 7th Int. Tech. Meeting of The Satellite Division of the Inst. of Navigation, Part 1, Salt Lake City, Utah, 20-23 September, pp. 17-24.

McCarthy, D. D. (1996). "IERS Conventions (1996)." IERS Technical Note 21. Central Bureau of IERS - Observatoire de Paris, Paris.

Rüeger, J.M. (1990). *Electronic Distance Measurement: An Introduction.* 3rd totally revised edition, Springer-Verlag, Berlin-Heidelberg-New York.

Rüeger, J.M. (1994). "Letters to the Editor." *The Australian Surveyor*, Vol. 39, No. 1, March, pp. 55-56.

Santala, J. and T. Parm (1994). "On the accuracy of a theodolite based measuring system." FIG XX Congress, Melbourne, Australia, 5-12 March, Commission 6, Paper TS 607.2, 18 pp.

Santerre, R. (1989). *GPS Satellite Sky Distribution: Impact On The Propagation Of Some Important Errors In Precise Relative Positioning.* Ph.D. thesis, Department of Surveying Engineering Technical Report No. 145, University of New Brunswick, Fredericton, N.B., Canada, 220 pp.

Schmidt, K. (1994). "Determination of the covariance matrix of double runs in motorized leveling of optical micrometer leveling with double-scale rods." *Surveying and Land Information Systems*, Vol. 54, No. 2, pp. 79-80.

Searle, S. R. (1971). "Topics in variance component estimation." A Biometrics invited paper, *Biometrics 27*, March, pp.1-76.

Secord, J.M. (1989). "Report of Work and Results of Surface Subsidence Monitoring Surveys." Department of Surveying Engineering, University of New Brunswick.

Sideris, M. G (1993). "Tests of a gravimetric geoid in GPS networks." *Surveying and Land Information Systems*, Vol. 53, No. 2, pp. 94-102.

Sliwa, L. (1987). "Some aspects on bench mark stability." *Surveying and Mapping*, Vol. 47, No. 2, June, pp. 155-163.

Snay, R. A. (1989). "Accuracy Analysis." Chapter 19 in "North American datum of 1983", Ed. C. A. Schwarz, NOAA Professional Paper NOS 2, U.S. Department of Commerce, Rockville, MD 20852, U.S.A., pp.193-219.

Specification Series, (1978). "Specifications and Recommendations for Control Surveys and Survey Markers." Energy, Mines and Resources Canada, Surveys and Mapping Branch, Ottawa, Canada.

Steeves, R. R. (1984). "Mathematical models for use in the readjustment of the North American geodetic networks." Geodetic Survey of Canada Technical Report No. 1, Energy, Mines and Resources Canada.

Swift, E. (1994). "Improved WGS84 coordinates for the DMA and Air Force GPS tracking sites." *Proceedings of ION GPS-94*. 7th Int. Tech. Meeting of The Satellite Division of the Inst. of Navigation, Part 1, Salt Lake City, Utah, 20-23 September, pp. 285-292.

Tellumat (1988). *Operators Handbook for Tellurometer MA200 Electronic Distance Measuring System*. Preliminary issue August 1988, 862-00020-K, Tellumat Limited, Surbiton, Surrey, England.

Thomson, D. B., M. P. Mepham and R. R. Steeves (1977). "The stereographic double projection." Technical Report No. 46, Department of Surveying Engineering, University of New Brunswick, N.B., Fredericton, Canada.

United States Naval Observatory (1994). "Activation of anti-spoofing (A-S)." Notice Advisory to Navstar Users (NANU) 050-94042, R 112045Z, February.

Vaníček, P. and E. J. Krakiwsky (1986). *Geodesy: The Concepts*. 2nd ed., Elsevier Science Publishers B.V., Amsterdam, The Netherlands.

Vaníček, P.(Ed.), P. A. Cross, J. Hannah, L. Hradilek, R. Kelm, J. Mäkinen, C. L. Merry, L. E. Sjöberg, R. R. Steeves and D. B. Zilkoski (1987). "Four-dimensional geodetic positioning." *Manuscripta Geodaetica* Vol. 12, No. 3, pp.147-222.

Vincenty, T. (1980). "Height-controlled three-dimensional adjustment of horizontal networks." *Bulletin Géodésique*, 54, pp. 37-43.

Vincenty, T. (1982). "Methods of adjusting space systems data and terrestrial measurements." *Bulletin Géodésique*, 56, pp. 231-241.

Walford, J. (1995). "*GPS Subsidence Study of the Costa Bolivar Oil Fields, Venezuela.*" M.Sc.E. thesis, Department of Geodesy and Geomatics Engineering Technical Report No. 174, University of New Brunswick, Fredericton, N.B., Canada, 137 pp.

Wassef, A. M. (1987). "Comparison of methods of analysis and evaluation of levelling errors." Technical Report No. 14, Centre for Surveying Science, University of Toronto.

Wilkins, F. J. (1989). "Integration of a coordinating system with conventional metrology in the setting out of magnetic lenses of a nuclear accelerator." M.Sc.E. thesis, Department of Surveying Engineering Technical Report No. 146, University of New Brunswick, Fredericton, N.B., Canada, 163 pp.

IMAGE EVALUATION
TEST TARGET (QA-3)

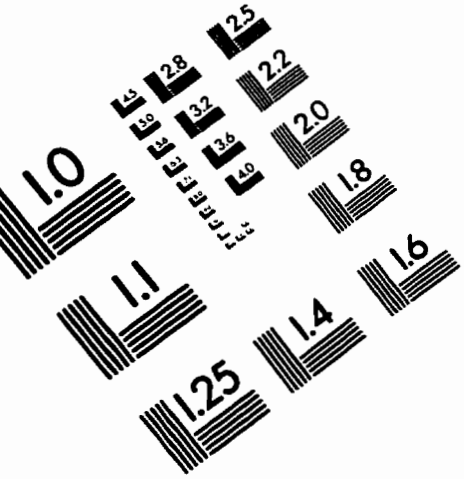

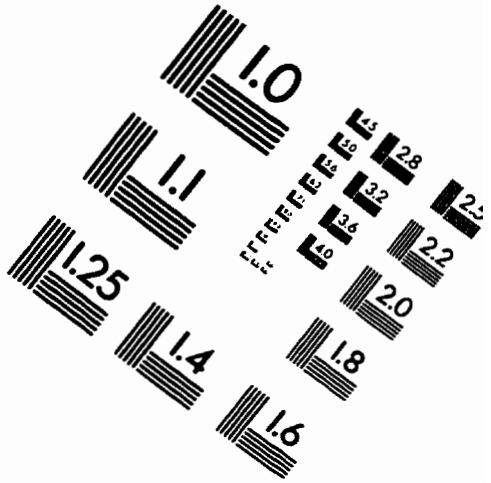

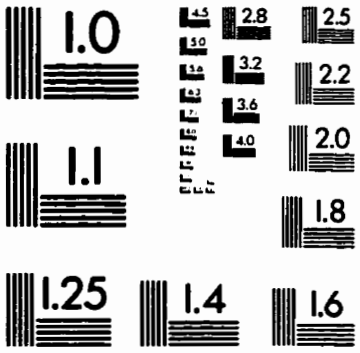

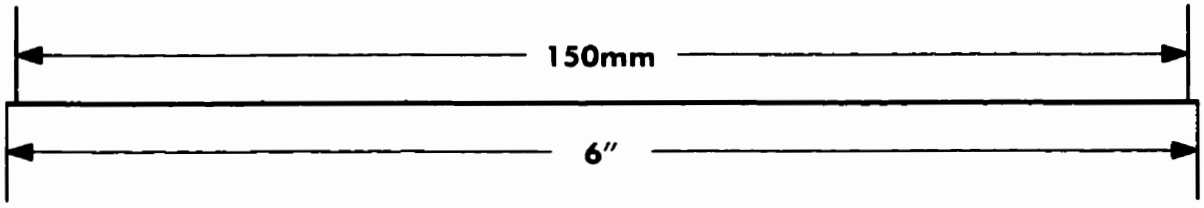

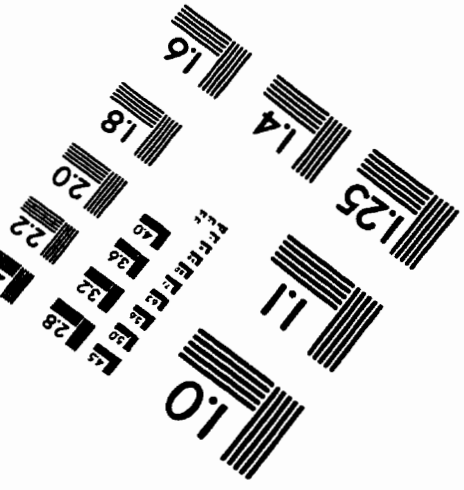

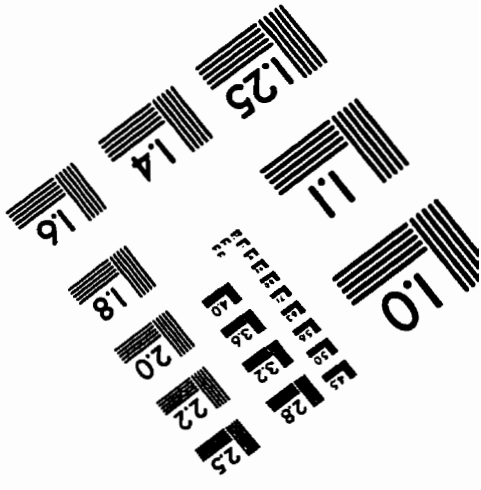

APPLIED IMAGE, Inc
1653 East Main Street
Rochester, NY 14609 USA
Phone: 716/482-0300
Fax: 716/288-5989